POLYSTYRENE-BASED AND CARBON FABRIC-REINFORCED POLYMER COMPOSITES CONTAINING CARBON NANOTUBES: PREPARATION, MODIFICATION AND CHARACTERIZATION

A THESIS SUBMITTED TO
THE GRADUATE SCHOOL OF NATURAL AND APPLIED SCIENCES
OF
MIDDLE EAST TECHNICAL UNIVERSITY

BY

BERRAK ERKMEN

IN PARTIAL FULFILLMENT OF THE REQUIREMENTS
FOR
THE DEGREE OF DOCTOR OF PHILOSOPHY
IN
CHEMICAL ENGINEERING

NOVEMBER 2020

Approval of the thesis:

POLYSTYRENE-BASED AND CARBON FABRIC-REINFORCED POLYMER COMPOSITES CONTAINING CARBON NANOTUBES: PREPARATION, MODIFICATION AND CHARACTERIZATION

submitted by **BERRAK ERKMEN** in partial fulfillment of the requirements for the degree of **Doctor of Philosophy** i**n Chemical Engineering, Middle East Technical University** by,

Prof. Dr. Halil Kalıpçılar
Dean, Graduate School of **Natural and Applied Sciences** _____

Prof. Dr. Pınar Çalık
Head of the Department, **Chemical Engineering** _____

Prof. Dr. Göknur Bayram
Supervisor, **Chemical Engineering, METU** _____

Examining Committee Members:

Prof. Dr. Süleyman Ali Tuncel
Chemical Engineering, Hacettepe University _____

Prof. Dr. Göknur Bayram
Chemical Engineering, METU _____

Prof. Dr. Cevdet Kaynak
Metallurgical and Materials Engineering, METU _____

Assoc. Prof. Dr. Erhan Bat
Chemical Engineering, METU _____

Asst. Prof. Dr. Cemal Merih Şengönül
Manufacturing Engineering, Atılım University _____

Date: 23.11.2020

I hereby declare that all information in this document has been obtained and presented in accordance with academic rules and ethical conduct. I also declare that, as required by these rules and conduct, I have fully cited and referenced all material and results that are not original to this work.

Name, Last name : Berrak, Erkmen

Signature :

ABSTRACT

POLYSTYRENE-BASED AND CARBON FABRIC-REINFORCED POLYMER COMPOSITES CONTAINING CARBON NANOTUBES: PREPARATION, MODIFICATION AND CHARACTERIZATION

Erkmen, Berrak
Doctor of Philosophy, Chemical Engineering
Supervisor: Prof. Dr. Göknur Bayram

November 2020, 200 pages

Carbon Fabric-Reinforced Polymers (CFRPs) attract attention due to their high mechanical properties, electrical conductivity, and providing weight reduction solutions in aerospace, automotive, marine, and energy industries. Since recycling, long processing times, non-visible damages, and complex repair procedures of thermoset-based CFRPs cause problems, studies are performed on the application of thermoplastic-based CFRPs. This study aims to produce polystyrene (PS)-based and carbon nanotubes (CNTs) and carbon fabric (CF)-reinforced multilayer composites and to improve their multifunctional properties by applying modifications to PS, CNTs, and CF.

The thesis consists of six parts. In the first part, CNTs were modified with surfactants, silane coupling agents, and a copolymer to disperse them homogeneously in the polymer matrix. The suspension stability of the modified CNTs in PS/toluene solution was investigated. Then, PS-CNTs binary composites were produced at different melt mixing conditions and characterized by optical microscope, electrical resistivity measurements, tensile and impact tests. Poly[styrene-b-(ethylene-co-butylene)-b-styrene] grafted with maleic anhydride (SEBS-g-MA) elastomer was also added to selected binary composites to improve the processability and create a

soft segment in the structure. PS-SEBS-gMA-CNTs were characterized in terms of morphology, electrical, mechanical, and shape memory properties. Results revealed that H_2SO_4-HNO_3 solution and (3-Trimethoxysilylpropyl)methacrylate (MSPM) treated CNTs were well dispersed in the polymer matrix and improved the properties of PS in the presence of elastomer.

In the second part, PS was synthesized with the bulk polymerization method at 0.01, 0.008, and 0.005 mol/L initiator concentrations. The chemical structure, melt flow index, average molecular weights, and thermal properties were used to compare the properties of synthesized PS with commercial PS. The results showed that PS was successfully synthesized with all initiator concentrations, but the properties were close to that of commercial PS at 0.005 mol/L initiator concentration. In the third part, PS-CNT masterbatches were produced with in-situ polymerization at 0.005 mol/L initiator concentration and then characterized in terms of their chemical structure and thermal properties. PS-CNT masterbatches were successfully synthesized with unmodified CNTs, and MSPM treated CNTs.

In the fourth part, to investigate the effect of composite preparation techniques on the mechanical, electrical, and shape memory properties, polymer layers of the multilayer composites were prepared using the methods of direct melt mixing and dilution of PS-CNTs masterbatches. Based on the results, the composite produced with the masterbatch dilution method containing MSPM-CNTs had 33% higher tensile strength and 34% higher tensile modulus than the sample fabricated with the direct melt mixing.

The fifth part of the thesis aimed to improve the interfacial adhesion between the layers of the multilayer composites by modifying the CFs with a silane coupling agent, a copolymer, PS-based coatings, and forming nanofibers with the electrospinning of polyamide 6. Among all the modification techniques applied to the CFs, the highest peel strength was obtained in CFRP containing MSPM modified CF as the value of 1962 N/m, which was 21% higher than as-received CF.

In the final part of the thesis, multilayer composites were fabricated with one, three, and five CF layers. A five-layered sample was also prepared with MSPM treated CFs (MSPM-CFs) to observe the surface treatment effect on the improvement of interfacial adhesion between the composite layers. The composites were characterized by morphology, mechanical, electrical, thermal, and shape memory properties. Increasing the number of CF layers from one to five, tensile strength, tensile modulus, and electrical resistivity were improved by 527%, 125%, and 70%, respectively. More homogeneous impregnation of polymeric material through the fibers was obtained in the multilayer composite fabricated with MSPM-CFs. Electrically triggered shape recovery of all the multilayer composites was achieved 100% within one minute.

Keywords: Carbon Fabric-Reinforced Polymers (CFRP), Carbon Nanotubes, Surface Treatment, In-situ Polymerization, Shape Memory Properties.

ÖZ

POLİSTİREN BAZLI VE KARBON KUMAŞ İLE GÜÇLENDİRİLMİŞ KARBON NANOTÜP İÇEREN POLİMER KOMPOZİTLERİ: HAZIRLANMASI, MODİFİKASYONU VE KARAKTERİZASYONU

Erkmen, Berrak
Doktora, Kimya Mühendisliği
Tez Yöneticisi: Prof. Dr. Göknur Bayram

Kasım 2020, 200 sayfa

Karbon Kumaş ile Güçlendirilmiş Polimerler (CFRP'ler), yüksek mekanik özellikleri, elektriksel iletkenliği ve havacılık, otomotiv, denizcilik ve enerji sektörlerinde ağırlık azaltma çözümleri sunması nedeniyle dikkat çekmektedir. Termoset-bazlı CFRP'lerin geri dönüşümü, uzun işleme süreleri, gözle görülmeyen hasarları ve karmaşık onarım prosedürleri sorunlara yol açtığı için termoplastik bazlı CFRP'lerin uygulanması konusunda çalışmalar yapılmaktadır. Bu çalışma, polistiren (PS) bazlı ve karbon nanotüpler (CNT'ler) ve karbon kumaş (CF) ile güçlendirilmiş çok katmanlı kompozitler üretmeyi, ve PS'e, CNT'lere ve CF'e modifikasyonlar uygulayarak onların çoklu fonksiyonel özelliklerini geliştirmeyi amaçlamaktadır.

Tez altı bölümden oluşmaktadır. İlk bölümde, CNT'ler yüzey aktif maddeler, silan bağlama ajanları ve bir kopolimer ile modifiye edilerek polimer matriks içinde homojen olarak dağıtılmıştır. Modifiye edilmiş CNT'lerin PS/toluen çözeltisinde süspansiyon stabilitesi araştırılmıştır. Daha sonra, PS-CNT'lerin ikili kompozitleri farklı eriyik karıştırma koşullarında üretilmiş ve optik mikroskop, elektriksel direnç ölçümleri, çekme ve darbe testleri ile karakterize edilmiştir. Ayrıca, maleik anhidrit ile aşılanmış poli[stiren-b-(etilen-ko-butilen)-b-stiren] (SEBS-g-MA) elastomeri,

işlenebilirliği geliştirmek ve yapıda yumuşak bir segment oluşturmak için seçilen ikili kompozitlere eklenmiştir. PS-SEBS-gMA-CNT'ler morfoloji, elektriksel, mekanik ve şekil hafıza özellikleri açısından karakterize edilmiştir. Sonuçlar, H_2SO_4-HNO_3 solüsyonu ve (3-Trimetoksisililpropil) metakrilat (MSPM) ile muamele edilmiş CNT'lerin polimer matriks içinde iyi dağıldığını ve elastomer varlığında PS'in özelliklerini geliştirdiğini ortaya çıkarmıştır.

İkinci bölümde, PS 0,01, 0,008 ve 0,005 mol/L başlatıcı konsantrasyonlarında yığın polimerizasyonu yöntemi ile sentezlenmiştir. Sentezlenen PS'nin özelliklerini ticari PS ile karşılaştırmak için kimyasal yapı, eriyik akış indeksi, ortalama moleküler ağırlıklar ve termal özellikler kullanılmıştır. Sonuçlar, PS'nin tüm başlatıcı konsantrasyonları ile başarılı bir şekilde sentezlendiğini, ancak özelliklerin 0,005 mol/L başlatıcı konsantrasyonunda ticari PS'ninkine yakın olduğunu göstermiştir. Üçüncü bölümde, PS-CNT derişik karışımları 0,005 mol/L başlatıcı konsantrasyonunda yerinde polimerizasyon ile üretilmiş, ve sonra kimyasal yapıları ve termal özellikleri açısından karakterize edilmiştir. PS-CNT derişik karışımları, modifiye edilmemiş CNT'ler ve MSPM ile işleme tabi tutulmuş CNT'ler ile başarıyla sentezlenmiştir.

Dördüncü bölümde, kompozit hazırlama tekniklerinin mekanik, elektriksel ve şekil hafıza özelliklerine etkisini araştırmak için, çok katmanlı kompozitlerin polimer katmanları, doğrudan eriyik karıştırma ve PS-CNT derişik karışımlarının seyreltilmesi metotları ile hazırlanmıştır. Sonuçlara göre, MSPM-CNT'leri içeren derişik karışımların seyreltilmesi metodu ile üretilen kompozit, doğrudan eriyik karıştırma ile üretilen numuneye göre %33 daha yüksek gerilme mukavemetine ve %34 daha yüksek elastik modülüne sahip olmuştur.

Tezin beşinci bölümü, çok katmanlı kompozitlerin katmanları arasındaki arayüzey yapışmasını, CF'leri bir silan bağlama ajanı, bir kopolimer, PS bazlı kaplamalar ile modifiye ederek ve elektroeğirme ile poliamid 6 nanofiberler oluşturarak geliştirmeyi amaçlamıştır. Tüm modifikasyonlar arasında CF'lere uygulanan

tekniklerde, en yüksek sıyrılma mukavemeti, alınan CF'den %21 daha yüksek bir değerde 1962 N/m olarak MSPM modifiye edilmiş CF içeren CFRP'de elde edilmiştir.

Tezin son bölümünde, çok katmanlı kompozitler bir, üç ve beş kat CF ile üretilmiştir. Kompozit katmanları arasındaki arayüzey yapışmasının iyileştirilmesi üzerinde yüzey işlemi etkisini gözlemlemek için MSPM ile muamele edilmiş CF'ler (MSPM-CF'ler) ile beş katmanlı bir numune ayrıca hazırlanmıştır. Kompozitler morfoloji, mekanik, elektriksel, termal ve şekil hafıza özellikleriyle karakterize edilmiştir. CF katmanlarının sayısının birden beşe çıkarılması, gerilme mukavemetini, elastik modülü ve elektriksel özdirenci sırasıyla %527, %125 ve %70 artırmıştır. MSPM-CF'ler ile üretilen çok katmanlı kompozitte polimerik malzemenin fiberler boyunca daha homojen emdirilmesi sağlanmıştır. Tüm çok katmanlı kompozitlerin elektrikle tetiklenen şekil geri kazanımı bir dakika içinde %100 olarak elde edilmiştir.

Anahtar Kelimeler: Karbon Kumaş ile Güçlendirilmiş Polimerler (CFRP), Karbon Nanotüpler, Yüzey İşlemleri, Yerinde Polimerizasyon, Şekil Hafıza Özellikleri.

To my precious family…

ACKNOWLEDGMENTS

I would wish to express my deepest gratitude to my supervisor Prof. Dr. Göknur Bayram, for her guidance, advice, criticism, encouragement, and insight throughout the research. I would also thank her for her support and for sharing her experiences while shaping my future career. I will always feel lucky that I had a chance to study with her. I want to thank Prof. Dr. Cevdet Kaynak and Assoc. Prof. Dr. Erhan Bat, for their valuable suggestions and comments.

This work is funded by METU Scientific Research Projects Coordination under grant number BAP-03-04-2016-004 and DKT-304-2018-3730.

I would like to express my gratitude to Selin Şahin, Refik Barış Yılmaz, and Deniz Okan Bayraktar for their friendship and help. I would also thank my friends Merve Demirel and Almira Çaldıklıoğlu from our research group, and Öznur Doğan for her support during this study.

I would sincerely thank Özge Batır, Özge Şen, Cihan Ateş, Ceren Ateş, Dilara Gülçin Çağlayan, Berna Öztok, Deniz Kaya, Beril Tabak, and Sibel Öztürk for their unlimited support, precious friendship and creating an enjoyable environment during this journey. I want to express my most profound appreciation to Hande Özkablan and Günay Atak. No matter how far we are, our friendship will always continue.

I would thank my manager in SOCAR Turkey, Dr. Ayhan Ezdeşir, for his tolerance and support. I want to acknowledge my lovely co-workers, Bige Batı, Seda Hayta Tuğçe Oturakkaya, Dr. Alp Alparslan, Ali Küçük, for their endless support and kind friendship.

Finally, I would thank my beloved mother, Berrin Erkmen, and my precious sister Buket Ünsal for their endless love, patience, and unlimited support, a must for me to complete this study with success. Of course, my family, my success wouldn′t have been possible without their encouragement and love.

TABLE OF CONTENTS

LIST OF TABLES

TABLES

LIST OF FIGURES

FIGURES

LIST OF ABBREVIATIONS

ABBREVIATIONS

AIBN	Azobisisobutyronitrile
APTES	(3-Aminopropyl)triethoxysilane
ATR	Attenuated Total Reflection
CF	Carbon Fabric
CFRP	Carbon Fabric-Reinforced Polymer
CNT	Carbon Nanotubes
DSC	Differential Scanning Calorimetry
EAP	Electroactive Polymers
EDX	Energy-dispersive X-ray spectroscopy
EVA	Ethylene-vinyl acetate
FTIR	Fourier Transformed Infrared Spectroscopy
GLYMO	(3-Glycidyloxypropyl)trimethoxysilane
GPC	Gel Permeation Chromatography
HNT	Halloysite Nanotubes
LBD	Light Blue Daylight
MFI	Melt Flow Index
MSPM	(3-Trimethoxysilylpropyl)methacrylate
PA6	Polyamide 6
PS	Polystyrene

PSMA	Poly (styrene-co-maleic anhdyride), cumene terminated
PTFE	Polytetrafluoroethylene
PUD	Polyurethane Dispersion
RTM	Resin Transfer Molding
SDBS	Sodium Dodecyl Benzene Sulphonate
SDS	Sodium Dodecyl Sulfate
SEBS-gMA	Poly[styrene-b-(ethylene-co-butylene)-b-styrene] grafted with maleic anhydride
SEC	Size Exclusion Chromatography
SEM	Scanning Electron Microscopy
SMA	Shape Memory Alloys
SMC	Shape Memory Ceramics
SMP	Shape Memory Polymers
SMPC	Shape Memory Polymer Composites
sPS	Synthesized PS with bulk polymerization
SPU	Segmented Polyurethane
TGA	Thermogravimetric Analyzer
TX100	Polyethylene glycol tert-octylphenyl ether (Triton X-100)
VARTM	Vacuum Assisted Resin Transfer Molding

LIST OF SYMBOLS

SYMBOLS

a	Empirical constant of Mark-Houwink-Sakurada equation
A_0	Initial cross sectional area of tensile specimen, mm^2
D	Diameter of CF fibers, µm
E	Modulus of elasticity, MPa
F	Tensile load, N
K	Empirical constant of Mark-Houwink-Sakurada equation
k′	Constant of Huggins' equation
k″	Constant of Kraemer's equation
l	Distance between the crocodile probes, mm
L_i	Gauge length of tensile specimen, mm
L_0	Initial length of the gauge portion, mm
ΔL	Change in gauge length, mm
M_n	Number average molecular weight, g/mol
M_v	Viscosity average molecular weight, g/mol
M_w	Weight average molecular weight, g/mol
M_z	Z-average molecular weight, g/mol
PDI	Polydispersity index
R	Electrical resistance, ohm
S	Cross sectional area which is perpendicular to the current flow, mm^2

T_g	Glass transition temperature, °C
T_m	Melting temperature, °C
T_{trans}	Transition temperature, °C
W_a	Work of adhesion, mJ/m^2

GREEK LETTERS

ρ	Volumetric electrical resistivity, ohm.cm
σ	Engineering stress, MPa
ε	Engineering strain, mm/mm
θ_i	Initial angle, °
θ_f	Final angle, °
η	Intrinsic viscosity, dl/g
η_{red}	Reduced viscosity, dl/g
η_{inh}	Inherent viscosity, dl/g
η_r	Relative viscosity, dl/g
η_{sp}	Specific viscosity, dl/g
θ	Average contact angle for the test liquid on the test specimen, °
γ_l	Surface tension of the test liquid, mJ/m^2
γ_l^d and γ_s^d	Dispersion component of surface tension of the test liquid and solid, respectively, mJ/m^2
γ_l^p and γ_s^p	Polar component of surface tension of the test liquid and solid, respectively, mJ/m^2

CHAPTER 1

INTRODUCTION

High-performance composites reinforced with fibers take the place of structural materials produced with metal and metal-like materials due to their ability to ensure lightweight and high strength (Koumoulos et al., 2019). Carbon Fabric-Reinforced Polymers (CFRPs) have been investigated over the past half century, and their superior properties make them widely used in the applications of aerospace, automotive, marine, sporting goods, civil infrastructures, and energy industries (Díez-pascual et al., 2014). Airbus designed an aircraft namely 'A350 XWB' which was built with over 70% advanced materials and 53% of these materials were carbon composites ("A350 XWB," 2019). 'Boeing 787' contains a significant amount of composite material in the airframe compared to other commercial aircraft. According to their design, nearly half of the airframe is composed of CFRPs and other composites ("Boeing 787 from the Ground Up," 2019).

Commonly in literature, thermoset polymers were used as the matrix in CFRPs (Chung, 2017). Nowadays, there is an increasing tendency for using thermoplastic polymers instead of thermosets due to the environmental concerns and recycling problems aroused by thermosets. The CFRPs fabricated with thermoset matrices cannot be processed again after use, and they are landfilled; thus environmental pollution is inevitable (B. Liu et al., 2017). The main problems that occurred in thermoset resins are high costs of raw materials, high energy consumption, long processing times, non-visible damages, and complex repair procedures (Pelin et al., 2016). The main advantages of thermoplastics over thermosets are their flexibility, high impact resistance, toughness, easiness of fabrication, short molding cycle,

damage tolerance, excellent chemical and corrosion resistance, and thermal stability (Shonaike, 2000).

In CFRPs; interfacial adhesion is an important parameter that affects the properties of the composites. Due to the inert surface of the fabrics, weak adhesion and poor interfacial bonding between the polymer layers and the fabric are observed. Surface treatment is a common method to overcome the weak interaction between the layers of the composite structure. Surface treatment methods, which are mainly applied, are acid oxidation, plasma treatment, gamma irradiation, rare earth treatment, silane coupling agent treatments, and polymer coating applications (S Tiwari & Bijwe, 2014). Thermoplastic polymer matrix-based CFRPs are usually produced higher than 60% fiber volume fraction to reach comparable properties with thermoset-based CFRPs (B. Liu et al., 2017). In the present study, multilayer composites were prepared with different fiber fractions and characterized in terms of morphologies, mechanical, electrical, and shape memory properties.

The mechanical behavior of CFRPs are widely investigated over decades, and the investigations of the functionality of these kinds of composites are relatively new due to the interest in multifunctional structural materials and smart structures (Chung, 2017). Shape memory polymers (SMPs) are a type of stimuli responsive materials that can recover their original shape from a temporary shape upon exposure to external stimuli such as heat (B. Xu et al., 2010), electricity (Pelin et al., 2016; Shonaike, 2000), magnetic fields (Mu et al., 2018), light (Lendlein et al., 2005) and pH (Han et al., 2012). Thermal responsive shape memory polymers are extensively investigated in recent years; however they did not show their full potential due to the demand for external heaters for actuation. Thereby, the application and significance of electroactive polymers (EAPs) are rising nowadays (Y. Liu et al., 2009). Polymer-based functional materials are mostly electrical insulators, and it is essential to form a conductive pathway by incorporating conductive fillers. Formation of the conductive pathway of the fillers in polymer matrix is a challenging issue due to the intermolecular interactions between the nanosized conductive fillers which make them prefer each other to form agglomerates (Mu et al., 2018; Tiwari et al., 2014).

CNTs were used in this study as conductive fillers. There are different approaches to provide a uniform distribution of CNTs in the polymer matrix, such as blending with high power dispersion techniques, in-situ polymerization, and chemical functionalization (X. L. Xie et al., 2005).

Pretreatments must be applied before adding the nanosized fillers into the matrix (Lu et al., 2010). Mainly, there are two methods used for surface modification of CNTs: covalent and non-covalent techniques (S. W. Kim et al., 2011). Covalent surface modification is based on the chemical functionalization with the covalent bond formation on the CNTs surface. In the non-covalent surface modification methods, low molecular weight polymer chains are wrapped around the nanotubes or surfactant molecules are adsorbed on the surface of nanotubes with physical bonding (Mittal, 2011).

Another approach to provide well-dispersed nanofillers was the application of different nanocomposite preparation techniques such as solution mixing, melt mixing, and in-situ polymerization method (Kaseem et al., 2016). In the in-situ polymerization method, nanofillers are added to pre-polymer during the polymerization process, and homogeneous dispersion of nanofillers and a strong interface between filler and polymer matrix are achieved simultaneously (Annala et al., 2012; Yoo et al., 2006). This preparation technique leads to nanocomposites that have better mechanical properties, thermal stability, and electrical conductivity.

Polystyrene (PS), the matrix material used in this study, is widely preferred for commodity products. In our study, the SMP blend was prepared using PS due to the recyclability and inexpensiveness considerations as an alternative to thermoset PS-based SMP and shape memory precursor mixture containing PS (Ahmad et al., 2011). For modification of PS, a compatible elastomer (SEBS-gMA) was added to form soft segments of the designed electrically and thermally controllable polymer blend. No studies exist on the preparation and characterization of PS-based and CF-reinforced multilayer composites with electroactive shape memory property to the best of our knowledge. This thesis study may be of interest for potential usage of

thermoplastic-based CF-reinforced multilayer composites in different application areas where improved mechanical properties, electrical conductivity, and shape memory properties are required.

In this thesis study, PS-SEBS-gMA-based multilayer polymer composites, consisting of nano-sized conductive filler, continuous CF, and polymer matrix were prepared using the compression molding technique. Polymer blend was reinforced with as-received and modified CNTs, and fabricated with two different methods, masterbatch dilution and melt mixing. The effect of polymer nanocomposite preparation technique on the mechanical properties, electrical resistivity and shape memory behavior of multilayer composites was investigated. Surface modifications were applied to CF in order to improve the adhesion between polymeric layers and CF plies. To confirm the existence of modification between the layers, FTIR analysis was conducted and multilayer composites were characterized, in terms of their adhesion strength, work of adhesion (W_a) values and morphology. By increasing the number of CF layers, improvement of the mechanical, electrical and shape memory properties of the multilayer composites was further aimed. Also, the effect of silane treatment applied to the CF surface was investigated on the properties of the multilayer composite that had the highest carbon fabric amount. CF content, morphology, mechanical properties, electrical conductivity, and electrically stimulated shape memory properties of multilayer composite samples were characterized by ash content and TGA analyses, SEM, mechanical tests, two-point probe method, and bending test, respectively. Thus, the multilayer composites produced in this thesis study may have an excellent potential to be considered as multifunctional engineering materials, which may be of interest to the aerospace and automotive industries.

CHAPTER 2

BACKGROUND

2.1 High Performance Carbon Fabric-Reinforced Polymers

Fiber-reinforced polymers are a class of composite materials that own superior strength to weight and modulus to weight ratios comparable with metallic materials (Njuguna et al., 2012). Carbon Fabric-Reinforced Polymers (CFRPs) with woven carbon fibers are produced to satisfy the needs of light-weight, high mechanical properties, chemical, and environmental resistance.

CFRPs are widely used in aerospace, automotive, marine, and energy industries and also in the production of sporting goods and civil infrastructures (Díez-pascual et al., 2014). With the development of technology, new demands are emerging from the industry to use these composites in place of traditional materials. Crash absorbing structures in the automotive industry, gas diffusion parts for fuel cells, high-pressure composite hydrogen tanks composed of adsorptive fibers, energy storage systems, fabric-reinforced carbon concrete applications in turbine rotor blades are the examples of applications of CFRPs in areas that require high performance. Cell-compatible fibers to replace nerve tracts in paraplegia and prosthetics with suitable properties to prevent stress shielding are the new applications of these composites in medicine (Koumoulos et al., 2019).

Commonly in industrial applications, thermoset resins are used as polymer matrix and epoxy is the most preferred thermoset resin in the production of CFRPs. Epoxy-based fiber-reinforced polymer composites are prepared with hand lay-up, filament winding, resin transfer molding, liquid resin infusion, and pultrusion techniques (Mahrholz et al., 2003; Rajak et al., 2019). Despite the fact that thermoset matrices

are preferred in the industry, there is an increasing tendency for using thermoplastic matrices due to the lack of curing step during processing, less hazardous chemical compositions, recycling and mass production opportunities (Yao et al., 2018).

Carbon fabric-reinforced thermoplastic polymer composites are fabricated with melt impregnation, but poor adhesion is observed in these methods when highly viscous thermoplastics are used as matrices. The main approach in the literature to decrease the viscosity of the thermoplastic matrix and improve the impregnation by first dissolving the polymer matrix in a suitable solvent and then molding with hot-pressing.

2.2 Modification of Composite Constituents

2.2.1 Modification of Polymer Matrix

Fiber-reinforced polymer composites are usually composed of layers of fabrics wetted with the polymer matrix. Interlaminar regions between these layers are matrix rich areas and in these areas weak points that cause failure or delamination are formed. The reasons for interlaminar failure are the production process, impact damage, and structural defects. When interlaminar failure occurs between the layers of the composite, the load carrying ability of the composite decreases. To maintain the high-performance of the composites, it is essential to prevent failure by applying modifications to the polymer matrix to improve the mechanical properties in weak areas (Boon & Joshi, 2020).

High impact strength is one of the significant property which is expected from CFRPs. The impact strength of the CFRPs is controlled by the polymer matrix. If the polymer matrix is brittle, it shows low resistance to crack initiation and growth (Misumi & Oyama, 2018). Fracture toughness can be increased with blending soft rubbers with epoxy matrix in epoxy-based CFRPs. Core-shell type rubber particles including butadiene/styrene core and a methyl methacrylate shell (F. Xu et al., 2016),

nanocarboxylic acrylonitrile butadiene rubber (Ozdemir et al., 2016) and acrylic block copolymers (Choi et al., 2017) are examples of these type additives.

Other techniques to enhance the interlaminar fracture toughness are the usage of nanosilica particles, carbonaceous nanoparticles such as graphene nanoplatelets, graphene oxide, carbon nanotubes and halloysite nanotubes (Ayatollahi, Barbaz Isfahani, & Moghimi Monfared, 2017; Ye, Chen, Wu, & Chan, 2011). Multilayer composites consisting of nanofillers and micro-sized fibers show synergistic effect of these fillers and give the multifunctionality to multilayer composites besides improving the mechanical properties.

2.2.2 Surface Modification of CNTs

CNTs were discovered in 1991 by Iijima while he was analyzing products of arc discharge experiments (Iijima, 1991). There has been extensive research on CNTs owing to their superior mechanical, thermal, magnetic and electrical properties. Besides these outstanding properties, there are some drawbacks restrict the usage of CNTs as conductive fillers. CNTs are chemically inert due to the low amount of defects sites and functional chemical groups on their surfaces and the perfect order of hexagon rings without any dangling bonds (Jeon, et al., 2012; Lin et al., 2003; Yesil, 2010). Dispersion of CNTs into polymer matrix is a challenging issue due to the intermolecular interactions between CNTs, making them agglomerate in composites.

Electrical and structural properties are reduced by the metal catalyst, catalyst support residues, and carbon-based particle traces during the production process present in the tubes. To overcome these difficulties; surface functionalization and modification are essential procedures for the production of polymer-CNTs nanocomposites.

Surface modification of CNTs is divided into two groups: covalent and non-covalent techniques. Possible functionalization mechanisms are given in Figure 2.1. Suitable

treatment techniques for dispersing CNTs homogeneously in different polymer matrices are listed in Table 2.1.

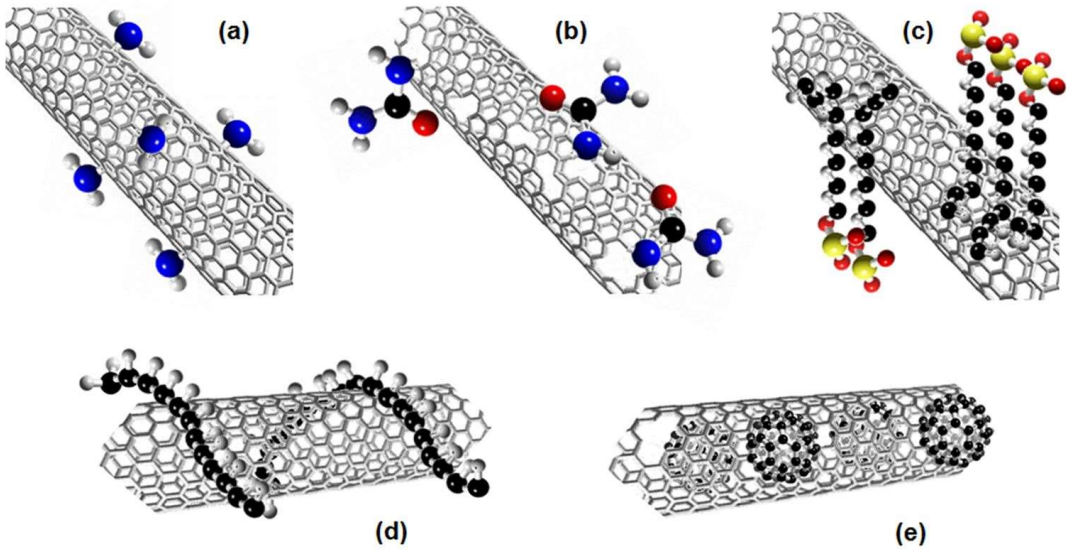

Figure 2.1. Surface modification methods of CNTs (a) covalent sidewall functionalization, (b) covalent defect sidewall functionalization, (c) non-covalent adsorption of surfactants, (d) polymer wrapping, (e) endohedral functionalization with C60 (Ávila-Orta et al., 2013).

Table 2.1 Suggestions for functional groups that can interact better with selected polymer matrices (Avilés et al., 2018).

Surface Treatment Techniques	Polymer Matrices
Fluorination	Epoxy resin
Fluorination and alkylation	Olefins
Thiolation	Unsaturated rubber matrices
Hydroxylation and silanization	Vinyl ester resin
Hydroxylation, silanization and amination	Epoxy resin
Amination	Natural rubber and SPU
Carboxylation	EVA and SPU
Carboxylation and amide formation	Nylon
Carboxylation and amine formation	Epoxy resin, PP-gMA or PET
Carboxylation, amine formation and vinylization	Acrylics and Olefin resin
Acylation and ester formation	Polyester resin

Covalent surface modification is based on chemical functionalization with covalent bond formation on the CNTs surface. Functionalization with this method depends on change of hybridization from sp^2 to sp^3 and a simultaneous loss of p-conjugation system on graphene layer (Jeon et al., 2011).

Besides producing oxidative groups and defect sites on the CNTs sidewalls, there are disadvantages of covalent surface modification techniques. Large number of defects are produced with severe process conditions such as high concentration of strong oxidizers and damaging ultrasonication process, leading to fragmentation of CNTs and reduced conductivity and mechanical properties. Damages formed after oxidative treatments are shown in Figure 2.2. These damages lead to a change in the hybridization of CNTs from sp^2 to sp^3 and deterioration of the π electron system in CNTs. Also, the chemicals used for functionalization are harmful for the environment (Jeon et al., 2011).

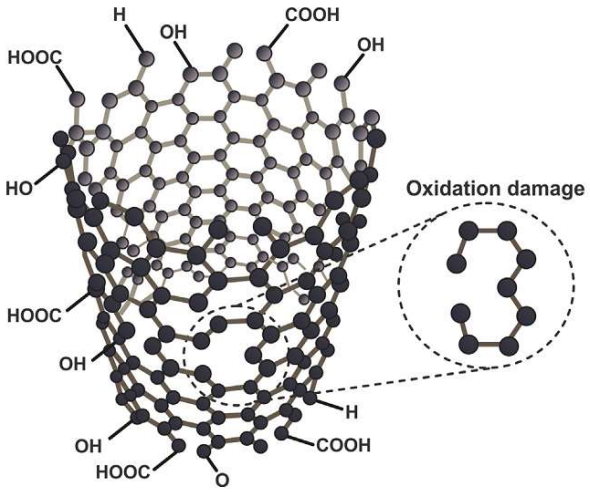

Figure 2.2. Schematic representation of oxidative functional groups and structural damages formed after oxidation treatment (adopted from Avilés et al., 2018 with permission).

In non-covalent surface modification methods, low molecular weight polymer chains are wrapped around the nanotubes or surfactant molecules are adsorbed on the surface of nanotubes with physical bonding (Mittal, 2011). Physical properties are not affected with non-covalent functionalization, and also solubility and processability are improved. This method includes the addition of aromatic molecules, conjugated polymers, surfactants, biomacromolecules onto the CNTs sidewalls activated with -OH, -COOH, -C=O functional groups with covalent modification (Jeon et al., 2011).

Surfactants decrease the surface tension of the CNTs, hinder the formation of agglomerations and enhance the wettability of CNTs by polymer with the aid of functional groups or miscible parts on their long tallow (Yesil, 2010). CNTs treated with surfactant molecules defeat the van der Waals forces by electrostatic/steric repulsive forces. A representative scheme of possible adsorption mechanisms of widely used surfactants onto CNT surface is given in Figure 2.3.

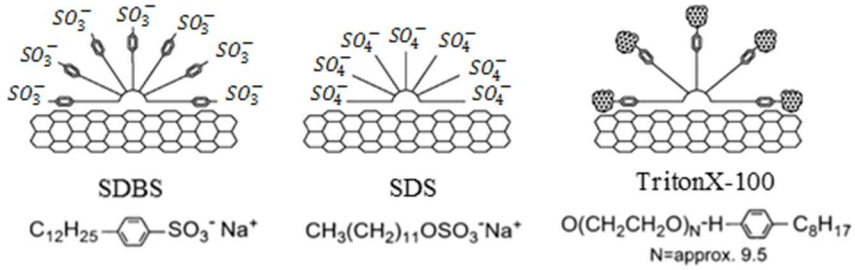

Figure 2.3. Schematic view of sodium dodecyl benzene sulphonate (SDBS), sodium dodecyl sulfate (SDS) and polyethylene glycol tert-octylphenyl ether (Triton X-100) adsorption onto CNT surface, respectively (Islam et al., 2003).

2.2.3 Surface Modification of CFs

Failure mechanisms of fiber-reinforced polymer composites are fiber breaking, fiber bridging, fiber pullout, matrix cracking, interface debonding, and delamination. A schematic view of these mechanisms is shown in Figure 2.4. However, the order and relation of failure modes are subjected to the type of loading, the properties of composite parts and the interfacial shear strength (Iftekhar, 2004).

Delamination is a failure mechanism resulting from weak fiber-matrix interfacial bonding, brittleness of the polymer matrix and growth of the cracks formed between the plies of multilayer composites and causes reduction in stiffness and strength (Díez-pascual et al., 2014). Continuous fabric structure provides extraordinary in-plane properties to CFRPs; however, out-of-plane properties are poor, which are dominated by the polymer matrix. Resin-rich regions are formed between the layers, and fibers are not aligned in the out-of-plane direction (Bekyarova et al., 2007; H. Xu et al., 2016). In these regions, crack initiation and propagation start quickly under compression, bending, and impact loading. Processing conditions such as molding temperature, pressure and pressure application time are also important for achieving adhesion without delamination and avoiding void formation in CFRPs. Mechanical properties depend on the void content of the composites. The higher the void content,

the lower tensile strengths of composites due to the poor adhesion between polymeric and fabric layers (Shonaike, 2000).

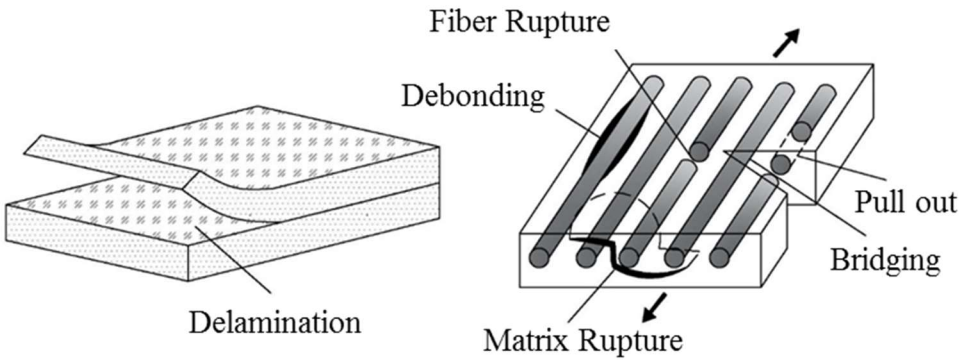

Figure 2.4. Failure mechanisms of laminated composites (Noels, 2018).

To improve the insufficient interlaminar properties and overcome the weak interaction between the two layers of the composites, modification techniques are developed. Toughening the matrix resin with elastomers, interleaving the interlaminar regions with tough polymers, short fibers, metal layers and polymeric nanofibers, applying through-thickness reinforcing (3D textiles, stitching, z-pinning and braiding), adding micro or nanoscale fillers and treating the fiber surface with silane coupling agents for strengthening the interface are widely applied (Daelemans et al., 2018; J. W. Kim et al., 2016; Ma et al., 2017; Palazzetti et al., 2017; H. Xu et al., 2016).

Small active specific surface area due to the smooth surfaces of the fibers, low surface energy, lipophobic surface properties, non-polar characteristics and chemical inertness of fabrics lead to weak interfacial adhesion thus poor stress transfer from matrix to the fibers occurs (Semitekolos et al., 2018).

To acquire a strong and homogeneous interfacial adhesion in CFRPs, mainly applied surface treatment methods are acid oxidation (Su et al., 2005), plasma treatment (Tiwari et al., 2011), rare earth treatment (Tiwari et al., 2014) gamma irradiation (Tiwari et al., 2011), and silane coupling agent treatment (Latif et al., 2019). Other treatment methods are laser treatment (Xie et al., 2020), chemical grafting, polymer

coating, polyurethane dispersion (PUD) sizing (Yang et al., 2018; D. Zhao et al., 2019), stitching (Bilisik et al., 2020), interleaving polymeric nanofibers in interlaminar regions (Daelemans et al., 2015) and synthesizing carbonaceous structures on CFs (An et al., 2012; Wang et al., 2019).

2.2.3.1 Silane Coupling Agent Treatment

Silane coupling agents are able to create bonds between organic and inorganic materials. The general formula of silane coupling agents is $R\text{-}(CH_2)_n\text{-}Si\text{-}X_3$. 'R' is the orgonofunctional group which is a non-hydrolyzable radical group and responsible for providing the desired functionality. 'X' is the hydrolyzable group consisting of alkoxy, acyloxy, halogen, or amine (Arkles, 2014).

Reaction steps between the silane coupling agent and a substrate are given in Figure 2.5. The first step is the hydrolysis of the three unstable groups. In the second step, condensation occurs, and oligomers are formed. These oligomers bond with the OH groups of the substrate by creating hydrogen bonds. Finally, covalent bond formation between silanol groups and the substrate is completed after water loss during drying or curing.

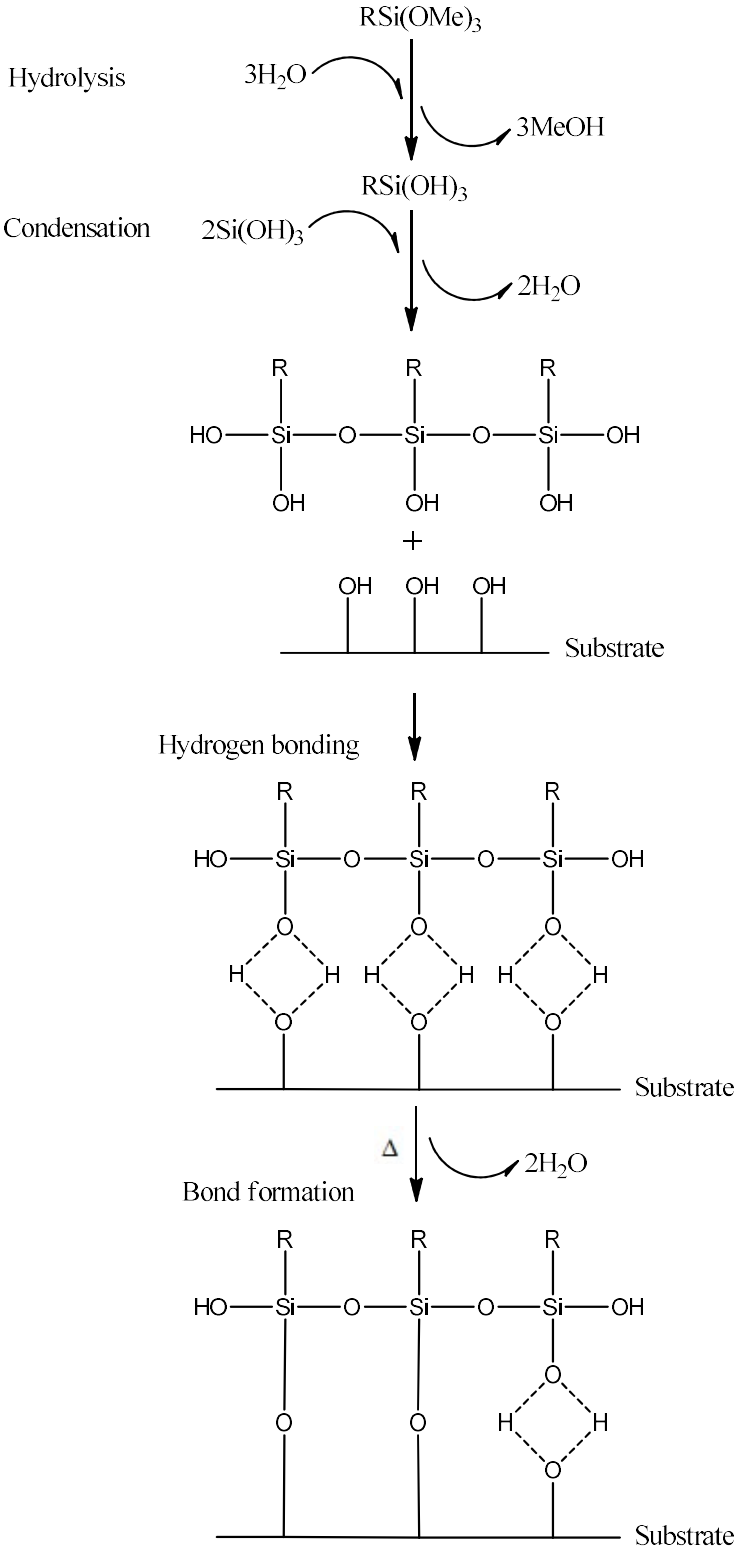

Figure 2.5. Reaction steps of hydrolytic deposition of silanes (Arkles, 2014).

2.3 Processing Techniques of Composites

2.3.1 Processing Techniques of PS-CNT Nanocomposites

Three main methods are generally used for preparing PS-CNT composites: solution mixing, melt mixing and in-situ polymerization.

In the solution mixing method, CNTs are dispersed in a solvent, polymer is added to the solution medium and after a certain time of mixing polymer films are formed by casting or precipitation. Toluene and dimethylformamide (DMF) are used generally as a solvent medium. The viscosity of the polymer solution should be low in order to achieve better dispersion of nanoparticles with agitation using the mechanical stirrer or ultrasonication techniques (M. Bhattacharya, 2016). There are some disadvantages of this method to prepare composites such as evaporating huge amount of solvent, not appropriate for mass production and vigorous ultrasonication applied to CNTs to achieve good dispersion cause damages on CNTs and result in low structural properties.

Melt mixing is the preparation technique, which is the most economical and environmentally friendly compared to other techniques. High temperature and high shear forces are applied and this method causes chemical or physical interactions between inorganic fillers and polymer matrix. Fillers and polymer matrix are blended with a single or a twin screw by co-rotating or counter rotating extruders. The mixing yields shear and elongational stress which lead to breakage of the agglomerates and dispersion of the nanofillers (M. Bhattacharya, 2016).

Processing conditions are essential factors that affect the performance of the mixing. Feeding from the hopper or a side feeder (Müller, Krause, Kretzschmar, & Pötschke, 2011), screw speed (McClory, Po, & Mcnally, 2011), temperature, screw design and residence time (M. Bhattacharya, 2016) are the main parameters. Higher screw speeds increase the shear forces and lead to the breakup of agglomerates. Lower screw speeds impart lower cutting and kneading forces and favor erosion processes.

Lowering the screw speed increases the residence time of the material inside the extruder, enhancing dispersion due to better infiltration of primary nanotube agglomerates, but for which consideration must be made for thermal degradation effects of the polymer matrix (McClory et al., 2011). Optimization of extrusion conditions should be done for better dispersion, electrical and mechanical results.

With the in-situ polymerization method, homogeneous dispersion of nanofillers and a strong interface between filler and polymer matrix can be achieved simultaneously (Annala et al., 2012). This leads to nanocomposites that have high mechanical properties, high thermal stability and high electrical conductivity. In this method, nanofillers are dispersed in the monomer and then polymerization starts with increasing the temperature and addition of chemicals such as initiators. At the end, CNTs grafted with polymer on the walls and polymer-CNTs composites that are not easy to produce with other techniques due to the thermal instability and insolubility in common solvents of the polymer are acquired (M. Bhattacharya, 2016).

2.3.2 Processing Techniques of Multilayer Composites

Fiber-reinforced polymer composites are fabricated by several processing techniques, which include lay-up, molding, winding, pultrusion and laminating composites starting from prepregs. Prepregs are the fibers that are combined with uncured resin or pre-impregnated with a thermoplastic matrix. These materials are ready to use and composites are formed by only applying heat.

In the lay-up process; plies of fabrics are placed in a mold and polymer resin is poured or applied with a brush or a machine. Resin is impregnated into the fabrics using rollers or introducing high pressure or vacuum to provide effective interaction between the reinforcement and the polymer matrix (Das, Ghosh, & Das, 2019).

Resin transfer molding (RTM) is the most common technique to produce epoxy-based CFRPs. In this technique, first fabric prepregs are placed into a mold cavity and then mold is closed. The resin is pumped into the mold until it is filled. After

filling, curing of the resin is started and when curing is completed, composite structure is cooled and product is ejected (Das et al., 2019). Vacuum infusion or vacuum assisted resin transfer molding (VARTM) technique is a similar approach with RTM, but there is a perforated tube that is placed between the vacuum bag and a resin container. The application of vacuum leads to the resin impregnated through the tube over the fabric to strengthen the composite (Rajak et al., 2019).

In the compression molding method, there is a hydraulic or mechanic hot-press and molds are placed between the trays of the press. Prepregs are put into the molds and the product with the desired shape is fabricated between the trays of the hot press at a specific temperature, molding time and pressure application. This method provides short cycle time, high production rate and dimensional stability (Rajak et al., 2019).

In the pultrusion process, continuous fibers are pulled through a resin bath. After fibers coated with resin, they are combined in a heated die. Filament winding is a very similar technique with pultrusion, but this process is an automated technique. Fibers are collected over a rotating mandrel after coating with resin in a resin bath and, when the desired shape is achieved, the product is cured at room temperature (Rajak et al., 2019).

2.4 Characterization of Blends and Composites

2.4.1 Mechanical Tests

Mechanical characterization of the composites is essential in order to define the performance of the materials and design new products. Knowing the behavior of materials under different load types is necessary to understand whether this material has sufficient properties for use in any applications. Tensile, shear, flexure, compression, torsion, fatigue, impact, tear resistance, hardness and abrasion resistance tests are mechanical characterizations applied to polymers. In this study, tensile, impact and t-peel tests were applied as mechanical characterizations.

The most informative mechanical characterization technique is the tensile test. The test is conducted by measuring the force continuously occurred during the elongation of the sample at a constant rate of extension. The stress-strain curve is plotted after the test and tensile strength, tensile modulus, yield strength and elongation at break values are defined from this plot. In universal testing machine, standard tensile test specimens are clamped between grips, one of which is attached to a moving crosshead and the other one is fixed. When the test is started, the applied load is recorded until the breakage of the specimen. In the end, time, force and stroke values are reported.

In order to calculate the tensile properties; engineering stress and strain should be calculated. Engineering stress is calculated as given in Equation 2.1 where F is the force and A_0 is the cross-section area before the force applied.

$$\sigma = \frac{F}{A_0} \tag{2.1}$$

Engineering strain is calculated as given in Equation 2.2 where L_i is the length of the specimen after test and L_0 is the original length of the specimen.

$$\varepsilon = \frac{L_i - L_0}{L_0} = \frac{\Delta L}{L_0} \tag{2.2}$$

Tensile strength (σ, MPa); is the maximum stress that the specimen can resist without breakage and this value is the ratio of the maximum load to initial cross-section area. Tensile modulus (E, MPa) is determined from the slope of the linear part of the stress-strain plot. Elongation at break (%) is the ratio of the length of the specimen after test to the original length of the specimen (Brostow, 2007).

Impact test provides information about the brittleness and toughness of the materials. The absorbed energy by the specimen during failure, which is also defined as toughness, is determined with this test. The impact strength of the specimen is calculated by dividing the energy to the cross-sectional area of the standard shaped

specimen and reported as in the unit of J/m^2. Toughness can also be calculated from the area under the stress-strain curve.

Specimens can be notched or unnotched. Charpy and Izod tests are the types of impact test. The specimen stands horizontal in the Charpy test and vertical in the Izod test, respectively. Impact test is performed by a pendulum with known weight hitting the specimen. From the pendulum movement after breaking the specimen, the loss in the kinetic energy is measured as the energy required to break the specimen (Brostow, 2007).

T-peel test is the widely applied method to evaluate the adhesion between the adhesive and the substrates. There are several t-peel test standards in terms of different angles and apparatus. Basically, a rectangular specimen, which has unsealed ends, is clamped between tensile tester grips. These unsealed ends are pulled to reverse directions at a constant speed. The force required to peel the specimen is recorded. Peel strength is calculated as the ratio of the force to the width of the specimen (Morris, 2016).

2.4.2 Electrical Resistivity Measurements

The effect of surface modification applied to CNTs and CFs on the electrical conductivity of the prepared composites were determined with electrical resistivity measurements. Electrical resistivity is defined as the resistance to the current which flows through the unit volume of a material. The electrical resistivity of the composites were measured using two-point probe method in this study.

In two-point probe method, two crocodile probes are connected to the specimen with a known distance. Electrical current passes through one probe to the other. The current between these probes is measured at constant voltage and electrical resistance is calculated with Ohm's law. The electrical resistivity of the specimen is calculated using Equation 2.3. where ρ stands for electrical resistivity in ohm.cm, R is resistance

in ohm, l shows the distance between the probes and S is the cross-sectional area, which is perpendicular to the current flow (Şengör, 2013).

$$\rho = R \times \frac{S}{l} \tag{2.3}$$

2.4.3 Morphological Analyses

Scanning Electron Microscopy (SEM) is a microscopic characterization technique to collect images representing the surface morphology of the samples. In this technique, a fine beam of electrons, formed by the electron gun, is scanned across the surface of an opaque specimen. The surface of the specimen should be conductive; thus surface coating with a conductive layer of gold, platinum or carbon is applied before analyzing the samples. When the beam hits the specimen, signals, which are produced by the emission of secondary electrons, backscattered electrons or x-ray photons, are collected and detected by the detector. The changes in the intensity of signals cause to observe the scanned images of the samples on the screen (S. N. Bhattacharya, Kamal, & Gupta, 2006; Billmeyer, 1984).

Optical microscopy is another technique to examine the surface texture and have magnified images of the surfaces. Images can be taken if the specimen parts reflect or absorb the light or possess different refractive index with this method. Transmitted-light microscopy, which is a suitable technique for the investigation of transparent specimens that can be prepared as thin films, is applied by sending the light from the bottom of the sample. Reflected-light microscopy method is applied for imaging of opaque specimens and light passes through the top of the specimen in this technique. The dispersion of CNTs, which were modified with different techniques in the PS matrix, was investigated in thin films of PS-CNT nanocomposites using an optical microscope with transmitted-light microscopy. Polymer layer and as-received CF surfaces, unbonded, polymer and CF sides of T-peel test specimens were also investigated with reflected-light microscopy method (Billmeyer, 1984).

2.4.4 Thermal Tests

The degradation temperature at maximum weight loss of synthesized PS and in-situ polymerized PS-CNT masterbatches were measured with Thermogravimetric Analysis (TGA). Besides, TGA was performed to control ash content analysis results applied to multilayer composites.

In TGA, the weight change of the sample as a function of temperature is recorded while the sample is placed in an oven and subjected to heat under nitrogen or air atmosphere. Weight change occurs due to the increase of the temperature with a constant heating rate. This change indicates the degradation of the sample. TGA applications are performed to the evaluation of thermal stability, decomposition temperature, and composition of the filled polymers (Balık, 2015; Billmeyer, 1984).

The glass transition temperatures (T_g) of synthesized PS and in-situ polymerized PS-CNT masterbatches were measured with Differential Scanning Calorimetry (DSC) analysis.

Enthalpy is the thermodynamic property observed in DSC. Transition in polymers which are glass transition, melting and crystallization, and also decomposition and oxidation reactions are studied using DSC. In this technique, a small sample and an inert reference sample are placed in pans that stand in an oven. Pans are started to heat with adjusted heating rate and control system adjusts and measures the power that is required for maintaining the sample and the reference pan at the same temperature. When a transition occurs in the sample, temperature versus signal proportional to the power difference is plotted as the DSC thermogram (Billmeyer, 1984; Rosen, 1993).

2.4.5 Measurement of Molecular Weight

2.4.5.1 Viscosity Average Molecular Weight (M_v)

Viscosity average molecular weight measurement is a relative method that used solution viscosity as a known quantity related to molecular weight, to calculate the average molecular weight of polymers. For measuring the solution viscosity; efflux time required for a specified polymer solution volume to flow through a capillary tube is compared with the corresponding efflux time of pure solvent (Billmeyer, 1984). The parameters that solution viscosity depends on are viscosity of the solvent, temperature, concentration of the solute and the particular polymer and solvent pair (Rosen, 1993).

In order to calculate the M_v, intrinsic viscosity is need to be determined. Intrinsic viscosity is defined as the fractional change in the viscosity of a solution per unit concentration of a polymer at infinite dilution. Measurements are done with a specified solvent and polymer pair at constant temperature and intrinsic viscosity is quantitatively related with molecular weight of the polymer (Rosen, 1993).

Intrinsic viscosity ([η]) is calculated by using Huggins equations which is the relation between reduced viscosity (η_{red}) and concentration (c) as given in Equation 2.4 (Billmeyer, 1984). Specific viscosity is denoted with η_{sp}.

$$\eta_{red} = \frac{\eta_{sp}}{c} = [\eta] + k'[\eta]^2 c \qquad (2.4)$$

By expanding the Huggins equation in terms of inherent viscosity (η_{inh}) into a power series, an equivalent form of the Kraemer equation is obtained (Equation 2.5) (Rosen, 1993):

$$\eta_{inh} = \frac{\ln(\eta_r)}{c} = [\eta] + k''[\eta]^2 c \qquad (2.5)$$

where $k'' = k' - 0.5$ and η_r is the relative viscosity.

Reduced and inherent viscosities are plotted regarding polymer solution concentration in order to determine the intrinsic viscosity. The intercept of the plots gives the accurate value of intrinsic viscosity.

By using the calculated intrinsic viscosity of polymer solution, viscosity average molecular weight can be calculated with Mark-Houwink-Sakurada equation (Equation 2.6).

$$[\eta] = K\,\overline{M_V}^{a} \qquad (2.6)$$

K and a are the empirical constants specified for a given polymer and a solvent at a certain temperature. These values are $1.2x10^{-4}$ dL/g and 0.71 for polystyrene at 30°C, respectively (Mark, 1999).

2.4.5.2 Gel Permeation Chromatography (GPC)

Gel Permeation Chromatography, also known as size-exclusion chromatography (SEC), is used to determine average molecular weight and molecular weight distribution of polymers. Number average (M_n), weight average (M_w) and z-average (M_z) molecular weight distributions and polydispersity index (PDI or M_w/M_n) are measured by applying GPC technique.

The separation occurs in a column filled with beads of a rigid porous gel such as highly cross-linked porous polystyrene and porous glass. A solvent stream flows through with a constant flow rate and a sample of dilute polymer solution is injected to the column. Polymer molecules in the solution pass through the porous beads and diffuse into the pores of the gel depending on their size (Billmeyer, 1984).

Small polymer molecules in the sample easily reach to the pores of the gel, diffuse into them and follow a long pathway throughout the column. The larger polymer molecules cannot fit into the pores and can pass without diffusing into the pores. They have a shorter pathway to access the exit and elute from the column first. Thus, polymer chains of different molecular weights are effectively separated with this

method due to the difference in the elution time of the polymer chains exiting the column.

2.4.6 Fourier Transformed Infrared Spectrometer (FTIR)

Infrared spectroscopy is the technique which can be explained as the interaction of infrared light with material. With this technique, the unknowns in the samples are determined by detecting the chemical bonds or functional groups in the molecule structure. The most common type of spectrometer is Fourier Transformed Infrared Spectrometer (FTIR).

The infrared spectrum is plotted absorbance or transmittance versus and wavelength the position of the peaks and bands show certain chemical bonds and functional groups present in the molecular structure of the sample. When the sample is exposed to infrared radiation, it absorbs the radiation and the chemical bonds in the structure vibrate. The existence of the chemical bonds is the requirement of the infrared absorbance to occur. There are certain wavenumber ranges that functional groups absorb the infrared radiation. This behavior provides to determine the unknown molecular structure of the sample with the aid of the correlation between the infrared band positions and chemical structures (Oliver, 1999).

2.4.7 Contact Angle Measurements

The performance of the fiber-reinforced polymers depends mostly on the strong adhesion between the fabric and polymer layers. Sufficient adhesion can be measured by the wettability of the fibers with polymer matrix. The surface wettability of CF is estimated by the surface energy. Better wettability between CF and polymer matrix is promoted by high surface energy of the fibers. Surface energy of CF is affected by the surface functionality and roughness. To use CFs as reinforcement materials, surface modifications should be applied to improve the compatibility between the polymer matrix and fibers by changing their surface

energy. Thus, the effectiveness of the surface modification applied on the CF surface is directly evaluated with surface energy calculations (D. Jiang et al., 2014).

In the content of the thesis, total surface free energy calculations were performed with sessile drop method according to ASTM D7490-08 standard in which two testing liquids are dropped onto the surface and after waiting for a certain time, contact angles are measured. One of these testing liquids is in polar characteristic and the other one possesses a non-polar characteristic. Total surface free energy is the sum of intermolecular forces, such as dispersion, polar and hydrogen bonding. By using the Owens-Wendt-Kaelble equation which is given in Equation 2.7, dispersion and polar components of surface free energy can be calculated.

$$\frac{\gamma_l(1+\cos\theta)}{2} = \left[\left(\gamma_l^d\gamma_s^p\right)^{1/2} + \left(\gamma_l^p\gamma_s^d\right)^{1/2}\right] \quad (2.7)$$

In this equation, θ represents the average contact angle for the test liquid on the test specimen, γ_l represents the surface tension of the test liquid in mJ/m^2, γ_l^d and γ_s^d represent the dispersion component of surface tension of the test liquid and solid, respectively and γ_l^p and γ_s^p represent the polar component of surface tension of the test liquid and solid, respectively. The properties of these probe liquids are given in Table 2.2.

Table 2.2 Surface free energy components (in mJ/m^2) of the probe liquids ("ASTM D7490-08, Standard Test Method for Measurement of the Surface Tension of Solid Coatings, Substrates and Pigments using Contact Angle Measurements," 2008).

Probe Liquid	Total surface free energy, γ^l	Polar component of surface energy, γ^p	Dispersive component of surface energy, γ^d
Water	72.8	51.0	21.8
DIM	50.8	1.3	49.5

The work of adhesion (W_a) gives information about the strength of the adhesion between an adhesive and a substrate. Higher values of W_a indicate better

compatibility and easy wettability between the fibers and polymer matrix and strong bond formation at the interface of the composite layers (J. Zhang, 2013). W_a between the CF plies (1) and polymer layers (2) was calculated from Young-Dupre equation which is given in Equation 2.8 (Baldan, 2012).

$$W_a = 2\left[\left(\gamma_1^d \gamma_2^d\right)^{1/2} + \left(\gamma_1^p \gamma_2^p\right)^{1/2}\right] \quad (2.8)$$

where γ_1^d and γ_2^d represent the dispersion component of surface tension of the CF ply and the polymer layer, respectively and γ_1^p and γ_2^p represent the polar component of surface tension of the CF ply and the polymer layer, respectively.

2.4.8 Shape Memory Tests

Shape changing with external stimuli is a concept inspired from nature. Animals and plants are using this skill as a survival mechanism. Researchers have developed artificial materials demonstrating shape changing abilities with external driving forces, including shape memory alloys (SMAs), shape memory ceramics (SMCs) and shape memory polymers (SMPs) (Lei et al., 2019; Li et al., 2019). SMPs are a type of stimuli responsive materials that can recover their original shape from a temporary shape upon exposure to external stimuli such as heat (B. Xu et al., 2010), electricity (Pelin et al., 2016; Shonaike, 2000), magnetic fields (Mu et al., 2018), light (Lendlein et al., 2005) and pH (Han et al., 2012).

The shape recovery mechanism of SMPs is illustrated in Figure 2.6. Mechanism is moving through four steps given as follows: (1) production of shape memory polymer in original shape, (2) heating the sample above the transition temperature (glass transition (T_g) or melting temperature (T_m)) and deforming to give temporary shape by applying load, (3) fixing the temporary shape by decreasing the temperature below transition temperature and removing applied load, (4) heating again the sample above transition temperature to regain the original shape.

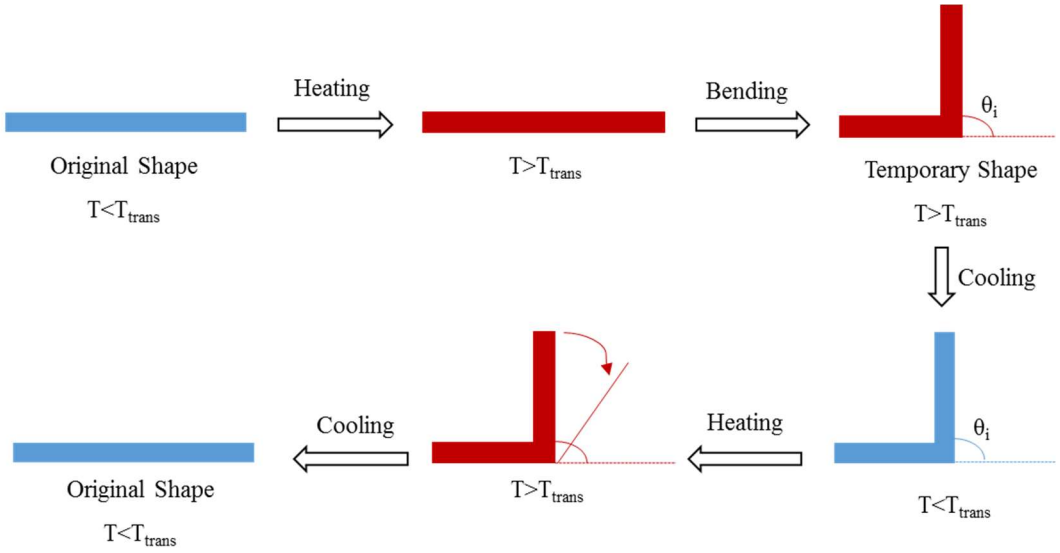

Figure 2.6. Thermomechanical cycle of shape recovery behavior of SMPs.

The benefits of SMPs which make them preferable over SMAs and SMCs are; their low density, low cost, high recoverable strain, high elastic deformation and easy processing (Hassanzadeh-aghdam et al., 2019; Li et al., 2019). On the other hand; weaknesses of SMPs are valid such as lower recovery stress, smaller energy output, poor mechanical properties, and shorter cycle life (Lei et al., 2019; Li et al., 2019; Y. Liu et al., 2014). Insulating properties of polymers due to the low thermal conductivities are resulted in longer shape recovery time in SMPs. Thermal responsive shape memory polymers are extensively investigated in recent years; however they cannot show their full potential due to the demand of external heaters for actuation.

To eliminate these shortcomings, shape memory polymer composites (SMPCs) are improved to provide better performance to shape memory polymers. Polymer-based functional materials are generally electrical insulators and it is essential to form a conductive pathway with incorporating conductive fillers. Thereby, the application and significance of electroactive polymers (EAPs) are rising nowadays (Y. Liu et al., 2009). Conductive fillers improve the thermal and electrical conductivity of the polymer matrix and allow faster Joule heating mechanism that leads to shortening in

recovery time (Ponnamma et al., 2017). Conducting fillers like carbon nanotubes (Cho et al., 2005; H. Lee et al., 2011; Yang Liu et al., 2019), carbon black (K. Wei et al., 2012), carbon nanofibers (Tang et al., 2013), short carbon fibers (Leng et al., 2007), graphene (Tang et al., 2013), metal particles (Leng et al., 2007; Lu et al., 2015), and conducting polymers (Sahoo et al., 2007) are added to SMPs to provide high mechanical properties and electrical conductivity.

2.5 Previous Studies

2.5.1 Modification of Polymer Matrix

Many studies and researches are conducted to develop practical and applicable methods for preventing delamination in multilayer composites. Toughening the polymer matrix is one of the widely implemented methods.

Fracture toughness can be increased with blending soft rubbers with the epoxy matrix. Core-shell type rubber particles including butadiene/styrene core and a methyl methacrylate shell (F. Xu et al., 2016), nanocarboxylic acrylonitrile butadiene rubber (Ozdemir et al., 2016) and acrylic block copolymers (Choi et al., 2017) were investigated in the literature. With the addition of rubbery phase, fiber pullout was rarely observed, fiber bridging and interphase formation were clearly seen compared to neat epoxy-based samples in microscopic investigations.

Silane coupling agent is a type of chemical responsible for the formation of chemical bonding at the interface between the fibers and the resin. It is commonly applied as sizing on the fabric surface but also used as a matrix modifier to produce reactive sites. The effect of two different silane coupling agents (n-(2-aminoethyl)-3-amino-propyltrimethoxysilane and n-(2-aminoethyl)-3-aminopropylmethyl-dimethoxysilane) on the tensile, flexural and interlaminar shear properties were investigated in epoxy/CF multilayer composites (J. Yang et al., 2013). Tensile properties were improved slightly, but flexural properties were increased

significantly with silane coupling addition. Viscosity of the resin system and contact angle of the resin system on the single carbon fiber were decreased as an indication of better wetting of the resin.

Multilayer composites consisting of nanofillers and micro-sized fibers show synergistic effect of these fillers and give the multifunctionality to multilayer composites. Ayatollahi et al. added CNTs and nanosilica particles to the epoxy matrix with ultrasound and high-speed shearing methods. Mechanical properties were increased with 0.5 wt.% nanofiller addition. The toughness, strength and stiffness of the composites were enhanced with nanofiller addition and CNTs were increased the properties higher than nanosilica particles (Ayatollahi et al., 2017).

Wei et al. investigated the effect of nano-TiO_2 and a hybrid filler mixture, which was nano-TiO_2 and CNTs on the tribological properties of epoxy-based CF-reinforced multilayer composites. 3 wt.% nano-TiO_2 was determined as the optimum concentration for low coefficient of friction and high wear life. With hybrid filler system containing 3 wt.% nano-TiO_2 and 0.4 wt.% CNTs; the synergistic effect was resulted in a significant decrease in the friction coefficient and an increase in wear life. The wear patterns changed to adhesive wear and abrasive wear from brittle exfoliation (Wei et al., 2018).

Wang et al. investigated the synergistic effect of the application of HNO_3 treatment and toughening the epoxy matrix with CNTs on tribological properties. The active groups that were produced during the oxidation process was responsible for the strengthening of the bonding strength and increase in friction and wear properties (Wang et al., 2020).

Halloysite nanotubes (HNTs) were used to toughen the epoxy matrix. Fracture resistance and interlaminar shear strength were improved considerably with HNT addition. According to microscope analyses, HNTs were not distributed homogeneously, but this microstructure formed by HNT rich sections were led to the absorption of a large amount of energy and prevented the crack propagation (Ye et al., 2011).

Generally, matrix modification studies were conducted in epoxy-based composites, but similar approaches were also applied in thermoplastic resin-based fiber-reinforced composites. Nanofiller addition was the most common method in the literature and fillers such as non-functionalized and functionalized silica particles (Pedrazzoli & Pegoretti, 2013), expanded graphite nanoplatelets (Pedrazzoli & Pegoretti, 2014), alumina, clay and CNTs (Arao et al., 2013) were extensively used in thermoplastic-based fiber-reinforced composites.

2.5.2 Surface Modification of CNTs

CNTs are good candidates as nanofillers with their high L/D ratios, superior mechanical properties, thermal and electrical conductivities. CNTs tend to agglomerate due to van der Waals interactions. Thus; dispersion and alignment of them in polymer matrix are very difficult and surface treatment is essential for hindering agglomeration, introducing reactive groups and improving the interfacial interactions between CNTs and polymer matrix. Besides, addition methods of CNTs to the polymer matrix are also an essential factor for providing homogeneous dispersion.

Many studies in the literature concentrated on dispersion of CNTs homogeneously and in better alignment for providing strong interfacial interactions to improve load transfer across the CNT/polymer interface (Gopal et al., 2010).

Covalent surface modifications are the most effective technique. This approach is applied by the reaction of molecules which have high chemical reactivity such as strong oxidizing acid and base mixtures (Ling et al., 2013; S. Su et al., 2008; Yesil et al., 2010), amines (Chen et al., 2012; Jimeno et al., 2009; Ramanathan et al., 2005), silane coupling agents (Fu et al., 2002; Kathi, 2008), formaldehyde (X. L. Xie et al., 2005),vinyl monomers (Xie et al., 2005), polymeric and oligomeric materials (Peng et al., 2005; H. F. Wei et al., 2007).

Non-covalent functionalization is obtained through an interaction of delocalized π-bonds on the CNT wall due to sp^2 hybridization with the π-bonds of the polymer molecules, leading to polymer wrapping around the CNTs (Patole et al., 2013). Poly(acrylic acid) (A. Liu et al., 2006), polyvinylpyrolidone (Connell et al., 2001), poly(4-styrenesulfonate) (Connell et al., 2001), polyaniline (Konyushenko et al., 2006), poly(2-ethyl-2-oxazoline) (Tan et al., 2007), poly(ethylene glycol) (Yesil et al., 2011) are examples of polymers commonly used in the literature.

Surfactants take their names from charge of their head groups as ionic and non-ionic surfactants. The surfactants applied for the dispersion of CNTs studied in literature is given as follows: (i) non-ionic surfactants; polyoxyethylene octylphenylether (Triton X-100), polyoxyethylene (20) sorbitan monolaurate (Tween 20), polyoxyethylene (20) sorbitan monooleate (Tween 80) (Rastogi et al., 2008), (ii) anionic surfactants, sodium dodecyl sulfate (SDS) (L. Jiang et al., 2003), sodium dodecyl benzene sulfonate (SDBS) (Camponeschi et al., 2006), (iii) cationic surfactants; hexadecyl-trimethyl-ammonium bromide (CTAB) (Ayewah et al., 2010).

2.5.3 Surface Modification of CFs

Introduction of acidic functional groups to the surface of the CFs and increasing surface area with oxidative surface treatment methods are widely applied in the literature. HNO_3 treatment was applied to CFs to enhance the tribological properties such as wear and friction. Zhang et al. prepared polyimide-based CF-reinforced composites with wet lay-up method, and anti-wear and friction reduction abilities of composites improved with HNO_3 treatment (X. Zhang et al., 2009).

A comparison of modification techniques was also studied in the literature. Su et al. modified CFs with strong HNO_3 etching, plasma bombardment, and anodic oxidation methods. By applying dip-coating method in a phenolic resin, CF-reinforced composites were prepared with 65 wt.% of CF. According to their results,

the composite made of CFs modified with anodic oxidation showed the best tribological and mechanical properties (Su et al., 2005). Another study from the literature concluded that the effects of air plasma treatment were superior to HNO_3 etching. They introduced nano-TiO_2 onto the CF surface in order to provide an improvement in the interfacial adhesion. Changes in matrix morphology of the CF/PTFE composites and modification with 4 wt.% nano-TiO_2 provided the optimum wear resistance to the composites. In fact the combination of air plasma treatment and 4 wt.% nano-TiO_2 modification improved wear resistance of nano-TiO_2 modified CF/PTFE further (P. Liu et al., 2012).

Yapıcı et al. examined strong oxidative treatment with piranha and chromate solutions. The increase in the hydroxyl and carboxylic acid functional groups on the CF surface led to improve the bonding strength due to the high electronegativity and polar characteristics at the interface (Yapıcı et al., 2014).

Plasma treatment is a widely applied method for improving the adhesion strength and interaction between the CF and polymer matrix. Several types of plasma treatment techniques were used in the literature such as cold remote nitrogen-oxygen plasma treatment (Sharma et al., 2011; Tiwari et al., 2011), radio-frequency capacitive low-pressure plasma treatment in air (Garifullin et al., 2017), microwave plasma treatment (Lee et al., 2014), glow discharge plasma treatment at low discharge voltage (L. Zhao et al., 2020), atmospheric plasma treatment of compressed air, argon and nitrogen (Käppler et al., 2014). Introducing polar groups and roughening the smooth surfaces of CF with plasma treatment cause enhancement in mechanical interlocking and interaction between the polymer layer and CF.

Polyurethane is a candidate for surface coating agent due to its advantages such as low viscosity, strong bond formation ability, low cost, flexibility, good wear resistance and tear properties. Polyurethane dispersions (PUDs) were used as surface modifiers for glass fabric-epoxy and carbon fabric-PA6 in the literature (Liao et al., 2016; Ma et al., 2017). Applying PUDs on fabric surface provides more oxygen-containing groups, better matrix impregnation conditions, higher mechanical

properties, stronger interfacial interactions and better thermal stability than silane coupling agent treated and unmodified CF-reinforced composites (Yang et al., 2018; D. Zhao et al., 2019).

Wang et al. investigated modifying the CF surface with in-situ grown CNTs in order to improve the tribological properties of CF-reinforced phenolic composites. They reached higher thermal conductivity and tensile strength in CNT coated CF composites compared to the unmodified ones. Friction coefficient and wear resistance were also improved, which led to a considerable increase in the interfacial bonding of the composites (B. Wang et al., 2018).

Many solutions as discussed above were developed but in recent years interleaving with polymeric nanofibers in interlaminar regions has proven to be one of the most effective method to solve the delamination problem in thermoset-based multilayer composites. Electrospun nanofibers were used as the nanomodifiers due to their low thickness and lightness, high porosity and high mechanical properties. Nanofibrous mat can be prepared as direct electrospinning of nanofibers onto fabric, and collecting the nanofibers on support first and then transferring them to the composite structure as an interlayer. Daelemans et al. used polyamide 6 and polyamide 6,9-based electrospun nanofibrous interleaves to improve impact resistance of glass fiber reinforced polymers in their study (Daelemans et al., 2018). According to their results, the more impact energy was absorbed in the interleaved laminates by the nanofibers, the less damage to reinforcing fibers and matrix resin was produced. The same research group also studied improving the toughening mechanism in carbon-epoxy composite laminates. The main mechanism leading to higher interlaminar fracture toughness, both in Mode I and Mode II, was observed to bridge cracks by polyamide nanofibers. The effectiveness of the nanofiber bridging toughening mechanism depends on a proper load transfer to the nanofibers (Daelemans et al., 2015).

Silane treatment is generally applied in glass fabric-reinforced composites (F. Su et al., 2009). Limited studies were performed in the literature about surface

modification of carbon fabric. Latif et al. investigated the effect of silane coupling agent amount on the mechanical properties of vinylester-epoxy hybrid resin-based carbon fiber-reinforced polymers. The sample prepared with fibers treated with 2 wt.% of silane coupling agent showed the best mechanical performance in terms of tensile properties (Latif, Prabhakar, & Song, 2019).

Zhang et al. treated CF surface with HNO_3 oxidation, silane coupling agent treatment and the combination of these methods. According to their results, when acid oxidation and silane coupling agent treatment were applied together; friction and wear properties were decreased due to the increase in surface roughness. Introducing more oxygen-containing groups to the surface improved the adhesion between the fabric plies and phenolic resin with the combined treatment method (X. Zhang et al., 2008). Silane coupling agents are applied to ensure that other grafted materials interact strongly with the fabric surface. Jiang et al. performed silane coupling agent treatment to CF surface first and then grafted the silane treated surfaces with monofunctional and multifunctional POSS to improve the interfacial properties (D. Jiang et al., 2014).

2.5.4 Processing Techniques of PS-CNT Nanocomposites

Zhang et al. produced PS-CNT composites first with solution mixing under ultrasonication and after drying they applied melt mixing at 210°C in mixer with different mixing times. PS-CNTs composites were dissolved in chloroform ($CHCl_3$) and dispersed with ultrasonication. According to their observations, improvement in the solubility in $CHCl_3$ was observed when mixing time increased from 5 min to 60 min. Solutions remained stable and seemed homogeneously dispersed for three months. It was mentioned that the reason for the stability of the PS-CNT composites was the enhanced interaction during the melt mixing step (Z. Zhang et al., 2006).

Modification of CNTs with polymer matrix material is a widely used approach for achieving good dispersion and improving mechanical properties. Yuan et al.

introduced CNTs into PS matrix in two ways: directly incorporation into matrix and dilution of commercially available masterbatches of PS-CNT composites with pure polymer. Purified CNTs were modified via polymerization of styrene under microwave irradiation. Modified and purified CNTs were mixed with PS and THF to form masterbatch particles. PS-CNT composites were prepared by melt mixing in twin screw extruder with different CNT contents. It was concluded that the PS layer coated on the CNTs improved the dispersibility and compatibility of the CNTs, leading to a strong interface adhesion and nanotube orientation in the PS matrix. Impact strength increased by 250% with PS coated CNT addition and the increase was 150% in unmodified CNT based composites when compared to neat PS (Yuan et al., 2009).

McClory et al. investigated the influence of screw speed on electrical and rheological percolation of melt-mixed high-impact polystyrene (HIPS)-CNT nanocomposites prepared by twin screw intermeshing co-rotational extruder with different CNT composition. High dispersion was achieved at 70 and 100 rpm screw speeds and at higher screw speeds CNTs tended to agglomerate. For 100 rpm, rheological percolation at a loading between 1 and 3 wt.% CNTs was reached. Electrical percolation threshold values were achieved as 1-3 wt. % at 20, 70 and 100 rpm, 3-5 wt. % for 150 rpm (Mcclory et al., 2011).

Solution mixing studies were conducted in the literature comparatively with the melt mixing method. Pristine and modified CNTs such as phenyl propane ester and polystyrene functionalized CNTs as well as an in situ synthesized polystyrene masterbatch (Faraguna, Pötschke, & Pionteck, 2017), polyaniline (PANi)-coated CNTs (Sarvi & Sundararaj, 2014) were mixed with the solutions of polystyrene with ultrasonic mixing. According to the common results of these studies, low percolation threshold, less fragmentation and homogeneous dispersion of CNTs were observed due to the ultrasonication. The degradation of the polymer matrix during solution mixing process was low compared to melt mixing method.

With in-situ polymerization method, homogeneous dispersion of the nanofillers and a strong interface between filler and polymer matrix can be achieved simultaneously (Kaseem et al., 2016). Nanocomposites produced with this method possesses high mechanical properties, high thermal stability and high electrical conductivity.

PS-CNT composites were prepared with three different polymerization technique without oxidation and shortening of CNTs in Ham et al.'s study. They applied conventional emulsion polymerization and miniemulsion polymerization technique which was suitable for preparing polymeric nanoparticles and polymeric encapsulation of nanoparticles, and the mixing of CNTs with PS latex. According to their observations, among these methods, in conventional emulsion polymerization technique CNT bundles entirely were covered with PS, in miniemulsion technique there were regions not covered with PS and mixing CNTs with PS latex was not a successful method because PS was not crosslinked and dissolved in solvent, and nanotubes separated from PS precipitated. Mechanical and electrical properties depended on crosslinking and surface coverage of PS so the PS-CNT composite showed a lower electrical resistance, and higher mechanical strength than the other methods. The electrical conductivity increased with increasing the amount of CNTs in the composite prepared by the miniemulsion polymerization (Ham et al., 2006).

Zhang et al. developed a method for preparing core-shell nanospheres with PS as the core and CNTs as the shell structure via hydrogen-bonding self-assembly. Carboxylic acid modified PS nanospheres were fabricated by soap-free emulsion copolymerization using acrylic acid as comonomer. First, CNTs were modified with HNO_3 to form defect sites on the CNT surfaces. They were then grafted with poly(vinyl pyrrolidone) (PVP), in which the carbonyl oxygen act as proton acceptors to form hydrogen bonds with carboxyl acid groups. Surface modification with PVP made CNTs self-assemble onto the surface of acid modified PS nanospheres via hydrogen bonding. The core-shell structure formation was defined as reversible, and controlling of the morphology was possible by changing the pH value of the PS-CNT core-shell nanosphere production medium (C. Zhang et al., 2010).

Koziol et al. fabricated PS-based aligned CNTs-reinforced composites by taking into account the alignment of CNTs in the composite structure. Carbon nanotube carpets were stacked between two aluminum cylinders and liquid styrene wetted these layers, and PS-CNT composites were produced with high filler loading by radical polymerization. In compliance with the SEM images, CNTs were entirely coated with PS. According to the TGA analysis; 75 wt.% of the composite was polymer, 20 wt.% was CNTs and the rest was impurities of CNTs (Koziol et al., 2011).

Hatui et al. prepared PS-based nanocomposites reinforced with CNTs, expanded graphite (EG) and combinations of these fillers with in-situ polymerization technique. Thermomechanical properties, morphologies and electrical conductivity of the composites were investigated. Firstly, CNTs were modified with 3:1 concentrated acid mixture of H_2SO_4:HNO_3 and then washed. For composites, including EG-CNT hybrid nanofillers; better dispersion and homogeneity were observed. CNTs filled the spaces between the graphite layers and provided the potential penetration of the polymer chain inside the layers of expanded graphite. The dual filler system also enhanced the thermal stability of composite and decreased the electrical resistivity sharply compared to PS-CNT and PS-EG composites. Mechanical properties such as tensile strength and tensile modulus had the highest values in PS-EG-CNT composites due to the easy penetration of polymer chains through the layers of EG which increased compatibility between fillers and polymer matrix (Hatui et al., 2014).

Zaragoza et al. applied in-situ bulk polymerization assisted with sonication to produce PS-CNT composites with different concentrations. Applying this method provides encapsulation and exfoliation of CNTs into the polymer matrix to enhance dispersion. FTIR analysis showed that there was no covalent interaction between PS and CNTs. They reported the effects of the strong cavitation forces induced by sonication during CNT dispersion. They suggested that a decrease in storage modulus can occur as a result of CNT fragmentation, which was observed in SEM images (Zaragoza-Contreras et al., 2009).

Khan et al. prepared PS-CNT composites with emulsion polymerization. Non-covalent modification with sodium dodecyl sulfate (SDS) and two different covalent modification approaches with HNO_3 and oleic acid were applied to CNTs. They measured the failure load with applying tensile load to PS-CNT films. The failure stress was increased nonlinearly with increasing the CNT amount in the composites due to the lack of alignment. This increment was relatively linear due to more homogeneous dispersion in oleic acid modified CNTs-reinforced composites (Khan et al., 2010).

In the study of Lahelin et al., the effect of different initiators, surfactants and CNTs on the in-situ emulsion and emulsion/suspension polymerization of styrene and methyl methacrylate and on the mechanical, electrical and thermal properties of the composites were investigated. Using this emulsion polymerization approach they prepared composites with high amounts of homogeneously dispersed fillers (up to 10 wt.%). They also reached higher modulus, electrical and thermal conductivity values with addition of CNTs compared to neat PS and PMMA (Lahelin et al., 2011).

As an application of PS-CNT composites in gas sensibility; Zhang et al. prepared the composites with in-situ bulk polymerization and solution mixing of PS with CNTs and measured the resistance responsivities against various organic vapors. Better dispersion of CNTs and lower electrical resistivity values were achieved in in-situ polymerized composites. Within short time exposure, the responsivity to organic vapors such as THF, benzene, toluene, chloroform etc. of in-situ polymerized composites was better than the composites produced with solution mixing and the resistance recovered to their original value faster when composites transferred into air (B. Zhang et al., 2005).

In order to improve the adhesion and dispersion between the PS matrix and CNTs; Hua et al. prepared styrene and styryl-functionalized CNTs by esterification and used them as fillers to produce PS-CNT composites by in-situ radical copolymerization. The presence of similarity in the composite structure led to improving the dispersion

and the thermal stability due to the covalently linked parts of the composite structure (Hua et al., 2013).

According to the literature survey results about PS-CNT composite preparation by in-situ polymerization, homogeneous dispersion of CNTs in polymer matrix can be achieved and conductive pathway formation occurs at lower concentrations of filler.

2.5.5 Processing Techniques of Multilayer Composites

Liu et al. prepared multilayer composites containing higher than 60 vol.% CF with Nylon-66, polyetherimide (PEI) and polyethylene terephthalate (PET) as matrices and they were compared their results with an epoxy-based multilayer composite. In their preparation technique, first thermoplastic polymers were dissolved in suitable solvents and hand lay-up method was used to impregnate the reinforcing fabric with the matrix solution. After solvent evaporation, hot press was applied to distribute uneven polymer on the CF surface and to remove the excess resin. For multilayer composite preparation, the prepregs were placed into a mold and compression molding was applied. Despite the fact that their mechanical test results not being as high as the one prepared with epoxy resin, the values were sufficient to meet the requirements of the industrial applications (B. Liu et al., 2017).

The concentration of polymer in the solution is one of the parameters that affect the mechanical performance of CFRPs. Pelin et al. studied the optimization of Polyamide 6 (PA6) concentration in formic acid to produce PA6-based CF-reinforced composites based on a multiple-stages technique that involves fabric impregnation and high-temperature pressing. Their tensile test results indicated that best mechanical performance was reached in the composite prepared using a solution of 20 wt.% PA6 in formic acid with the tensile strength of 540.5 MPa and Young's modulus of 63.6 GPa (Pelin et al., 2016).

Polypropylene (PP)-based prepregs were produced by Kim et al. by using PP films with different thicknesses before multilayer composite preparation. PP films and CF

were placed into a mold designed to have a space between the upper and lower molds to allow excess resin come out. PP films were inserted between eight plies of prepregs, and multilayer composites were produced using the compression molding method. The tensile strength and tensile modulus were decreased slightly with increasing thickness of the interleaved PP film due to the decrease in the volume fraction of CF in the multilayer composites (J. W. Kim et al., 2016).

Akkaoui and Bayram investigated the effects of the fiber concentration and molding parameters on the mechanical and thermal properties of PA6/Glass mat (GM) multilayer composites prepared by compression molding. PA6 pellets were put in the middle of the mold, and then a layer of GM and, the remaining amount of polymer was placed in the multilayer structure, respectively. The total polymer amount was kept constant in all the composites while increasing the GM layers in the composites. The most important parameter on the mechanical properties was GM content and tensile strength and modulus increased with increasing the number of GM plies from one (17 wt.%) to three (39 wt.%) layers in the composite structure (Akkaoui and Bayram, 2004).

Yaşar produced thermoplastic poly(ether)ester elastomer (TPEE)-based carbon black (CB)-reinforced polymer layers and combined these layers with five layers of CF by compression molding in her thesis study. Several surface modifications were applied to CB, such as silane coupling agent and paraffinic oil. The highest tensile strength (78.29 MPa) and tensile modulus (9275.3 MPa) were reached in the multilayer sample, which was produced with 3 wt.% of silane coupling agent and paraffinic oil modified CB (Yasar, 2014).

2.6 Motivation of the Thesis

Multifunctional composite materials, including CFRPs, are used extensively in many applications where advanced mechanical and structural properties are needed. Due to the processing, repairment, and recycling restrictions of thermoset matrices, high-

performance thermoplastic-based polymer composites have started to replace thermoset-based polymer composites in industrial applications.

The preparation of multilayer composites using PS, an inexpensive thermoplastic that is frequently used in commodity and daily life applications, was studied for the first time in this thesis study. The polymer matrix has been modified and enhanced in terms of mechanical, electrical conductivity, and shape recovery properties. CNTs were used to ensure electrical conductivity and shape recovery when an electrical voltage was applied. Oxidative treatment and surface modifications were conducted to CNTs with surfactants, silane coupling agents, and a copolymer. As multifunctionality, shape memory behavior of the prepared polymer nanocomposites, and multilayer composites were investigated with thermally and electrically bending tests. To enable soft segments in the structure, which are responsible for the recovery of the temporary shape of the samples, an elastomer (SEBS-gMA) was blended with PS.

Nanocomposites were produced with two different preparation techniques; direct melt blending of PS and CNTs, and PS-based CNT-reinforced composite synthesis with in-situ polymerization in order to achieve homogeneous dispersion of CNTs in the polymer blend.

Delamination between the layers of multilayer composites is the main failure mechanism in CFRPs. The application of the suitable surface modification technique is critical for enhancing the interfacial adhesion between the polymer matrix and fiber surface. Various treatments were applied to the fabric surface to provide roughness to ensure mechanical interlocking and chemical functionality to enhance adhesion between the polymer and CF layers.

In this thesis, composites containing PS, SEBS-gMA, CNTs and CFs were prepared using the compression molding technique. The multilayer composites were designed step by step. In the first section, CNTs were modified with silane coupling agents, surfactants and a copolymer. The best modification technique that provided better dispersion in binary PS-CNTs and ternary PS-SEBS-gMA-CNTs composites was

selected. After that, multilayer composites were produced with the polymer blends, reinforced using CNTs, and fabricated with two different methods, masterbatch dilution and melt mixing. The characterization results of the bulk polymerization of PS, PS-CNT masterbatches and multilayer composites were discussed in the second, third, and fourth sections.

In the fifth section, to prevent delamination before increasing the number of CF layers, several surface modifications were applied to the CFs, such as silane coupling agent treatment, polymer coating, and interleaving with nanofibers. At last, in the sixth section, multilayer composites with one, three, and five as-received CFs were produced. In order to see the effect of surface modification on the properties of the multilayer composites, CFs of the five-layered composite were modified with a silane coupling agent. CF content, morphology, mechanical properties, electrical conductivity, and electrically stimulated shape memory properties of the multilayer composite samples were characterized. The thermoplastic-based multilayer composites with improved mechanical, thermal, and shape memory properties possess high potential for aerospace, automotive, and related industries.

CHAPTER 3

EXPERIMENTAL

3.1 Materials

3.1.1 Polystyrene (PS)

Polystyrene (PS Crystal 1540, Total Petrochemicals) was supplied by Tekinplast Plastik Tic. Ltd. Şti., Turkey. The specifications of the material obtained from the supplier are given in Table 3.1.

Table 3.1 Properties of PS ("Technical Data Sheet of PS Crystal 1540," 2017).

Property	Method	Unit	Value
Melt Flow Index (200°C /5 kg)	ISO 1133 H	g/10 min	12
Unnotched Charpy impact strength	ISO 179-1:2010	kJ/m^2	8
Tensile strength at break	ISO 527-2	MPa	42
Elongation at break	ISO 527-2	%	2
Tensile modulus	ISO 527-2	MPa	3100
Surface Resistivity	ISO IEC 93	Ohms	$>10^{14}$

3.1.2 Elastomer (SEBS-gMA)

Poly[styrene-b-(ethylene-co-butylene)-b-styrene] grafted with maleic anhydride (SEBS-g-MA) with a trade name of Kraton® FG1924 G was used as a compatibilizer and also a soft segment in shape memory polymer composites. It was supplied by Dolder Kimya Dış Tic. A.Ş., Turkey. Its chemical structure and properties are given in Figure 3.1 and Table 3.2, respectively. Abbreviation of SEBS-g-MA is given as 'E' in sample coding.

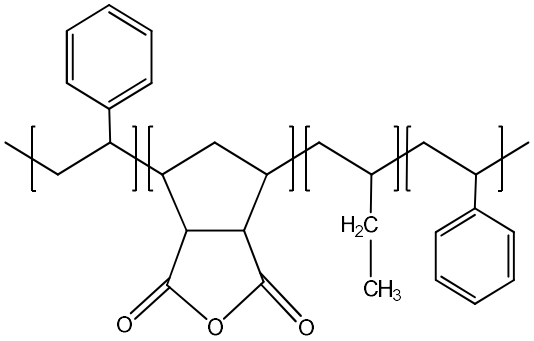

Figure 3.1. Chemical structure of SEBS-gMA ("Technical Data Sheet of Kraton FG 1924 G," 2017; Yeniova et al., 2010).

Table 3.2 Properties of SEBS-gMA (Kraton® FG1924 G) ("Technical Data Sheet of Kraton FG 1924 G," 2017; Yeniova et al., 2010).

Property	Method	Unit	Value
Melt Flow Index (230°C/5 kg)	ASTM D 1238	g/10 min	40
Tensile strength at break	ASTM D 142	MPa	23
Elongation at break	ASTM D 142	%	750
Maleic anhydride, Bound	Beta Attenuation Monitor (BAM) 1026	wt.%	0.7 to 1.3
Styrene/Rubber ratio	n/a	%	13/87

3.1.3 Multiwalled Carbon Nanotubes (CNTs)

Multiwalled carbon nanotubes, used as conductive fillers in this study was purchased from Nanocyl (Belgium) with a trade name of NC7000. Properties of the material are given in Table 3.3.

Table 3.3 Properties of MWCNTs (NC7000) ("Technical Data Sheet of NC7000," 2017).

Property	Method	Unit	Value
Average diameter	Transmission Electron Microscopy	nm	9.5
Average length	Transmission Electron Microscopy	μm	1.5
Carbon purity	Thermogravimetric Analysis	%	90
Transition metal oxide	Inductively Coupled Plasma Mass Spectrometry	%	< 1%
Amorphous carbon	High Resolution Transmission Electron Microscopy	-	-
Surface Area	BET Surface Area Analysis	m^2/g	250-300
Volume resistivity	Internal Test Method (Resistivity on Powder)	Ω.cm	10^{-4}

3.1.4 Surface Modifiers

For surface modification of CNTs; three different kinds of surfactants, two different silane coupling agents and a copolymer were used. Silane coupling agents were obtained from Cam Elyaf Sanayi A.Ş., Turkey, surfactants and copolymer were supplied by Sigma Aldrich. Properties and chemical structures of surface modifiers are given in Table 3.4.

Table 3.4 Chemical structures and properties of surface modifiers.

Materials	Chemical Structure	Properties
Sodium Dodecyl Sulfate (SDS)	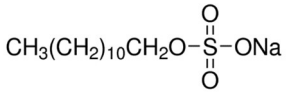	Anionic Surfactant, Molecular Weight: 288.38 g/mol, Critical Micelle Concentration: 7-10 mM ("Technical Data Sheet of SDS," 2019).
Poly (styrene-co-maleic anhdyride), cumene terminated (PSMA)	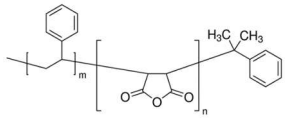	Avg. M_N: ~1600 by GPC, ~1.3:1 mole ratio of styrene:maleic anhydride, T_g: 154°C ("Technical Data Sheet of PSMA," 2019).
Sodium Dodecyl Benzene Sulphonate (SDBS)	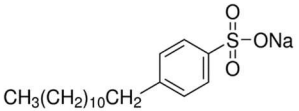	Anionic Surfactant, Molecular Weight: 348.48 g/mol, Critical Micelle Concentration: 1.5 mM ("Technical Data Sheet of SDBS," 2019).
Polyethylene glycol tert-octylphenyl ether (TX-100)	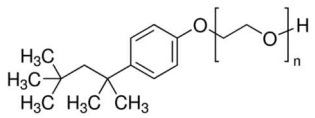	Nonionic Surfactant, Molecular Weight: 625 g/mol, Critical Micelle Concentration: 0.22-0.24 mM ("Technical Data Sheet of Triton X-100," 2019).
(3-Trimethoxysilylpropyl)methacrylate (MSPM)	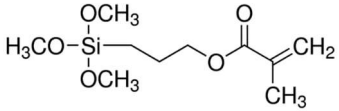	Molecular Weight: 248.35 g/mol, T_b: 190°C, Density: 1.045 g/mL at 25°C ("Technical Data Sheet of MSPM," 2019).
(3-Glycidyloxypropyl)trimethoxysilane (GLYMO)	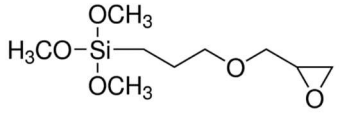	Molecular Weight: 236.34 g/mol, T_b: 90°C, Density: 1.07 g/mL at 25°C ("Technical Data Sheet of GLYMO," 2018).

3.1.5 Styrene

In in-situ polymerization studies, styrene was used as a monomer and it was purchased from Sigma-Aldrich. Chemical formula of styrene is illustrated in Figure 3.2 and its properties are given in Table 3.5.

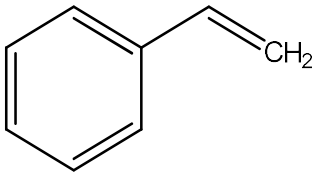

Figure 3.2. Chemical structure of styrene.

Table 3.5 Properties of styrene monomer ("Properties of Styrene Monomer," 2017).

Property	Unit	Value
Molecular weight	g/mol	104.15
Boiling point	°C	145-146
Melting point	°C	-31
Autoignition temperature	°F	914
Density	g/mL at 25°C	0.906

3.1.6 Azobisisobutyronitrile (AIBN)

AIBN was used as initiator in the PS synthesis. It was obtained from Sigma-Aldrich. Chemical formula of AIBN is represented in Figure 3.3 and its properties are given in Table 3.6.

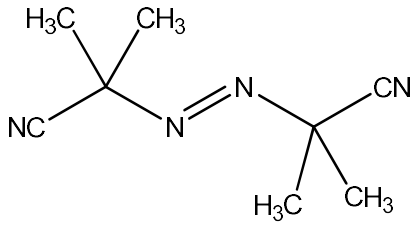

Figure 3.3. Chemical structure of AIBN ("Properties of AIBN," 2017).

Table 3.6 Properties of AIBN ("Properties of AIBN," 2017)

Property	Unit	Value
Chemical formula	-	$C_8H_{12}N_4$
Molecular weight	g/mol	164.21
Storage temperature	°C	2-8
Melting point	°C	102-104

3.1.7 Carbon Fabric (CF)

The carbon fabric used in this study was provided from Metyx Composites, Turkey. The type of the CF is designated as CW 245 B-Carbon 3K. It contains three thousands of filaments per tow with 2x2 twill woven weaving style and the areal density is 245 g/m^2. The sizing on the CF is compatible with polyester, vinylester and epoxy resins (Yasar, 2014).

3.1.8 Teflon Sheets

Teflon sheets with a thickness of 1.5 mm were used as releasing layers during the preparation of the polymeric layers and multilayer composites using a compression molding. It was obtained from Aydınlar Makina-Metal San. and Tic. Ltd. Şti., Turkey.

3.1.9 Polyamide 6 (PA6)

One of the surface modification methods that was applied to CF was coating the surface with PA6 electrospun nanofibrous layer. The PA6, namely Tecomid NB40, was supplied by Eurotec Engineering Plastics, Turkey. Properties of which are given in Table 3.7.

Table 3.7 Properties of PA6 ("Properties of Polyamide 6," 2018).

Property	Unit	Value
Density	g/cm^3	1.13
Melting point	°C	223
Processing temperature	°C	240-260
Moisture content	%	< 0.2

3.1.10 (3-Aminopropyl)triethoxysilane (APTES)

To improve the chemical interaction between electrospun PA6 layer and CF; silane coupling agent (SCA) treatment with APTES (Fig. 3.4) was first applied onto the CF surface. SCA was purchased from Sigma-Aldrich.

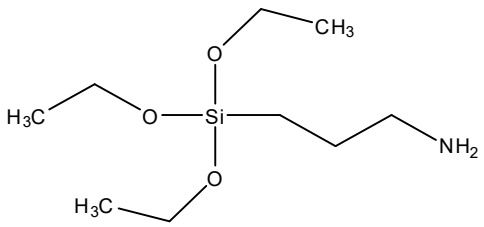

Figure 3.4. Chemical structure of APTES ("Properties of (3-Aminopropyl)triethoxysilane." 2017).

3.2 Experimental Methods

3.2.1 Surface Treatment and Modification of CNTs

Acid treatment was applied to the CNTs with the method given as follows. 5 grams of dried CNTs were dispersed in 100 mL H_2SO_4 and 100 mL HNO_3 mixture and ultrasonicated (Sonorex Super, Bandelin) at 80°C for 30 minutes. After diluting the black colored mixture 1:5 by volume with water, the mixture was filtered under vacuum and washed with excess hot and cold distilled water until pH of the filtered water was greater than 5 (Yesil, 2010).

Surface modification step was applied to improve the dispersion of CNTs in the PS matrix. Experimental procedures for acid modification (A-CNT), surface modification with surfactants which are sodium dodecyl benzene suplhonate (SDBS-A-CNT) and TritonX-100 (TX100-A-CNT) and surface modification with silane coupling agents which are (3-Trimethoxysilylpropyl)methacrylate (MSPM-A-CNT) and (3-Glycidyloxypropyl)trimethoxysilane (GLYMO-A-CNT) are given in Figures 3.5, 3.6 and 3.7, respectively.

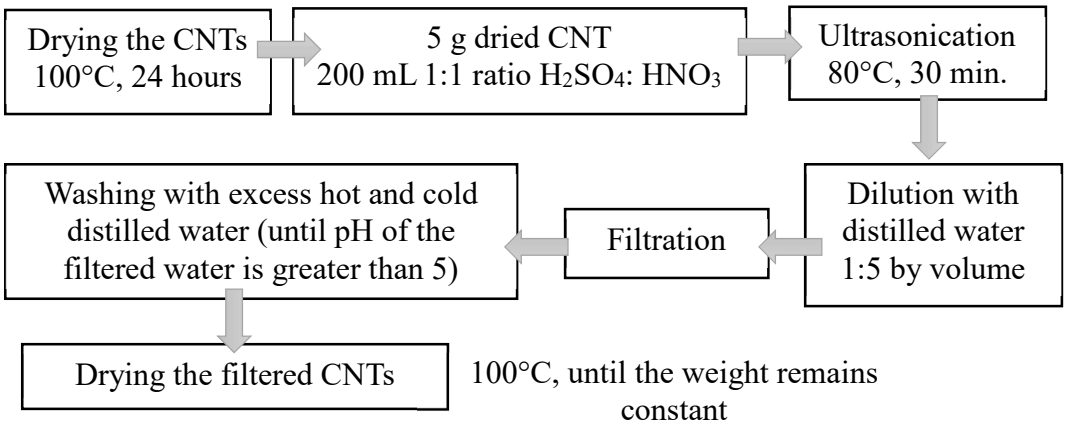

Figure 3.5. Flow chart of preparation steps of A-CNT sample.

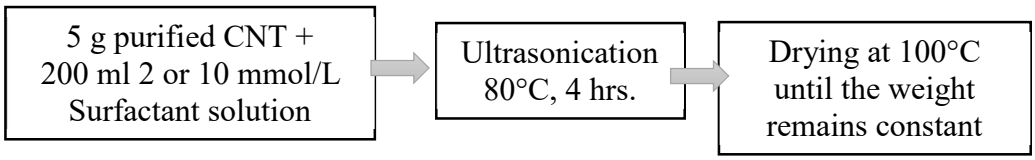

Figure 3.6. Flow chart of preparation steps of SDBS-A-CNT and TX100-A-CNT samples.

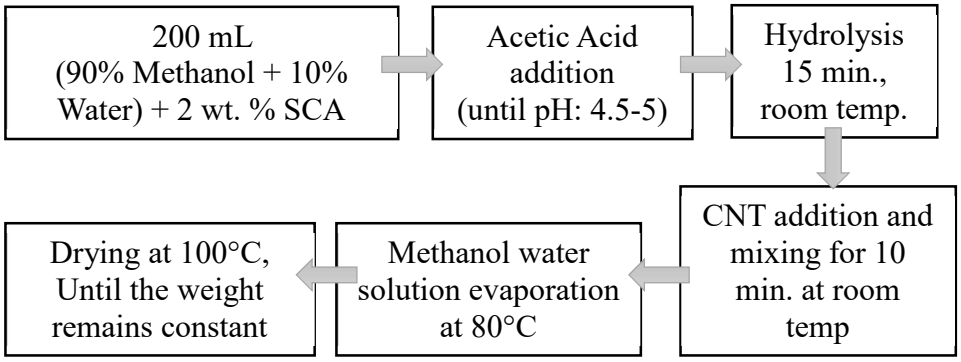

Figure 3.7. Flow chart of preparation steps of MSPM-A-CNT and GLYMO-A-CNT samples.

3.2.2 Preparation of PS-CNT Binary and PS-E-CNT Ternary Composites with Melt Mixing Method

In order to observe the effect of surface modification on dispersion of CNTs in PS, binary composites of PS and CNTs were produced with melt blending method. A co-rotating twin screw extruder (Thermoprism TSE-16-TC (L/D = 24)) was used for melt blending of composites in this study as shown in Figure 3.8.

In the first set of experiments, PS pellets were ground into smaller pellets using a Wiley mill intermediate model grinder (Arthur H. Thomas Co., Philadelphia). PS, modified and as-received CNTs were mixed in a beaker and fed from the hopper by hand. Extrusion process was performed with the temperature profile of 200°C-

240°C-240°C-240°C-240°C from hopper to die, at a screw speed of 150 rpm and feed rate of 25 g/min.

The second set of experiments were performed in order to observe the effects of feeding from hopper or main feeder, decreasing screw speed and feed rate on the homogeneous dispersion of CNTs. PS was not ground and fed from main feeder and CNTs were fed from hopper by hand in order to achieve 1 wt.% CNT addition. By this way, polymer was in melt state and feeding by hand from hopper was expected to form more homogeneous mixtue of PS and CNTs. Extrusion process was performed with the same temperature profile given above, at a screw speed of 100 rpm and feed rate of 15 g/min.

Figure 3.8. Co-rotating Twin Screw Extruder.

Ternary composites were prepared with 40 wt.% of SEBS-g-MA and 1 wt.% of modified and as-received CNTs. PS and SEBS-g-MA were fed from main feeder and CNTs were fed from hopper by hand in order to achieve 1 wt.% CNT addition. Extrusion process was performed with the temperature profile of 200°C-240°C-240°C-240°C-240°C from hopper to die, at a screw speed of 100 rpm and feed rate of 15 g/min. Sample codes and compositions are given in Table 3.8. Abbreviation of SEBS-g-MA is given as ‘E’ in sample coding.

Table 3.8 Sample codes and compositions of PS-SEBS-g-MA-CNT ternary nanocomposites.

Sample Codes	Compositions
PS-E	60% PS-40%Elastomer (SEBS-gMA) binary composites
PS-E-CNT	60% PS-40%Elastomer (SEBS-gMA) and 1wt.% of as-received CNTs added.
PS-E-A-CNT	60% PS-40%Elastomer (SEBS-gMA) and 1wt.% of 1:1 (H_2SO_4: HNO_3) Acid Modified CNTs added.
PS-E-SDBS-A-CNT	60% PS-40%Elastomer (SEBS-gMA) and 1wt.% SDBS modified CNTs added.
PS-E-TX100-A-CNT	60% PS-40%Elastomer (SEBS-gMA) and 1 wt.% TritonX100 modified CNTs added.
PS-E-MSPM-A-CNT	60% PS-40%Elastomer (SEBS-gMA) and 1 wt. % MSPM modified CNTs added.

3.2.3 Polymerization of Styrene and Masterbatch Production of PS-CNT Nanocomposites via In-situ Polymerization Method

Bulk polymerization technique was used to synthesize PS and the parameters such as reaction time, reaction temperature (90°C) and initiator concentration (0.01 mol/L) were taken from the previous work as a starting point (Balık, 2015).

Experimental set-up of bulk polymerization of styrene is given in Figure 3.9. Initiator concentrations such as 0.01, 0.008 and 0.005 mol/L were studied to find the amount that gave the similar MFI and molecular weight with the commercial PS. Sample codes and initiator concentrations of the synthesized PS are given in Table 3.9. According to this procedure; 100 mL of styrene was gradually added onto AIBN. This solution was stirred for 5 hours in 500 mL three necked balloon. After that, polymerization was initiated by applying heat. The polymerization reaction time was 3 hours and reaction temperature was 95°C. At the end of the reaction, highly viscous

polystyrene was poured onto aluminum mold and left for drying in an oven at 90°C for 18 hrs. Dried PS was taken from aluminum mold and crushed into small pieces in mortar.

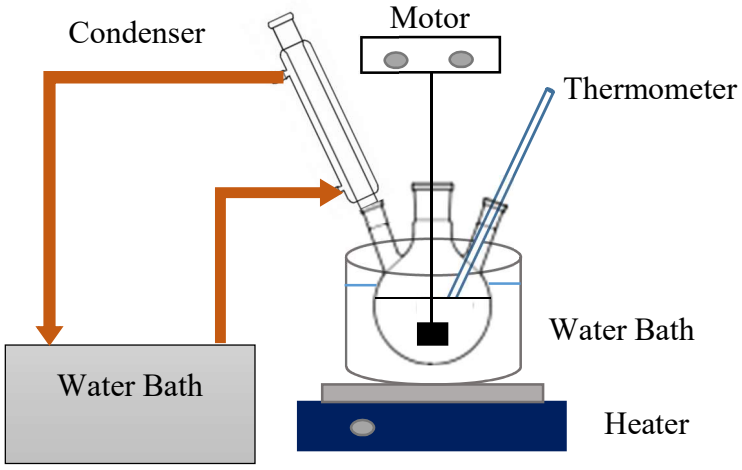

Figure 3.9. Schematic representation of bulk polymerization experimental set-up.

Table 3.9 Sample codes and initiator content of bulk polymerized PS.

Sample	Initiator Concentration, mol/L
PS	Commercial grade
sPS-1	0.01
sPS-2	0.008
sPS-3	0.005
sPS-4	0.005 (Scale-up with 200 mL Styrene)

For PS-CNT masterbatch production; 200 mL of styrene was gradually added into 0.005 mol/L AIBN. This solution was stirred for 5 hours in 1000 mL three necked balloon. After that, polymerization was initiated by applying heat. After the first hour of polymerization 2.3 g of CNTs were added gradually and other steps were followed as same as the bulk polymerization. After the polymerization, the CNT amount in the masterbathces were calculated as 3.2 wt.%. For A-CNT, in-situ polymerization

was performed two times but polymerization could not be achieved in both experiments due to the acidic characterization of reaction medium. After polymerization, the remaining CNTs in the balloon after pouring were collected and separated by applying centrifuge and washed with toluene several times in order to remove polymer. After drying, this unreacted CNTs were subtracted from the total added CNTs (2.3 g) and remaining amount of CNTs were used as feed for extrusion.

PS-CNT masterbatches were diluted to reach 1 wt.% CNT amount in PS-E-CNT nanocomposites. PS, PS-CNT masterbatches and elastomer were fed from main feeder. Extrusion process was performed using the same conditions with other nanocomposite productions. The sample designations of the masterbatches and characteristics of them are summarized in Table 3.10.

Table 3.10 Sample codes and content of sPS-CNT masterbatches.

Sample	Content of the masterbatches
sPS-CNT	Synthesized PS and as-received CNTs masterbatch
sPS-MSPM-A-CNT	Synthesized PS and acid treated and then MSPM modified CNTs masterbatch

3.2.4 Preparation of Multilayer Composites with Selected Compositions Produced with Melt Mixing and In-situ Polymerization Techniques

Masterbatch composites (sPS-CNTs), which were synthesized by in-situ bulk polymerization method, were diluted with commercial grade PS and combined with SEBS-gMA in extruder to obtain the composite formulation with 40 wt.% of SEBS-gMA and 1 wt.% of as-received and MSPM modified CNTs. PS, SEBS-gMA and sPS-CNTs were fed from main feeder. This procedure was called as method 1 (M1).

To compare the composite preparation methods, melt blending of PS, SEBS-gMA and CNTs was also performed with another approach. In this method, PS and SEBS-gMA were fed from main feeder and CNTs from hopper by hand. The amount of

CNTs fed to hopper was adjusted as 1% of the feed rate of polymer pellets. This procedure was called as method 2 (M2). Abbreviations and information about the composites are given in Table 3.11.

Table 3.11 Sample codes and information about PS-SEBS-g-MA-CNT-CF multilayer nanocomposites.

Sample	Information on usage of CNTs and modification technique	Preparation method of polymer composites	
		Method 1	Method 2
PS-E-CF	PS-E binary blend was prepared without CNT addition.	+	+
PS-E-CNT-CF	As-received CNTs were added.	+	+
PS-E-MSPM-A-CNT-CF	First, acid treatment was applied to CNTs according to Yesil, 2010. Then, MSPM treatment was performed according to Yasar, 2014.	+	+

Polymeric layers were prepared with PS-E binary and PS-E-CNT ternary composites, and they were combined with one layer of CF by using hydraulic compression molding device in order to form the multilayer composites (Figure 3.10). Compression molding process conditions for the polymer layers and the multilayer composites are given in Table 3.12.

PS-E-CNT Polymeric Layers | One Layer of CF | PS-E-CNT-CF Multilayer Composites

Figure 3.10. Flow chart showing preparation of the multilayer composites.

Table 3.12 Compression molding conditions.

Sample	Conditions	
Polymer layers	Frame Usage	150x150x1 mm^3
	Pre-heating	20 bar, 2 min.
		50 bar, 2 min.
	Heating	100 bar, 4 min.
	Cooling	Leaving at room temperature.
Multilayer Composites	Frame Usage	None
	Pre-heating	20 bar, 6 min.
		50 bar, 6 min.
	Heating	90 bar, 6 min.
	Cooling	Leaving at room temperature.

3.2.5 Surface Modification of CF

For improving the adhesion between the layers of multilayer composites, different modification techniques were applied to the CF plies, which were MSPM treatment, PSMA treatment, bulk polymerized PS coating, in-situ polymerized PS-E coating, electrospinning of PA6 on CF surface, the combination of MSPM treatment and in-

situ polymerized PS-E blend coating and the combination of APTES treatment and electrospinning of PA6 on CF surface. Sample codes and explanations were given in Table 3.13.

The procedure of silane coupling agent treatment with MSPM is as follows. 200 mL of 90% methanol solution was prepared with 2 wt.% of MSPM. The pH of the solution was adjusted to 4.5-5 by using acetic acid. The hydrolysis time was 15 min. Solution was poured onto the CF and left at room temperature for 45 min. The solution was filtered and then the sample was dried at 100°C until the weight of filter paper and CNTs were remained constant.

A copolymer which contains similar groups with our polymer layer, PSMA was also used for surface treatment of CF. 200 mL of acetone was mixed with 2 wt.% PSMA in a beaker. Solution was poured onto the CF and cooled to room temperature. The solution was evaporated at 100°C until the weight of the beaker remained constant.

Bulk polymerization of PS was conducted and viscous PS in liquid form was directly poured onto the CF for improving the compatibility between polymer layer and CF. sPS-CF was dried in the oven at 80°C for 18 hours. 50 wt.% of the CF was coated with PS after drying.

After this modification, bulk polymerization of PS was conducted in the presence of 10 g SEBS-gMA at the beginning of mixing step and viscous PS-E in liquid form was directly poured onto the CF. sPS-E-CF was dried at 80°C for 18 hours in the oven. 16 wt.% of the CF was coated with sPS-E solution after drying. To enhance the adhesion between the composite layers further, firstly, MSPM modification was applied to the CF and then sPS-E blend was poured onto the MSPM-CF. sPS-E-MSPM-CF layer was oven dried at 80°C for 18 hours.

In order to form a nanofibrous mat on the CF surface to increase the surface area; electrospinning of PA6 onto CF surface was conducted using a solution which contained 15 wt.% PA6 in the mixture of formic acid (FA) and acetic acid (AA) in 4:1 ratio. Electrospinning was performed at 30 kV voltage, 10 cm tip to collector

distance with 0.33 mL/hr flow rate for 2 hours by using plate collector. Then to increase the compatibility between the PA6 nanofibrous mat and CF, silane coupling agent treatment with APTES was conducted. 500 mL of 80% ethanol solution was prepared with 2 wt.% SCA. The pH of the solution was adjusted to 3.5 by using acetic acid. The hydrolysis time was 30 min at 70°C. Solution was poured onto the CF and left at room temperature for 45 min. The ethanol-water solution was evaporated at 100°C until the weight remained constant. After APTES modification, electrospinning of PA6 onto CF surface was conducted under the same conditions mentioned above for 30 min by using rotating drum collector.

Table 3.13 Sample codes and preparation methods of surface modifications applied to CF.

Sample Code	Explanations
CF	Polymeric layers were combined with one ply of unmodified CF.
MSPM-CF	Polymeric layers were combined with one ply of silane coupling agent (MSPM) modified CF.
PSMA-CF	Polymeric layers were combined with one ply of Poly(styrene-co-maleic anhydride), cumene terminated modified CF.
sPS-CF	Polymeric layers were combined with one ply of bulk polymerized neat PS coated CF.
sPS-E-CF	Polymeric layers were combined with one ply of in-situ polymerized PS-E blend coated CF.
sPS-E-MSPM-CF	Polymeric layers were combined with one ply of CF firstly modified with MSPM and then coated with in-situ polymerized PS-E blend.
PA6-ES-CF	Polymeric layers were combined with one ply of CF coated with electrospun PA6 layer.
PA6-ES-APTES-CF	Polymeric layers were combined with one ply of CF firstly modified with APTES and then coated with electrospun PA6 layer.

3.2.5.1 Desizing of CF

Silane coupling agent is present on as-received CF to enhance the compatibility between polymer matrix and fabric surface. According to the information from the supplier, the silane coupling agent applied on the CF that we used in our study is compatible with epoxy resins. In order to observe the effect of removing the silane coupling agent on peel strength of the multilayer composites, silane coupling agent was removed from the CF surface. CF layers with dimensions of 30x30 cm^2 were heated in muffle furnace at 500°C in air for 2 hours. Multilayer composites were prepared with one of this desized CFs (Desized-CF). Silane coupling agent treatment with MSPM was applied to the other desized CF and then multilayer composites were prepared (Desized-MSPM-CF). The effect of sizing removal was characterized with SEM and EDX analyses and T-Peel test.

3.2.6 Preparation of Multilayer Composites with Different Number of CF Plies

In order to form multilayer composites, PS-SEBS-g-MA-CNT ternary composites were first prepared as layers and then combined with one, three and five plies of CFs using compression molding machine. The multilayer composite was also prepared with five layers of CFs which were modified with MSPM to assess the effect of surface modification on the composite performance. Contents and abbreviations of composites are given in Table 3.14. The representative flow chart for the preparation of the multilayer composite containing three layers of CF is briefly shown in Figure 3.11.

Table 3.14 Sample codes and contents of PS-E-CNT-CF multilayer nanocomposites.

Sample Codes	Contents
PS-1-CF	Two layers of PS-E-MSPM-A-CNT combined with a ply of CF.
PS-3-CFs	Four layers of PS-E-MSPM-A-CNT combined with three plies of CF.
PS-5-CFs	Six layers of PS-E-MSPM-A-CNT combined with five plies of CF.
PS-5-MSPM-CFs	Six layers of PS-E-MSPM-A-CNT combined with five plies of MSPM modified CF.

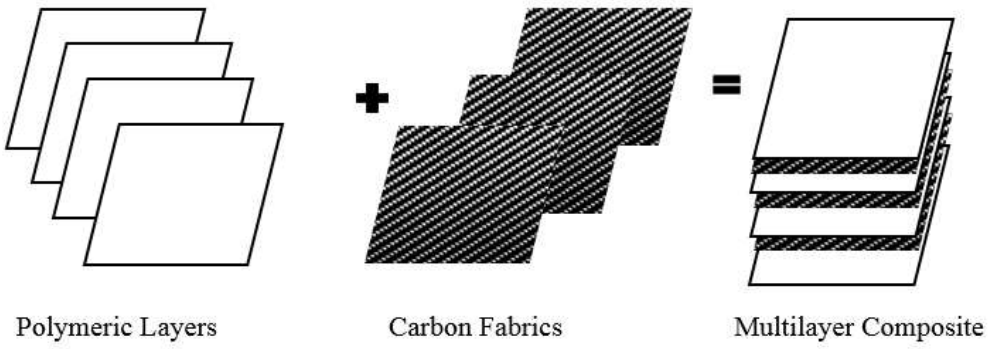

Figure 3.11. Flow chart showing the preparation of the multilayer composite.

Multilayer composites were prepared using a constant volume metal frame with dimensions of 18x18x2 cm^3 in order to obtain comparable tensile specimens. First, the weight of CF layers were measured and then the rest of the composites were completed with polymer layers to fulfill this constant volume. Therefore the polymer layers of the multilayer composites were produced separately with different processing conditions (Table 3.15). After preparing the layers, they were combined with CFs in order to fabricate the multilayer composites. Two metal plates were also used to distribute the applied pressure homogeneously throughout the multilayer composites. The program of compression molding process was followed as: first preheating without application pressure for 3 min, secondly compression at 20 bar

for 6 min, then compression at 50 bar for 6 min and finally at 90 bar for 6 min between the two PTFE sheets. Molding temperature in all the compression molding steps was 220°C. The layers and the multilayer composites were left at room temperature for cooling.

Table 3.15 Sequence of compression molding process pressure and pressure application time for the polymer layers of multilayer composites with one, three and five plies of CFs.

Sample	The polymer layers of the multilayer composites in;		
	PS-1-CF	PS-3-CFs	PS-5-CFs or PS-5-MSPM-CFs
Process Conditions	4 min 20 bar 2 min 50 bar 2 min 100 bar	3 min no pressure 2 min 20 bar 2 min 50 bar 2 min 100 bar	3 min no pressure 2 min 20 bar 2 min 50 bar 2 min 100 bar 2 min 150 bar

3.3 Characterization Methods

3.3.1 Suspension Stability Analysis of CNT Samples

Suspension stabilities of the modified and as-recieved CNTs in 15 mL PS-Toluene solution were determined by sonicating a certain amount of CNTs in PS-Toluene solution for 30 minutes at room temperature. CNT amount is 1 wt.% of the PS which was dissolved in toluene in 1:10 by weight. Pictures were taken during definite time intervals (after 3 hours, 24 hours, 96 hours, 720 hours and 960 hours) in order to observe the stability in PS solution and determine the better modification according to the observations.

3.3.2 Scanning Electron Microscopy (SEM)

Morphological analyses of ternary composites were performed by Scanning Electron Microscope (SEM) (QUANTA 400F Field Emission SEM) in METU Central Laboratory. SEM images were taken from fracture surface after impact test of injection molded bar shaped PS-E-CNT samples. In order to observe the effect of elastomeric phase in the morphology, samples were etched in an ultrasonic bath for 15 minutes at 30°C with n-heptane that dissolves the SEBS-gMA (Dike, 2011). To see the effect of etching on the samples, PS-E-CNT and PS-E-MSPM-A-CNT samples were analyzed without etching with n-heptane.

SEM images of multilayer composites were taken from the fracture surface of the tensile test specimen which were broken with the aid of liquid nitrogen. Before SEM analyses, all of the samples were coated with a thin layer of gold and palladium to prevent the accumulation of static electric field during imaging.

3.3.3 Mechanical Tests

3.3.3.1 Tensile Test

Tensile properties of binary and ternary composites were tested using a Shimadzu Autograph AG-IS 100 kN universal tensile testing instrument, according to ISO 527-2 standard for Type 5A specimen. Specifications of specimens are given in Table 3.16. Crosshead speed was taken as 3 mm/min for all the binary and ternary composites. Measurements were taken at room temperature and tensile properties were calculated from stress-strain plots. Results were given as the average of five samples and standard deviations were recorded.

Table 3.16 Dimensions of test specimens of binary and ternary composites.

Dimension	Value, mm
Overall length, minimum	75
Width at ends	12.5
Length of narrow parallel-sided portion	25
Width of narrow parallel- sided portion	4
Initial distance between grips	50
Gauge Length	50
Thickness, minimum	2

Tensile properties of multilayer composites were tested according to ASTM D638 standard. Specification of specimens are given in Table 3.17. Crosshead speed was taken as 4 mm/min and average of five samples were calculated and standard deviations were recorded.

Table 3.17 Dimensions of test specimens of the multilayer composites.

Dimension	Value, mm
Overall length, minimum	165
Width at ends	20
Length of narrow parallel-sided portion	75
Width of narrow parallel- sided portion	16
Initial distance between grips	95
Gauge Length	95
Thickness, minimum	2

3.3.3.2 Impact Test

Impact strength of the binary and ternary nanocomposite samples were determined using a Ceast Resil Impactor 6967 impact testing device according to ISO 179

Standards, instrumented with a 7.5 J hammer. Injection molded bar shaped specimens for impact tests had 4 mm thickness, 10 mm width and 80 mm length.

3.3.3.3 T-Peel Test

T-peel test specimens were prepared using compression molding process. Specimens were 22 cm in length and approximately 15 cm of them were bonded. A piece of baking paper was used as a release layer to separate the films at the edge. The samples were 2.5 cm wide. An unmodified CF layer was placed on top of the all specimens in order to increase the strength of the polymeric layer during application of tensile force. The tests were performed with Shimadzu Autograph AG-IS 100 kN universal tensile testing instrument according to ASTM D1876 standard. Crosshead speed was 10 cm/min. During the test, load versus peeled distance plot was obtained. The average force after the initial peak load divided by the specimen width was taken as the peel strength. The results were represented as average of five measurements and standard deviations were reported. Schematic representation of T-peel test specimen is given in Figure 3.12.

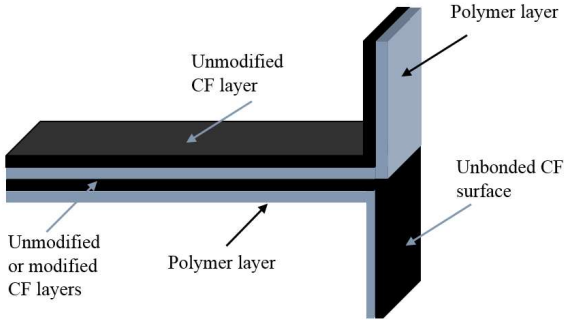

Figure 3.12. T-peel test specimen.

3.3.4 Electrical Resistivity Measurements

Electrical resistivity values of binary, ternary and multilayer composites were measured with two-point probe method, for which the probes were connected to a Keithley 2400 SourceMeter constant current source meter (Figure 3.13). Measurements were conducted by contacting the compression molded samples to the crocodile probes. Average result of twenty measurements was reported for each material.

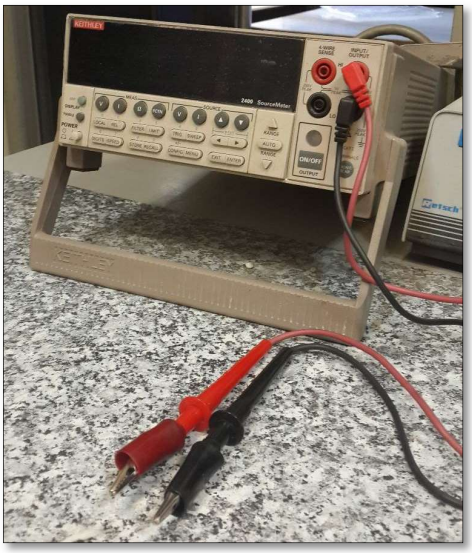

Figure 3.13. Keithley 2400 Constant Current SourceMeter.

3.3.5 Optical Microscopy

Olympus BX50 light microscope with a LBD (Light Blue Daylight) filter was used to obtain the optical microscopy images. To observe the agglomerates in the binary composites of PS and CNTs, imaging was performed in the bright-field mode with 10x objective.

Polymer layer, as-received CF surface, and the surfaces of T-peel test specimens, which are shown in Figure 3.12, were also investigated with an optical microscope. Imaging was obtained with Olympus BX53M light microscope in reflecting mode. During imaging objector was set as 4x, polarized light was used and exposure time was changed according to the brightness of the surface. Images for the peeled surface of bulk polymerized PS coated CF (sPS-CF) were taken with bright-field mode.

3.3.6 Fourier Transformed Infrared (FTIR) Spectroscopy

FTIR Spectroscopy analyses were performed using a Shimadzu, IR-Prestige-21 FTIR Spectrometer to determine the chemical groups of sPS, sPS-CNT masterbatches and CNT samples. To create the spectra of CNTs, they were pressed with KBr in powder form. FTIR spectra of the samples were recorded in the range of 600 cm^{-1}- 4000 cm^{-1} and number of scan was 12.

To confirm the existence of modification on the multilayer composite layers, a Perkin Elmer Spectrum Two FTIR Spectrometer instrument with attenuated total reflection (ATR) accessory was used. FTIR spectra of samples were recorded in the range of 500 cm^{-1}- 4000 cm^{-1} with scan number of 12.

3.3.7 Thermogravimetric Analysis (TGA)

The degradation temperatures at maximum weight loss of sPS and sPS-CNT masterbatches were determined with a Shimadzu, DTG-60/60H Thermal Gravimetric Analyzer (TGA). Samples were heated from 20°C to 700°C with a constant heating rate of 10°C/min, under nitrogen atmosphere with a flow rate of 70 ml/min. The results were represented as TGA plots from one measurement and the temperature range of degradation was recorded.

TGA was performed to control the results of ash content analysis applied to multilayer composites by heating the samples in air atmosphere from room

temperature to 900°C with a heating rate of 10°C/min. The results were represented as average of two measurements and standard deviations were recorded.

3.3.8 Differential Scanning Calorimetry (DSC)

The glass transition temperature (T_g) of sPS and sPS-CNT masterbatches were determined by using a Shimadzu, DSC-60 Differential Scanning Calorimeter. Samples were heated from 20°C to 250°C with a constant heating rate of 10°C/min, and then cooled to room temperature, and heated to 250°C again. The analyses were performed under nitrogen atmosphere.

3.3.9 Viscosity Average Molecular Weight (M_v) Measurements

The viscosity average molecular weight of sPS was calculated using intrinsic viscosity in Mark-Houwink-Sakurada equation. Dilute sPS solutions were prepared with different concentrations from 0.28 g/dL to 1.2 g/dL. Flow times of the solutions were measured at 30°C by using an Ubbelohde viscometer. Inherent and reduced viscosities were plotted with respect to the concentration of solutions to find intrinsic viscosity.

3.3.10 Gel Permeation Chromatography (GPC)

Average molecular weights of bulk polymerized neat PS were measured by GPC (Polymer Laboratories PL-GPC 220) in METU Central Laboratory. GPC (also known as size-exclusion chromatography, SEC) is also used for determining number average, weight average and Z average molecular weights and polydispersity index of prepared samples. The temperature of the module containing detectors was kept constant at 35°C. Molecular weight between 200-2x10^6 Da can be measured with triple detection which were light scattering, viscometer and reflective index. THF was used as solvent and 0.05 g of neat sample must be homogeneously dissolved in

this solvent. The flow rate of polymer solution passing through the column was 1 mL/min.

3.3.11 Melt Flow Index (MFI) Measurements

MFI measurements were carried out according to the ASTM D1238-13 standard with an Omega Melt Flow Indexer. The measurements were done at 200°C using 5 kg load. The weight of polymer melt which passes through the die in 10 seconds was measured and recorded. At least five measurements of each sample were taken to obtain more accurate results. The MFI value was reported in grams/10 min.

3.3.12 Contact Angle Measurements

Contact angle measurements were performed with sessile drop method according to ASTM D7490-08 standard. Water and diiodamethane (DIM) were the probe liquids. Water was used to calculate the polar component and DIM were used to calculate the dispersion component. Contact angles were measured using Drop Analysis-LB-ADSA plug-in in ImageJ (NIH, USA) software. The Owens-Wendt-Kaelble equation was used for calculating polar and non-polar components of surface tension and work of adhesion was calculated from Young-Dupre equation.

3.3.13 Ash Content Analysis

Fiber amount of the composites were determined with a procedure according to ASTM D5630 but with a different temperature determined from TGA curve of as-recieved CF sample given in Appendix A. Less than 4% of fiber loss was observed at 650°C and ash content analyses were conducted at this temperature. In this procedure, 2 grams of each specimen were heated in porcelain crucibles at 650°C in a furnace. First, empty crucibles (w_1) were weighed and recorded and then crucibles were weighed again after filling with samples and recorded as w_2. Finally, after

burning for 20 minutes, crucibles were placed into a desiccator and after cooling weight of the cooled crucibles were recorded as w_3. Fiber content of specimens were calculated according to the equation given below.

$$\text{Fiber content, wt. \%} = \frac{(w_3 - w_1)}{(w_2 - w_1)} \times 100 \quad (3.1)$$

3.3.14 Shape Memory Behavior Analyses with Bending Test Actuated by Heat and Electricity

Thermally triggered bending test specimens of the ternary and multilayer composites with the dimensions of 5x70 mm^2 were prepared by cutting them from the compression molded films. They were bended to 90° by heating to a higher temperature (110°C) than T_g (determined with DSC as 102°C) of PS-E-CNT composites in the oven. Samples were placed in a beaker to take the shape of 'L' and force was applied to its middle point. Then they were fixed to their temporary 'L' shape by dipping the beaker into the liquid nitrogen. As the final step, samples were put into the oven and heated again so the samples began to return their permanent shape.

Electrically actuated shape memory properties of the multilayer composites were determined using a temperature control and adjustable power supply which was designed by Entek Electronics Tic. Ltd. Şti., Turkey. "π" shaped specimens with the dimensions of 2 mm in thickness, 5 mm in width of both ends, 30 mm in length of both parallel arms and 25 mm in total width were used for testing (Yanju Liu et al., 2009). Firstly, the specimens were bent to a certain angle with the aid of the curvature of a beaker, and they were cooled down to their T_g with liquid nitrogen. 0.9 ampere was applied and the bending test was performed. To calculate the shape recovery ratios with respect to time, video was recorded with a camera. Shape recovery ratio is calculated by the equation given below:

$$\text{Shape recovery ratio, \%} = \frac{\theta_i - \theta_f}{\theta_i} \times 100 \quad (3.2)$$

where, θ_i is the initial deformation angle, θ_f is the final deformation angle. The elapsed time until the bended samples was recovered their initial shape was also recorded as shape recovery time. The plane with the crocodile probes to which the specimens were attached was taken as reference for the measurement of the angles which were at the beginning of the test and after recovery. When the sample was at the same level with this plane, %100 recovery was achieved. One heating cycle was applied and given results were the average of five samples.

CHAPTER 4

RESULTS AND DISCUSSION

4.1 Surface Treatment and Modification of CNTs

In this section, surface treatment and modification of CNTs were conducted. First, the suspension stability of the modified CNTs was observed. Then, PS-CNTs binary composites were produced at different melt mixing conditions and characterized by optical microscope analysis, electrical resistivity measurements, tensile and impact tests. Also, PS-E-CNTs ternary composites were produced with selected modified CNTs and characterized with SEM analyses, electrical resistivity measurements, tensile and impact tests, and bending tests triggered with heat.

4.1.1 Suspension Stability Analysis

The images of as-received CNTs and CNTs, which were modified with SDS, PSMA, TX100, SDBS, MSPM and GLYMO and then dispersed in PS-Toluene solution are given in Figure 4.1. CNTs without modification were started to precipitate after filling the sample containers immediately due to the lack of functional groups on the CNT walls to form the interaction between PS and CNTs.

Stability of the suspensions of CNTs was ranged as MSPM-A-CNT> SDBS-A-CNT> TX100-A-CNT> SDS-A-CNT> CNT> PSMA-A-CNT> GLYMO-A-CNT. According to the observations, weaker interaction was observed in SDS-A-CNTs than CNTs, which were modified with SDBS and TX100 due to the lack of benzene ring in the SDS structure. The benzene ring in the molecules is adsorbed strongly to the graphitic surface of CNTs due to π–π stacking type interaction (Youssry, Al-Ruwaidhi, Zakeri, & Zakeri, 2020). In terms of alkyl chain length, CNTs performed better stability when treated with SDBS (12-carbon alkyl chain) than TX100 (8-

carbon alkyl chain). Hydrophobic tail groups of surfactants showed a tendency to lie flat on the graphitic surface of CNTs due to the compatibility of the graphitic unit cells with the methylene units of hydrocarbon chains. Surfactants containing longer tails have high spatial volume and more steric hindrance, resulting in ensuring enhanced repulsive forces among CNTs (Rastogi et al., 2008). Also, different behavior of SDBS and TX100 arose from the different chemical structures of their head groups. The head group of TX100 (polyethylene oxide chain) is polar and larger than that of SDBS (SO_3^-) resulted in low packing density compared to that of SDBS (Islam et al., 2003). The stability of the PSMA-A-CNTs was not good in the PS-toluene solution. In this material, polystyrene and maleic anhydride groups were present, but these compatible groups cannot show enhancement in dispersion of CNTs. This may be due to the application of the modification technique with this modifier.

The worst stability was observed in GLYMO-A-CNT sample. GLYMO material is a bifunctional organosilane with three methoxy group in one side and on the other side there is an epoxy group. This material is generally used for reinforcing epoxy matrix (Hoepfner & Pezzin, 2016). This may be the reason of the non-compatibility of the GLYMO-A-CNT sample with PS matrix. The highest stability was reached in MSPM-A-CNT sample. MSPM is a methacrylfunctional silane coupling agent. The alkoxy group of this molecule hydrolyzes in the presence of the water to form methanol and silanol groups. This reactive groups are interacted with the polymer matrix. The composite structure of PS and MSPM-A-CNT may be evaluated as compatible according to the stability of the suspension of this sample. Based on the the results of these observations, binary nanocomposites of PS-CNTs were prepared with CNTs modified with SDBS, TX100 and MSPM.

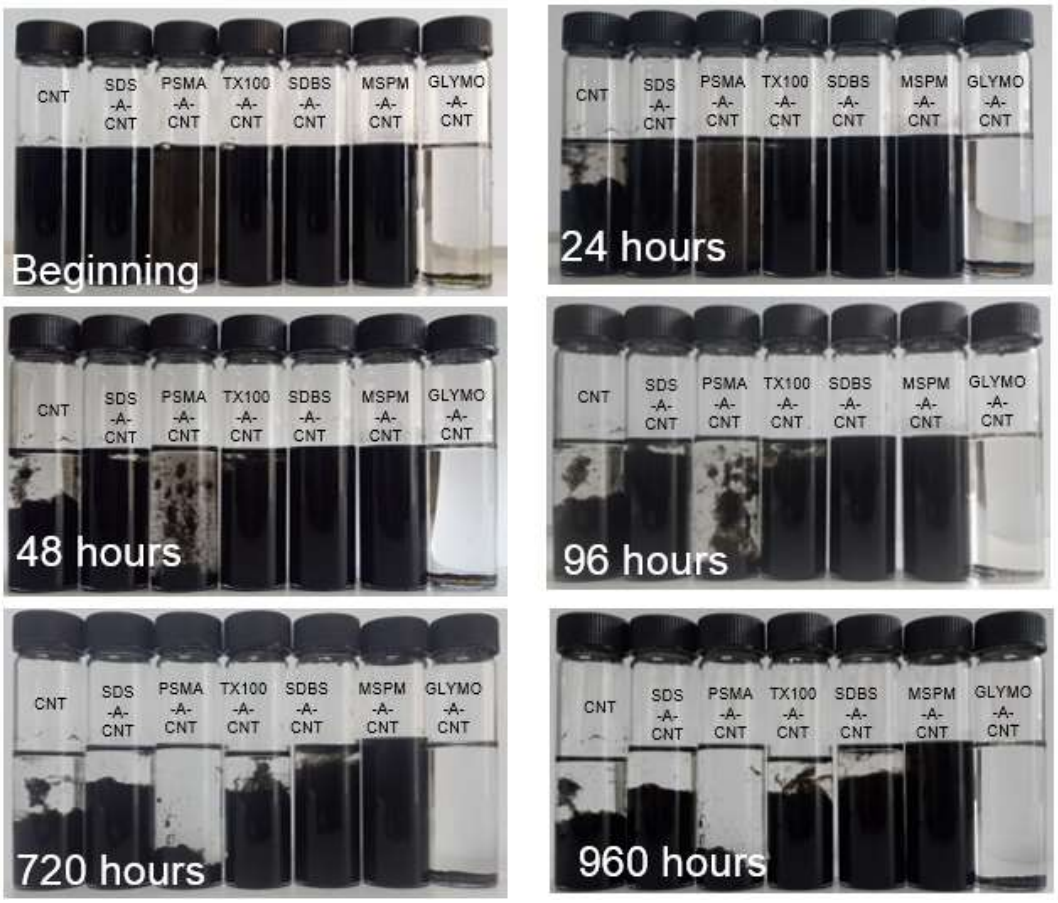

Figure 4.1. Suspension stabilities of CNT samples in PS-Toluene solution with and without surfactant assistance.

4.1.2 Characterization of PS-CNT Binary Composites

4.1.2.1 Optical Microscopy Analysis

Optical microscope imaging, performed from compression molded films (Figure 4.2), of binary PS-CNT nanocomposites prepared with first set of extrusion, which was performed with ground PS, at a screw speed of 150 rpm and a feed rate of 25 g/min, explained in Section 3.2.2 are shown in Figure 4.3. Dark spots of the images represent the agglomerate structures. The calculated percentage of the area covered

by the agglomerates in the images taken from at least three different regions of the film samples is given in Table 4.1.

The area covered by the agglomerates in the composites was decreased with surface modifications applied to the CNTs compared to PS-CNT composite. Surface modified CNTs tended to reagglomerate during the melt blending process when the conditions of high screw speed and high feed rate (first set) were observed from the optical images. The highest area covered by agglomerates was reached in PS-TX100-A-CNTs sample; as can be seen from the optical microscope images, the dispersion of CNTs seemed to be homogeneous but with large agglomerates. 32.9% agglomerate covered area was achieved in the PS-MSPM-A-CNT sample. When the results of the SDS-A-CNT and SDBS-A-CNT added composites were compared, in PS-SDBS-A-CNT sample, agglomerates were covered 20.2% of the image, and for the PS-SDS-A-CNT sample, this value was 25.7%. However, the standard deviation of PS-SDS-A-CNT sample was higher than the PS-SDBS-A-CNT sample. This was explained with non-homogeneous dispersion CNTs with SDS modification and the better dispersion of SDBS-A-CNTs due to the benzene group in the SDBS molecule. The lowest area covered by CNTs was observed in PS-PSMA-A-CNTs sample, as can be seen from the optical microscope images; this area was consisting of agglomerates. This modification was not suitable for homogeneous dispersion of CNTs in the PS matrix, as seen in Figure 4.2. Images of GLYMO-A-CNT samples cannot be taken because CNTs and PS phases were incompatible with each other, and the sample was transmitted the light directly from the CNT-free areas of the samples. The images were too bright to detect the CNTs in these films. Conditions of the extrusion process were reconsidered to achieve a more homogeneous dispersion of CNTs in PS, and the second set was designed with a lower screw speed (100 rpm) and feed rate (15 g/min). Changes in extrusion process conditions were expected to favor the dispersion of CNTs in PS. According to the suspension stability results and optical images of the samples, binary nanocomposites of PS-CNTs and ternary composites of PS-E-CNTs were prepared with CNTs modified with SDBS, TX100, and MSPM.

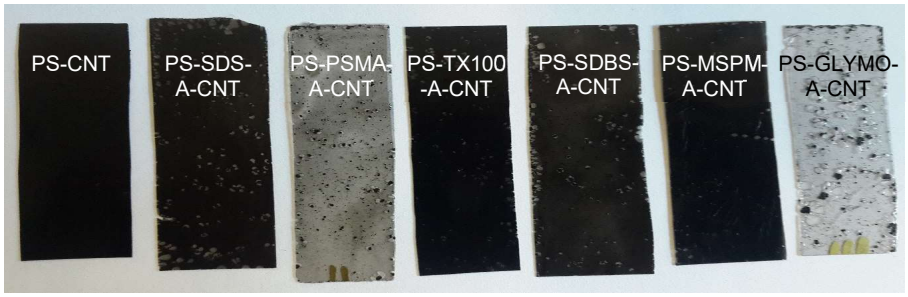

Figure 4.2. Film samples produced with binary composites of PS reinforced with as-received and modified CNTs.

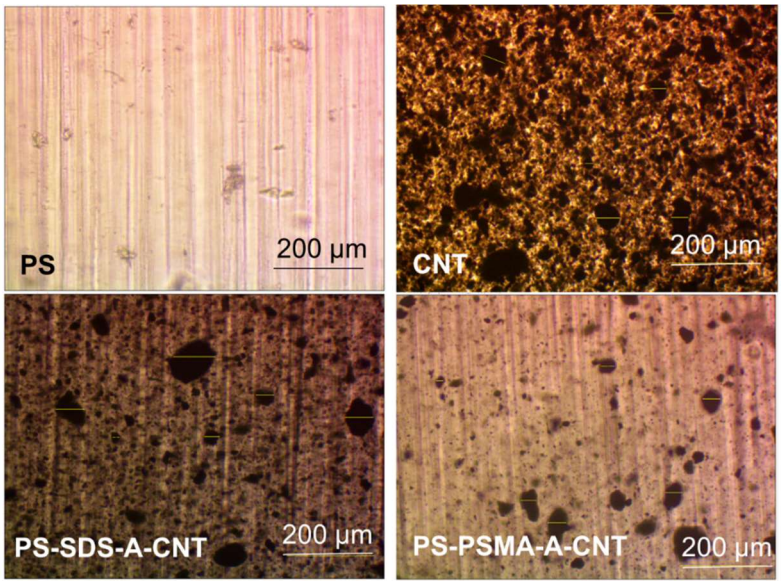

Figure 4.3. Optical Microscope images of PS-CNT binary composites prepared with different surface modifiers.

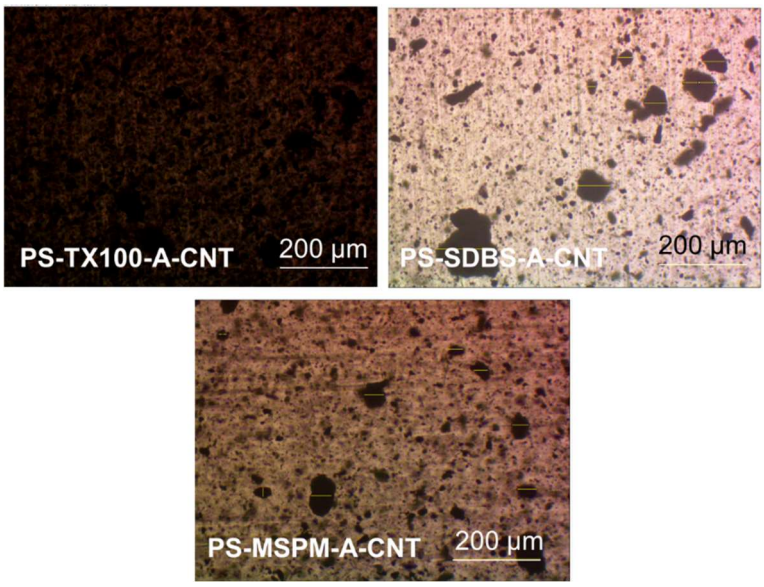

Figure 4.3. (cont'd) Optical Microscope images of PS-CNT binary composites prepared with different surface modifiers.

Table 4.1 The calculated percentage of the area covered by the agglomerates in the PS-CNT nanocomposites.

Sample code	Area, %
PS-CNT	69.5 ± 0.1
PS-SDS-A-CNT	25.7 ± 5.9
PS-PSMA-A-CNT	11.5 ± 4.6
PS-TX100-A-CNT	60.2 ± 3.6
PS-SDBS-A-CNT	20.2 ± 1.3
PS-MSPM-A-CNT	32.9 ± 2.6

4.1.2.2 Electrical Resistivity Measurements

The electrical resistivities of the PS-CNT composites prepared with 1 wt.% as-received and modified CNTs were measured with two probe method from the compression molded films (Figure 4.2). The comparison of the electrical resistivity values of all the composites is shown in Figure 4.4. The detailed measurements can be seen in Appendix B.

The percolation threshold is the definition of the critical point that beginning a sharp reduction of the electrical resistivity with increasing the filler content. Above the percolation threshold value, a transition from electrical insulator to conductor is observed due to the formation of the conductive pathway of the fillers. The fillers control the electrical conductivity of the sample above the percolation threshold value (Cheng Zhang, Zhu, Ma, & Sumita, 2009). According to the technical data sheet, volume resistivity of PS is 10^{14} ohm.cm ("Technical Data Sheet of PS Crystal 1540," 2017). The electrical resistivity values of the PS-CNT composites were lower than 10^{8} ohm.cm at 1 wt.% CNT loading, which revealed that the percolation threshold concentration of these composite systems was lower than this CNT content. According to the general conductivity range of conducting polymers, 10^{8} ohm.cm is the limit of the semiconductor region (Le, Kim, & Yoon, 2017). The CNT content of the samples was kept at 1 wt.% in all the composites.

The effect of process conditions of the melt mixing method on the dispersion of CNTs in PS was observed in PS-CNT sample significantly. The electrical resistivity of this sample was decreased to $10^{4.1}$ ohm.cm from $10^{5.5}$ ohm.cm with decreasing the screw speed to 100 rpm from 150 rpm and decreasing the feed rate to 15 g/min from 25 g/min. This result can be attributed to the fact that the agglomerates were contributed to the formation of the conductive pathway by breaking down, with the increase in the residence time of the material in the extruder resulted from the changes in the process conditions made in the second set.

The electrical resistivity increased with the addition of modified CNTs to approximately 10^8 ohm.cm, but still, these values were in the semiconductor region. Acid modification and surface modification affected the conductivity of CNTs negatively because oxygen-containing groups and also defects were formed on the surface of the CNTs led to a decrease in conductivity with modification on the surface (Braga, Zaggo, Montagna, & Passador, 2020; Moreno Marcelino, Vigueras Santiago, López Téllez, & Hernández López, 2014). It was expected that electrical resistivity values were high in composites prepared with homogeneously dispersed CNTs owing to the better interaction of surface modifier and a thick layer of surfactant on CNT surface. The surface modification also enhanced the interaction between polymer matrix and fillers, so conductivity decreased with wetting of CNT surfaces with PS. Similar behavior was observed in both processing sets in terms of electrical resistivity.

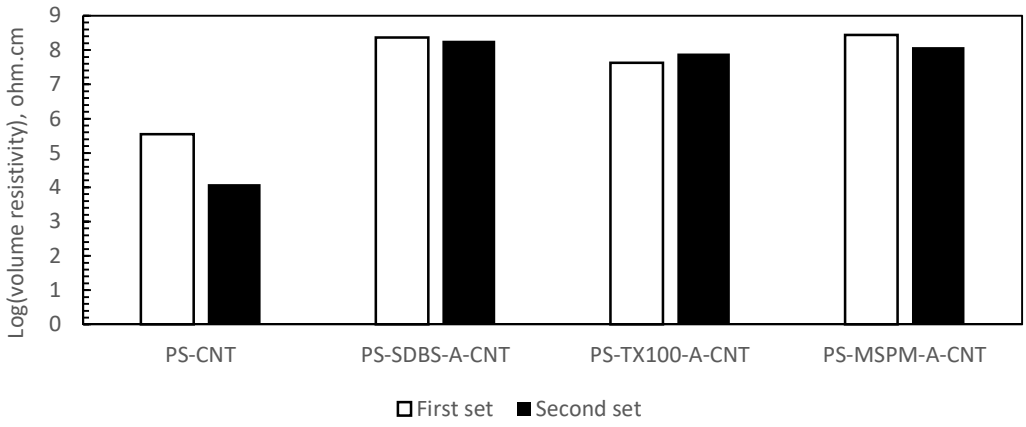

Figure 4.4. Electrical resistivity values of the binary composites.

4.1.2.3 Tensile Test Results

Tensile strength values of the binary composites produced with different melt mixing conditions are shown in Figure 4.5 and the detailed test results of the tensile test are given in Appendix C. Grinding process applied in the first set decreased the tensile

strength of neat PS to 34 MPa from 42 MPa which is given in the technical data sheet. A significant decrease in tensile strength to 22 MPa was observed with introducing CNTs to neat PS, in the PS-CNT sample due to the stress concentrated areas occurring from the highly agglomerated particles in the matrix.

In the second set of experiments, PS was not ground, fed from main feeder and CNTs fed from hopper by hand to achieve 1 wt.% CNT. The screw speed was decreased to 100 rpm from 150 rpm, and the feed rate was decreased to 15 g/min from 25 g/min. A similar tensile strength value with the technical data sheet was achieved without grinding and new melt blending conditions for neat PS samples. Tensile strength of the composites prepared with modified carbon nanotubes was higher than the composites produced with as-received CNTs in both methods. After acid treatment and surface modification, chemical compatibility in the composites was increased. The defect sites on the surface of CNTs can increase the mechanical interlocking and interaction between CNTs and polymer matrix (Yesil, 2010). An improvement in tensile strength was achieved with the conditions applied in the second set. Lower screw speeds allow lower cutting and kneading forces and favor erosion processes. Reducing the screw speed increases the residence time of the material inside the extruder, improving dispersion due to better rupture of nanotube agglomerates (McClory et al., 2011).

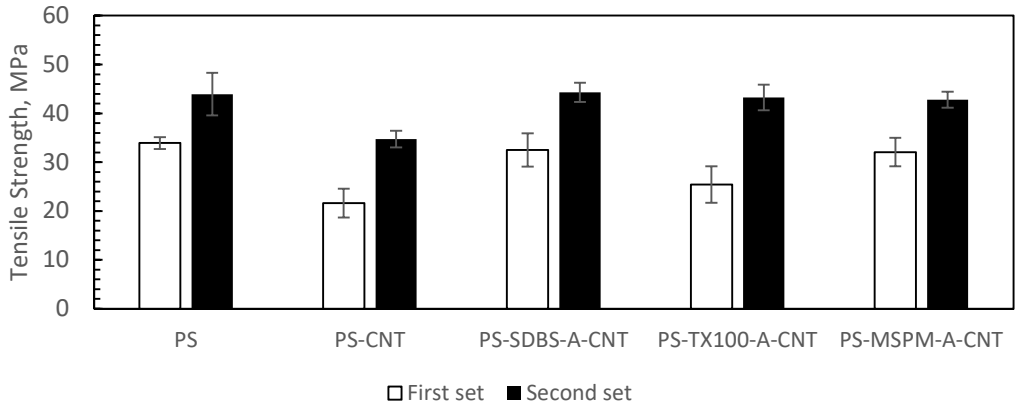

Figure 4.5. Tensile strength values of the binary composites.

Tensile moduli of the binary composites are given in Figure 4.6. Tensile modulus values of PS-CNTs composites were slightly higher than neat PS sample based on the increase in stiffness with the addition of CNTs in both sets of experiments. Defects on the CNTs surface are also expected to influence the mechanical properties. The methods of handling nanotubes, including acid treatments and sonication for a long time are known to shorten nanotubes results in decreasing aspect ratio and are detrimental to mechanical properties (Choudhary, Singh, & Mathur, 2013).

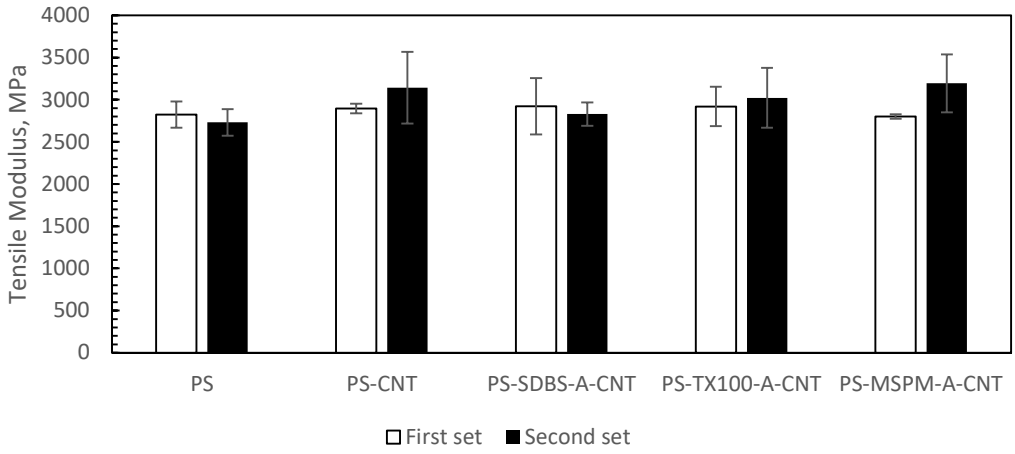

Figure 4.6. Tensile moduli of the binary composites.

Elongation at break values of the binary composites are given in Figure 4.7. In binary composites, elongation at break values did not show a trend in both sets of experiments. The value of neat PS decreased with the addition of 1 wt.% as-received CNTs due to the brittle structure of CNTs and the weak points that formed by the agglomerations. In the second set of experiments; PS-SDBS-A-CNT, PS-TX100-CNT and PS-MSPM-A-CNT composites showed higher elongation at break values than PS-CNT sample due to the development of dispersion of CNTs in the polymer matrix.

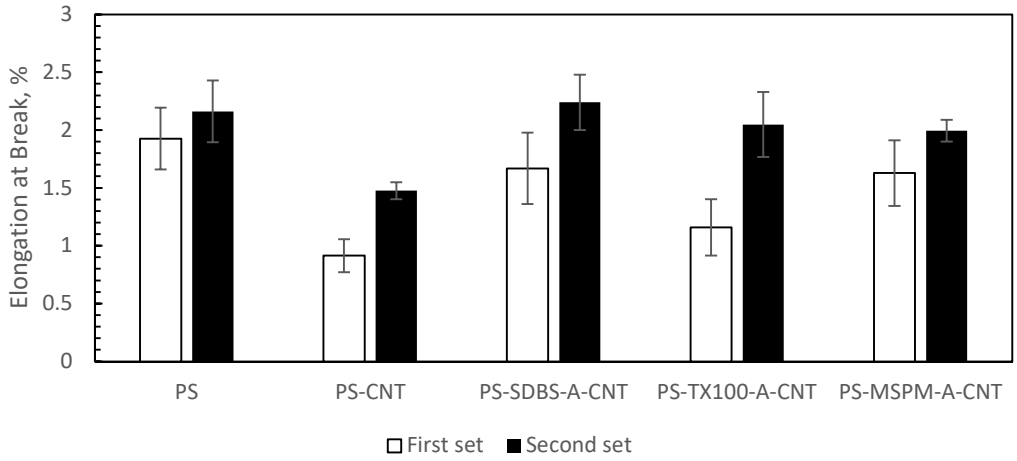

Figure 4.7. Elongation at break values of the binary composites.

4.1.2.4 Impact Test Results

The impact strength of the neat PS, PS-CNT, PS-SDBS-A-CNT, PS-TX100-A-CNT and PS-MSPM-A-CNT samples, which were given in terms of two sets of processing conditions based on grinding of PS pellets, screw speed and feeding rate are represented in Figure 4.8 and the detailed values are given in Appendix C. The impact strength values of the samples prepared with the first set almost did not change with the addition of CNTs. In the samples prepared with the second set, it is seen that the impact resistance was reduced in the CNT added samples when compared to the neat PS. Even if the agglomerates were dispersed to a certain extent by reducing the screw speed, it did not contribute to the improvement of the impact strength. The highest value was reached for PS at 11.9 kJ/m^2. Carbon nanotube addition to the PS matrix decreased the impact strength of these composites produced in both sets due to the lower impact energy absorbance of the rigid carbon nanotube particles. There was no significant difference in the impact strength of binary composites produced with modified CNTs by different modifiers.

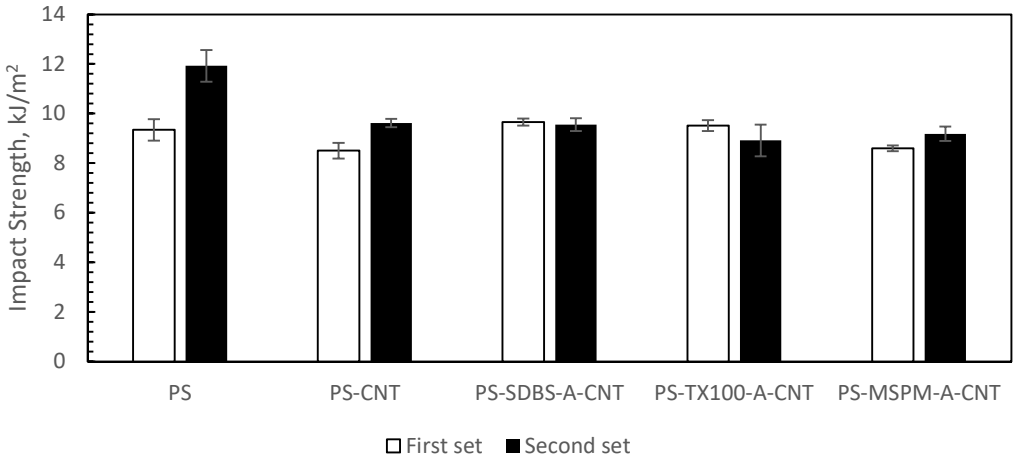

Figure 4.8. Impact strength values of the binary composites for surface modifier selection.

4.1.3 Characterization of PS-E-CNT Ternary Composites

The purpose of preparation of the ternary composites was to improve processability and shape recovery properties of the composites without sacrificing their mechanical properties. In the shape memory composites produced in this study, PS acted as a hard segment and the PS compatible elastomer (SEBS-gMA) was used to form a soft segment. On account of this, preliminary experiments were performed to determine the optimum concentration of the elastomer in the ternary composite structure.

The SEBS-gMA was blended with PS at different concentrations of 5 wt.%, 10 wt.%, 20 wt.%, 30 wt.% and 40 wt.% to determine the most suitable elastomer concentration. Melt mixing conditions were screw speed of 100 rpm, the feed rate of 15 g/min as determined in the PS-CNT composites production. Polymer layers were produced by compression molding with these blends. The images of the dog bone shaped PS-E-CF samples are given in Figure 4.9. Multilayer composites containing two layers of PS and 5wt.%, 10 wt.%, 20wt.% and 30wt.% SEBS-gMA and a CF layer were not sufficiently flexible, so they were broken the during preparation of the samples for the mechanical tests. When the elastomer concentration was

increased to 40 wt.%, tensile test specimens were obtained without cracks. Therefore the composites were prepared with 40 wt.% elastomer concentration in the present study.

Figure 4.9. PS-E-CF samples prepared with different amount of elastomer (SEBS gMA) addition.

4.1.3.1 Scanning Electron Microscopy (SEM) Analysis

Improving the toughness of PS is achieved by modification with rubbery block copolymers and this improvement is explained with the dispersion of the rubber phase in polymer matrix. The morphology of PS, elastomer phase, and CNTs were examined with SEM analysis. The elastomeric phase in the composites was observed by etching the samples with n-heptane (Dike, 2011). To see the effect of etching on

the samples, PS-E-CNT and PS-E-MSPM-A-CNT composites were analyzed without etching with n-heptane.

SEM micrographs of neat PS are given in Figure 4.10. Straight crack propagation lines were observed rather than tortuous lines, which represent the brittle nature of PS. The indication for the easy fracture of PS with a few amounts of energy is those straight lines. PS sample was also etched to check the insolubility of PS in heptane. Etching with n-heptane did not affect the crack propagation lines of PS as can be seen from the SEM images.

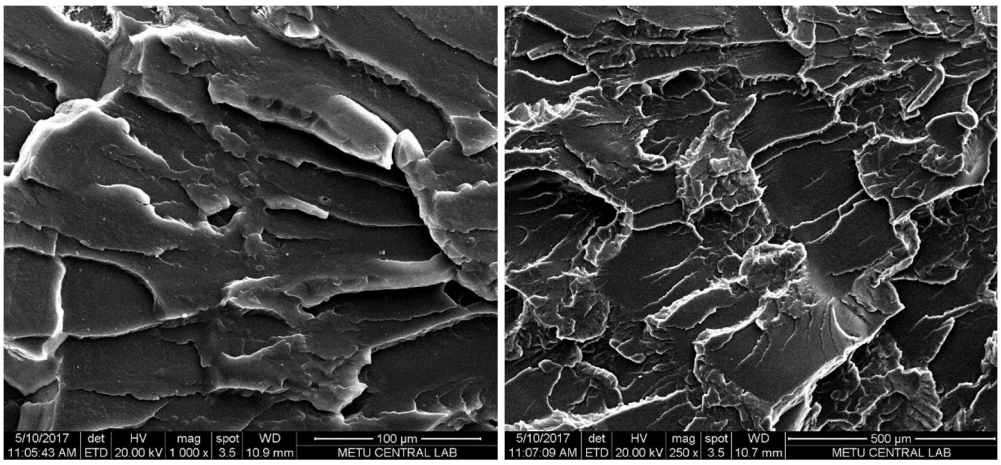

Figure 4.10. Neat PS sample from fracture surface at 1000x and 250x (etched with n-heptane).

SEM micrographs of the PS-E sample are illustrated in Figure 4.11. In these images, the crack lines were denser, resulting in an increase in the energy needed to keep the cracks moving for failure of the material (Dike, 2011). According to the phase inversion criterion, the phase with lower viscosity and higher volume fraction tends to be the continuous phase. PS was the continuous and SEBS-gMA phase was the distributed phase in our blends. The dispersed phase structure was transformed into a co-continuous structure with increasing elastomer content. A high quantity of polymer matrix and elastomer was required to form of co-continuous structures in polymer blends (Mekhilef et al., 1996). The concentration where the co-continuous

phase morphology becomes observable is called phase inversion point and this point was 40 wt.% content of SEBS-gMA in the present study.

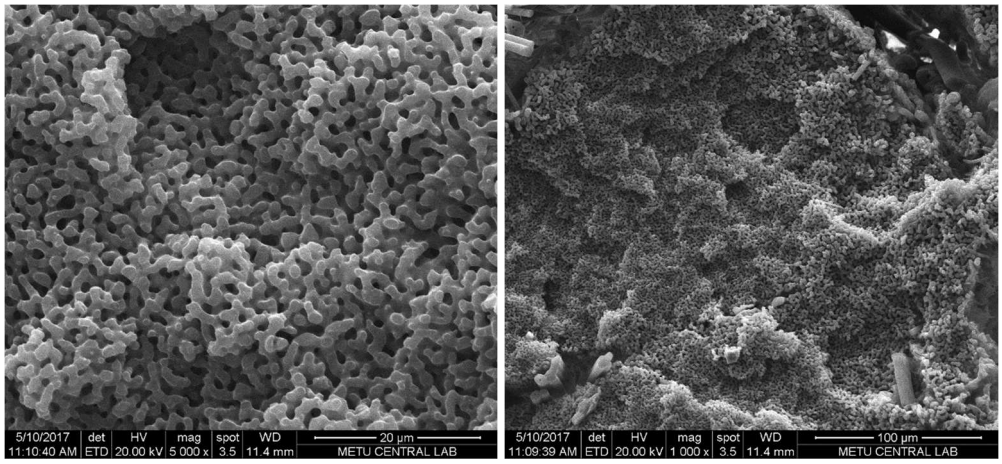

Figure 4.11. PS-E sample from fracture surface at 5000x and 1000x (etched with n-heptane).

SEM micrographs of binary composites of PS-E and ternary composites of PS-E-CNT samples are given in Figure 4.12. Agglomerates of CNTs with different sizes were observed in PS-E-CNT sample (Figure 4.12 (b)). Defects as deterioration in the co-continuous structure were detected in the A-CNTs added sample (Figure 4.12 (c)) and failure in the acidic characterization of the CNTs may be the reason for this behavior. With surfactant treatment using SDBS and TX100, vacancies of elastomer left in the samples were obtained to be smaller (Figure 4.12 (d) and (e)) and agglomerates of CNT were seen easily. Microfibrous structures were formed with silane coupling agent treatment with MSPM, and CNT clusters were homogeneously dispersed in this sample as seen in Figure 4.12 (f).

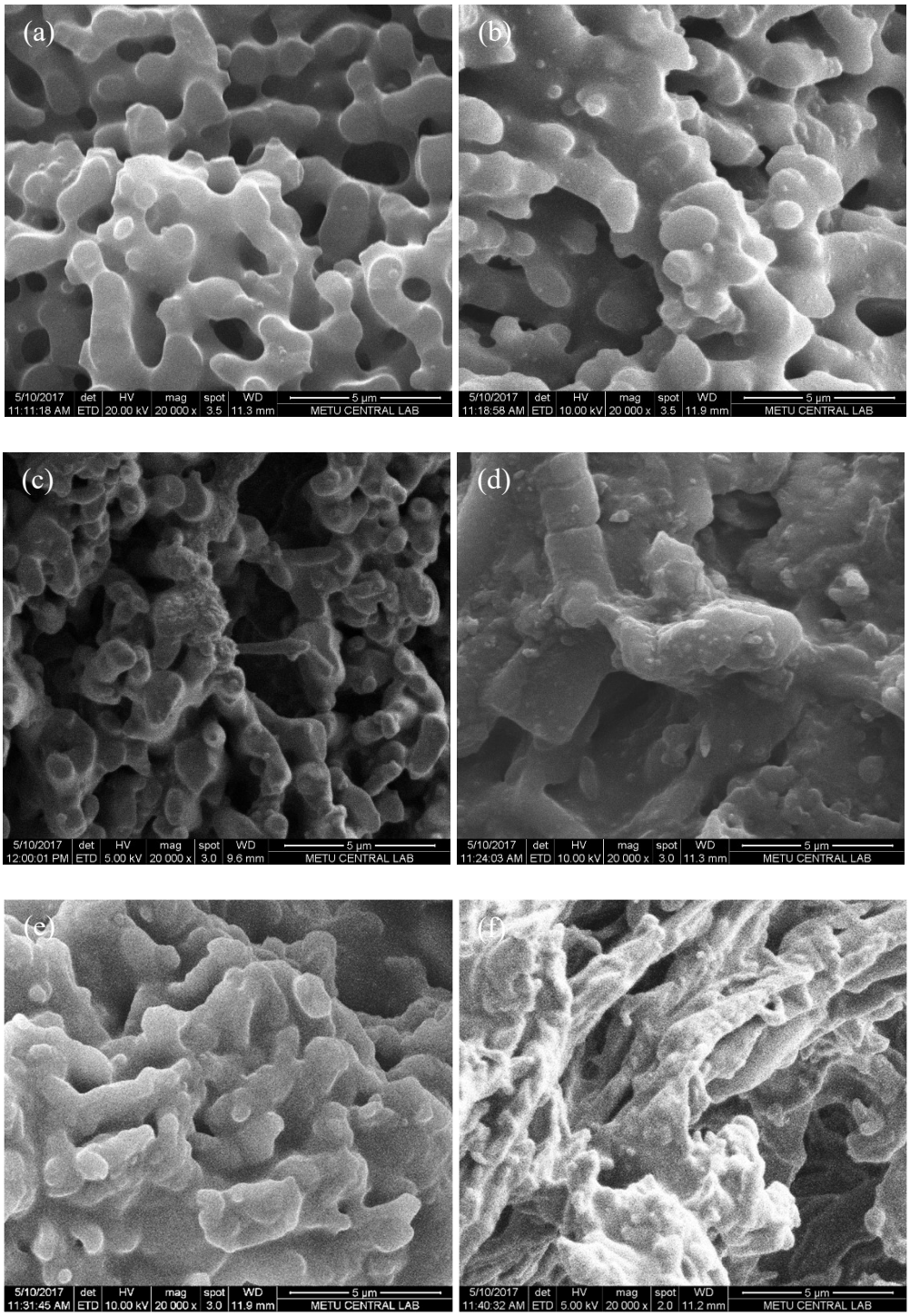

Figure 4.12. SEM images of (a) PS-E, (b) PS-E-CNT, (c) PS-E-A-CNT, (d) PS-E-SDBS-A-CNT, (e) PS-E-TX100-A-CNT, (f) PS-E-MSPM-A-CNT at 20000x magnification (etched with n-heptane).

In order to see the effect of etching; PS-E-CNT and PS-E-MSPM-E-CNT samples were analyzed from the fracture surface of impact specimens without etching with n-heptane (Figures 4.13 and 4.14). In the PS-E-CNT samples, CNTs distributed in the elastomer phase were observed, but these regions were not homogeneous. According to the physical appearance of the samples, the most homogeneous sample was PS-E-MSPM-A-CNT compared to PS-E-CNT composite due to the improvement of the dispersion of CNTs with silane treatment.

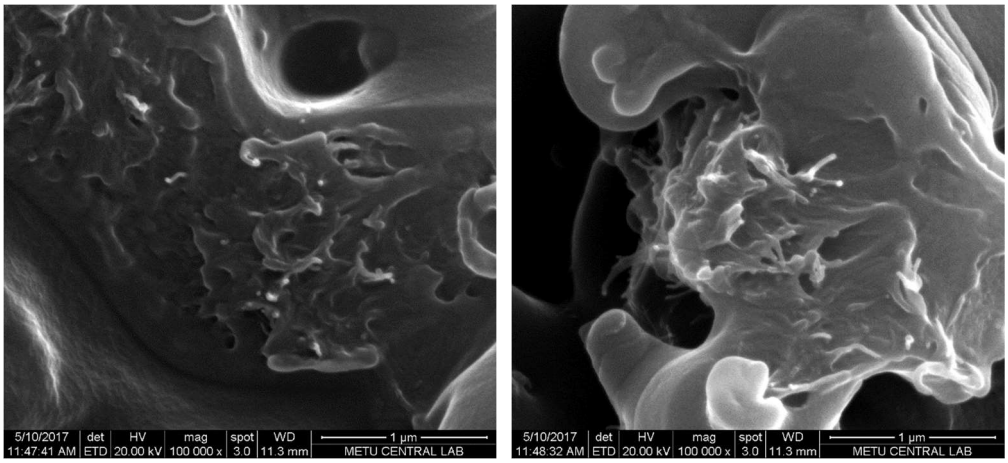

Figure 4.13. PS-E-CNT sample from fracture surface at 100000x (un-etched).

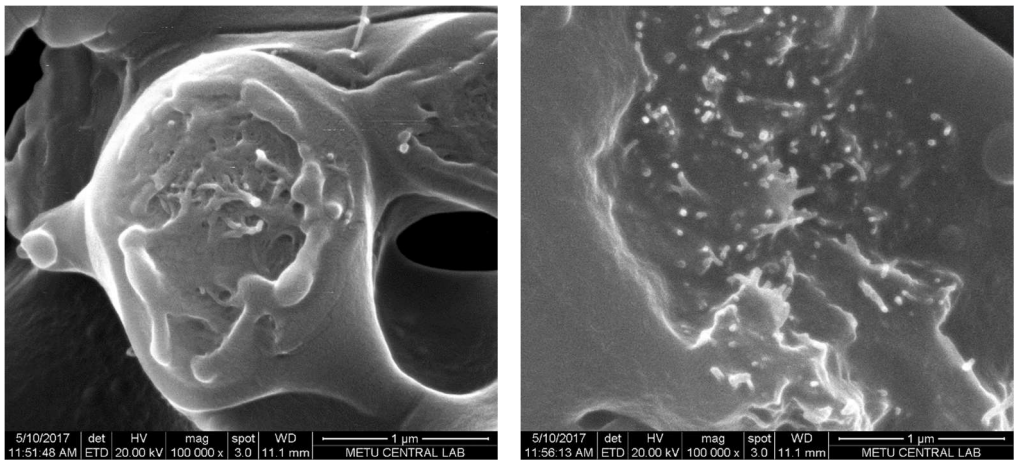

Figure 4.14. PS-E-MSPM-A-CNT sample from fracture surface at 100000x (un-etched).

4.1.3.2 Electrical Resistivity Measurements

The electrical resistivities of the PS-CNT and PS-E-CNT ternary composites prepared with as-received and modified CNTs measured with two probe method from compression molded films are shown in Figure 4.15. The detailed test results are given in Appendix B. Blending with elastomer was resulted in an increase to $10^{8.7}$ ohm.cm in electrical resistivity compared to PS-CNT sample, which was $10^{4.1}$ ohm.cm.

With surface modification, an insulating modifier layer was coated on CNTs surfaces. This layer did not allow the transportation of electrons effectively, which decreased the electrical conductivity of the CNT aggregates (Gojny et al., 2006). The lowest electrical resistivity was reached in MSPM-A-CNT added sample as $10^{8.2}$ ohm.cm. This may be resulted from the improved dispersion of CNTs and the formation of a longer conductive pathway of CNTs with silane coupling agent modification technique than the non-covalent modification technique applied with surfactants.

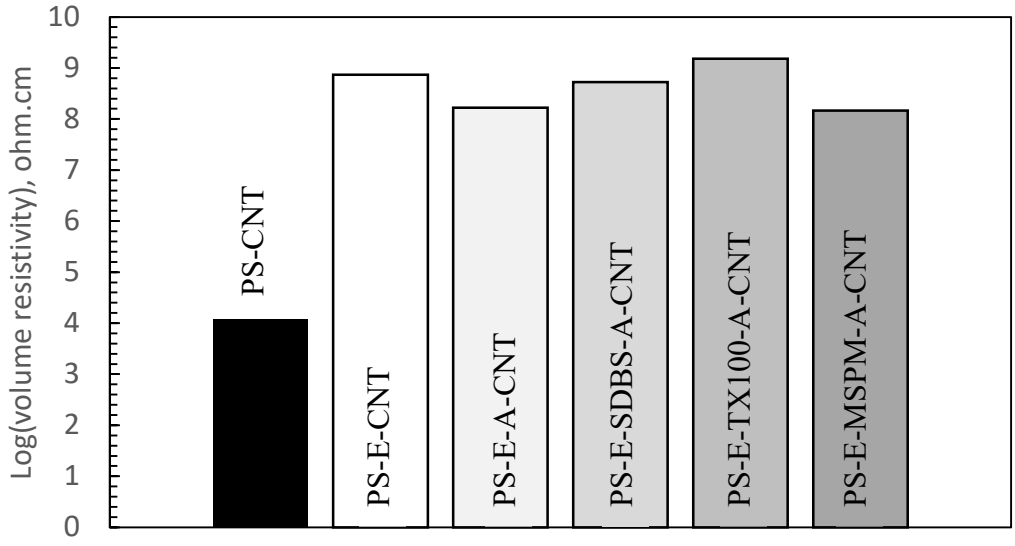

Figure 4.15. Electrical resistivities of the ternary composites.

4.1.3.3 Tensile Test Results

The tensile strength values of the ternary composites are shown in Figure 4.16, and the test results are given in Appendix C. Tensile strength value of PS, which was 44 MPa, decreased to 4.9 MPa with the addition of 40 wt.% of SEBS-gMA owing to the elastomeric nature of SEBS-gMA. When as-received and modified CNTs were introduced, there was a slight increase in tensile strength owing to the enhancement in the dispersion of CNTs. According to SEM results, elastomer content that was used in this study led to the phase inversion point. After phase inversion, CNTs were distributed homogeneously in both elastomer and PS phases and restricted the crack propagation. In co-continuous structure; both components are continuous and can thus fully contribute to the properties of the blends, the materials usually possess low mechanical properties. This is caused by weak interactions between two polymers and a larger interfacial area (Mekhilef et al., 1996). Thus, the addition of modified CNTs did not significantly affect the tensile strengths of the composites.

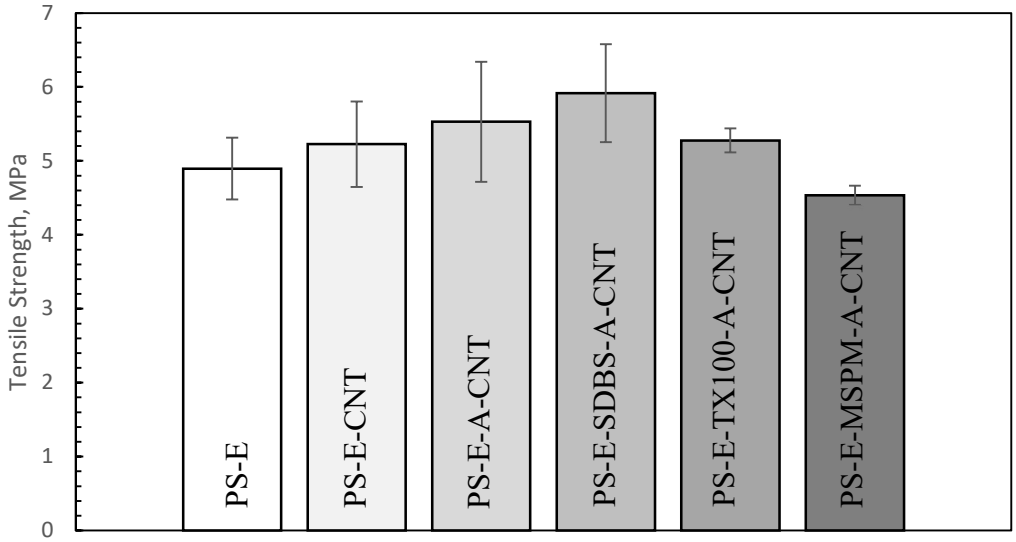

Figure 4.16. Tensile strengths of the ternary composites.

The tensile moduli of the ternary composites are illustrated in Figure 4.17. SEBS-g-MA had lower tensile modulus value compared to pure PS. When they were melt-blended, a dilution effect occurs and tensile modulus values were decreased in all the composites prepared with elastomer. When results were compared to see the effect of surface modification on tensile modulus, there was no significant improvement observed in the tensile moduli of the composites. Nevertheless, there was a small decrease in the tensile modulus value of PS-E-CNT. It was because of the non-homogeneous dispersion of CNTs in the blend structure.

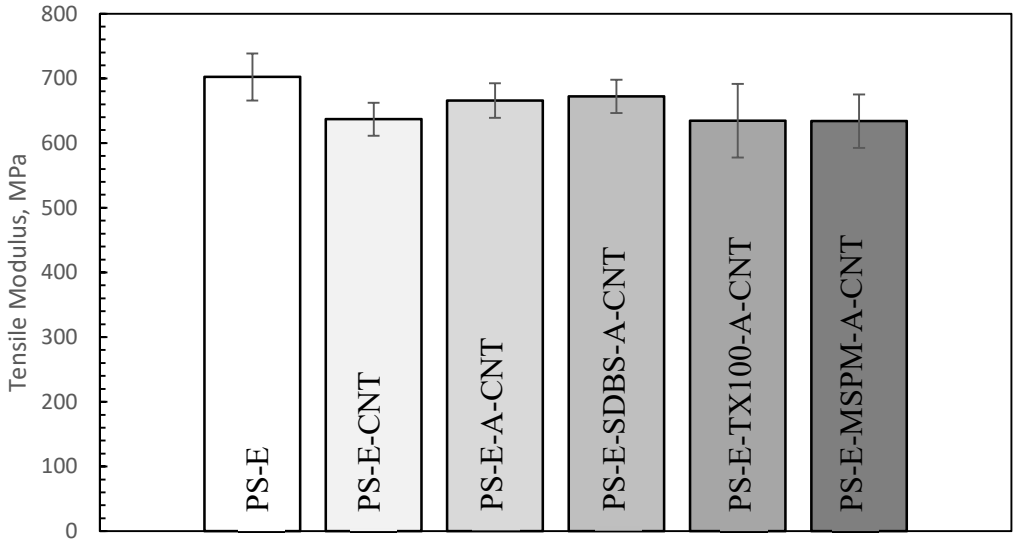

Figure 4.17. Tensile moduli of the ternary composites.

Elongation at break values of the ternary composites are shown in Figure 4.18. When these results were compared with those of the binary composites of PS and CNTs which was 1.48%; elongation at break values increased significantly due to the elastic behavior of the elastomer. It was expected that elongation at break decreased due to the addition of rigid fillers to rigid polymers. The increase in elongation at break with the addition of CNTs and their surface treatment can be explained with the presence of CNTs in the elastomeric domains was resulted in higher elastomer

phase coalescence rate and enlarged domains led to improved elongation at break values of the composites (Yeniova et al., 2010).

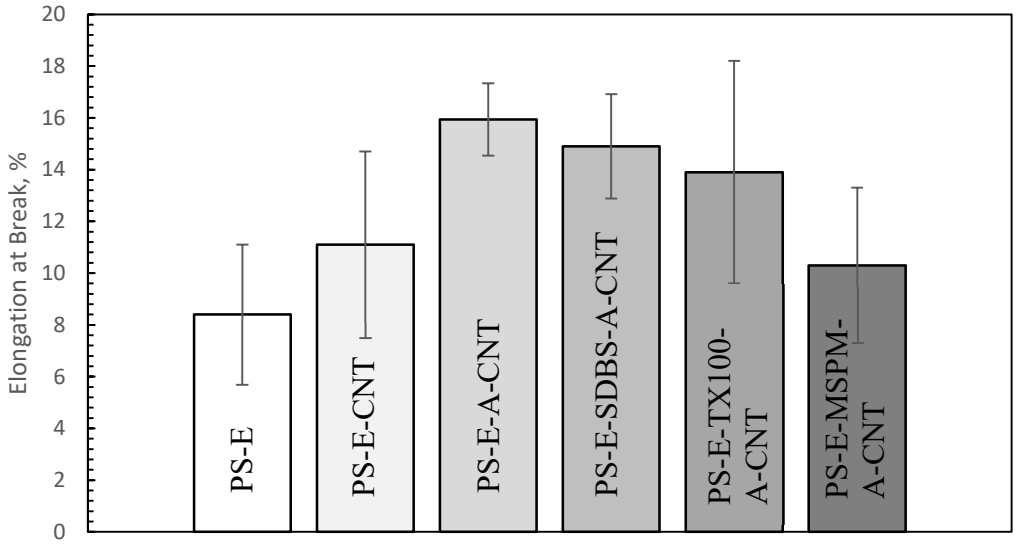

Figure 4.18. Elongation at breaks of the ternary composites.

4.1.3.4 Impact Test Results

Impact strength values of the ternary composites are shown in Figure 4.19 and detailed test results are given in Appendix C. Owing to the ductility of elastomeric domains; there was a significant increase in impact strength of all the ternary composites.

If nanoparticles form agglomerates or they prefer each other in polymer composites, stress concentrated regions form, and this situation leads to a significant loss in the impact energy of the specimen (J. Wang, Fang, Gu, Xu, & Liu, 2006). When the surface modified CNTs added composites were compared, the highest impact strength was reached in PS-E-MSPM-A-CNT as 62 kJ/m^2. With silane coupling agent treatment, the CNTs adhered to the matrix effectively through chemical bonding and ensured good interfacial interaction with the matrix.

The increase of impact strength with the incorporation of CNTs into the blend structure can be explained with a preferential affinity CNTs to the elastomeric phase. CNTs polarity was increased due to the presence of hydroxyl and carboxyl groups introduced by chemical treatment. The elastomer used in this study contained a polar and reactive group, which was maleic anhydride. The existence of these polar groups made elastomeric domains and CNTs prefer each other and improved the impact strength of the composite.

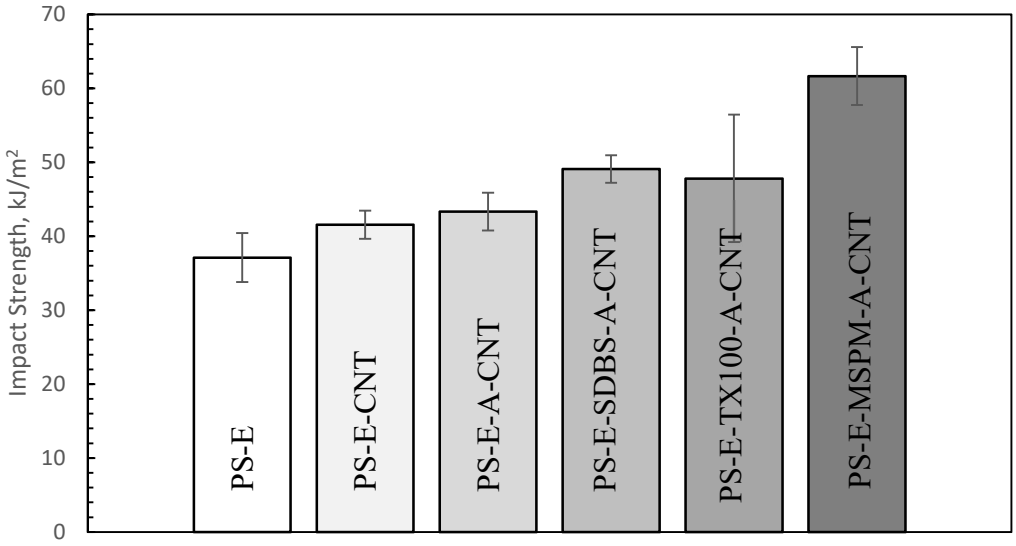

Figure 4.19. Impact strengths of the ternary composites.

4.1.3.5 Shape Memory Behavior Analysis with Bending Test Actuated by Heat

The thermally triggered bending test images of PS-E-MSPM-A-CNT-CF composite chosen as a representative sample, are shown in Figure 4.20. The shape recovery ratio and shape recovery time values of bending test specimens are given in Table 4.2. 100% shape recovery was achieved in all the composites and shape recovery times were three times higher than the PS-E binary blend. The effect of the hard segment in the shape memory polymer became dominant with CNT addition and this

decreased the effect of the soft segment on shape recovery time. Effect of CNT addition on the hard segment can be ranged as A-CNT>TX100-A-CNT>CNT>SDBS-A-CNT>MSPM-A-CNT. Better shape recovery behavior was observed when homogeneous CNT dispersion was achieved. This may be attributed to the increased stored energy resulting from homogeneously distributed nanotubes in the polymer matrix. The CNTs generated higher stored elastic strain energy and helped the composites gain higher recovery stress due to release of stored elastic strain (Deka et al., 2010). According to our results, lower shape recovery times were reached in the composites based on MSPM and SDBS modified CNTs times; thus better dispersion was considered to be achieved in these samples.

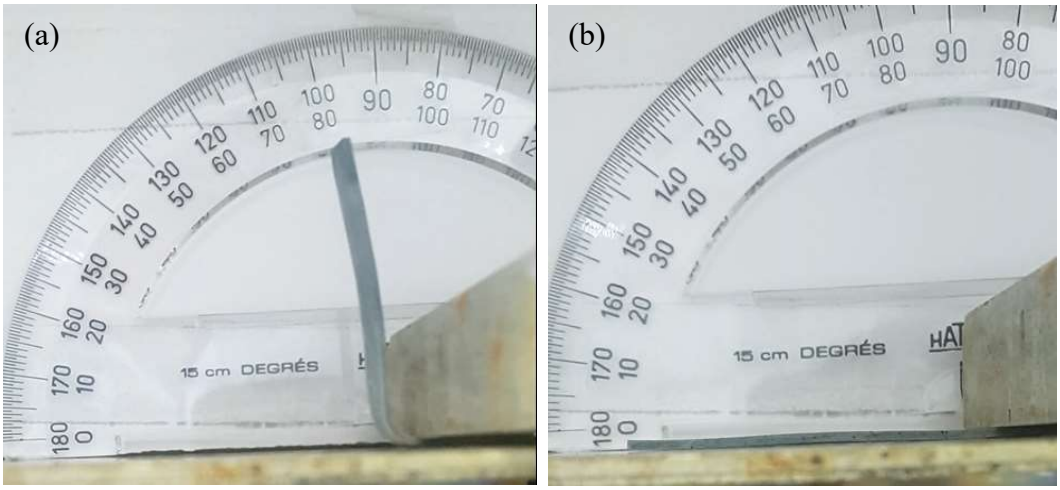

Figure 4.20. Bending test images of PS-E-.MSPM-ACNT samples (a) t=0, (b) t=1:09 min.

Table 4.2 Bending test results of the ternary composites.

Samples	Shape Recovery Time, min:sec	Shape Recovery Ratio, %
PS-E	0:34	100
PS-E-CNT	1:30	100
PS-E-A-CNT	1:35	100
PS-E-SDBS-A-CNT	1:21	100
PS-E-TX100-A-CNT	1:34	100
PS-E-MSPM-A-CNT	1:09	100

4.2 Characterization of Synthesized PS (sPS)

In this section, the characterization test results of polystyrene samples synthesized with bulk polymerization technique were given in comparison with those of commercial PS. The chemical structure of the samples was characterized using FTIR analysis. Molecular weights and MFI of the samples were examined and their thermal characterizations were discussed in terms of TGA and DSC analyses.

4.2.1 Fourier Transformed Infrared (FTIR) Spectroscopy Analysis

The FTIR spectra of styrene monomer, commercial PS and the sPS samples with different initiator concentrations (0.01, 0.008 and 0.005 mol/L) are illustrated in Figure 4.21. The difference between styrene and polystyrene was the double bond between the carbon atoms in the styrene structure. This C=C double bond corresponding to stretching vibration of the styrene vinyl group appeared at 1630 cm^{-1} (Hermán et al., 2015; Oliver, 1999). At the spectra of the polystyrene samples, this peak disappeared due to the successful polymerization of styrene.

The range from 3200 cm^{-1} to 2800 cm^{-1} is the region of the C-H stretching modes. The absorptions from the aromatic C-H stretching vibration peak were observed at

3022 cm^{-1}. The peaks observed at wavenumbers of 2846 and 2914 cm^{-1} were related with CH_2 symmetric and asymmetric stretching, respectively.

Aromatic C-C bond stretching vibrations in the ring structure were observed at 1600 cm^{-1}, 1492 cm^{-1}, and 1452 cm^{-1}. Also, the absorption at 1452 cm^{-1} resulted from both the ring breathing of the benzene and the deformation vibration of CH_2. The in-plane C-H bending of the phenyl ring was represented by the peak at 1026 cm^{-1} (Olmos, Martín, & González-Benito, 2014).

The range from 900 cm^{-1} to 675 cm^{-1} is the out-of-plane C-H bending, which is the characteristic of aromatic substitution. This pattern was observed at 694 cm^{-1} and 748 cm^{-1} in the spectra (Olmos et al., 2014).

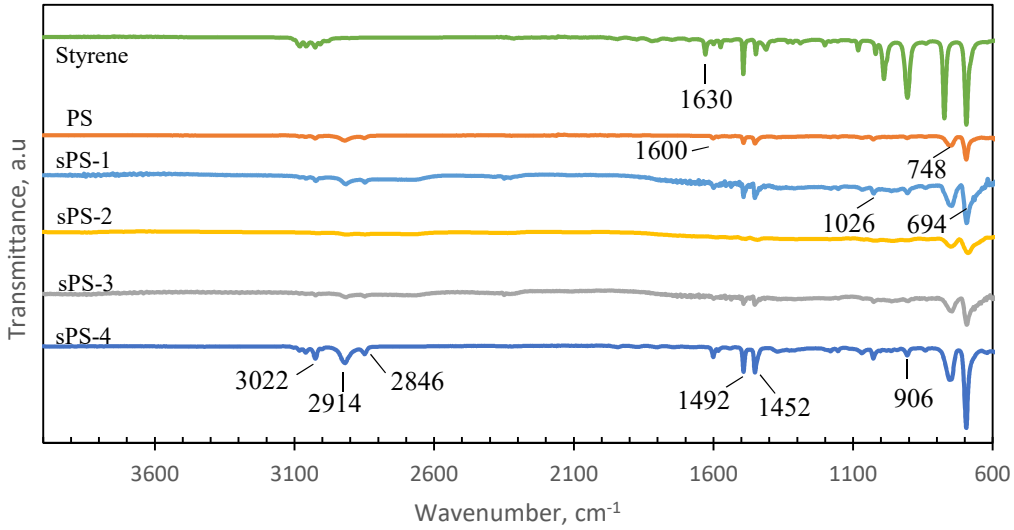

Figure 4.21. FTIR spectra of commercial PS and synthesized PS with different initiator concentrations.

4.2.2 Molecular Weight and Melt Flow Index (MFI) Measurements

Average molecular weight values and MFI values of commercial PS and sPS samples are given in Table 4.3. A sample calculation of viscosity average molecular weight

is given in Appendix E. To reach similar molecular weight and MFI value with the commercial PS, a parametric study was conducted in terms of different AIBN concentrations of 0.005 mol/L, 0.008 mol/L and 0.01 mol/L. According to the results, the molecular weight of commercial and the synthesized polystyrene were in the same order of magnitude but with relatively higher PDI values. MFI of PS samples were also measured to compare the effect of decreasing initiator concentration. Commercial PS had a higher number, weight and viscosity average molecular weights and lower MFI value compare to the synthesized PS with 0.01 mol/L AIBN concentration. Results show that the sample prepared with 0.005 mol/L AIBN concentration had nearly the same number and viscosity average molecular weights and MFI values. This concentration was chosen to be used in the in-situ polymerization of PS-CNT masterbatches. The sample named sPS-4 was synthesized at 0.005 mol/L AIBN concentration and 200 ml styrene to provide a large mixing medium for masterbatch production. Weight average molecular weight and MFI values of the sPS-4 sample were acceptable for performing masterbatch production.

Table 4.3 Molecular weight and melt flow index values of PS Crystal 1540 and sPS.

Sample	Initiator Concentration, mol/L	MFI, g/10 min	M_n*10^{-3}, g/mol	M_v*10^{-3}, g/mol	M_w*10^{-3}, g/mol	PDI, (M_w/M_n)
PS	Commercial grade	14	105	229.96	224.8	2.14
sPS-1	0.01	27	61	216.35	206	3.38
sPS-2	0.008	22	60.3	222.46	192	3.18
sPS-3	0.005	13	86	231.65	323.7	3.76
sPS-4	0.005	17	65.7	220.00	222.4	3.38

4.2.3 Thermal Characterization

TGA curves of commercial PS and sPS samples produced with different initiator concentrations are given in Figure 4.22. The initial decomposition temperature

(approximately the temperature at 1 wt.% weight loss), the temperature at maximum degradation (T_{max}) and the temperature at 5 wt.% weight loss are given in Table 4.4.

The decomposition of the commercial PS was observed in the range of 250 to 416°C. This range was 146 to 414°C for sPS-1, 174 to 416°C for sPS-2, 240 to 419°C for sPS-3 and 219 to 419°C for sPS-4. During the thermal degradation of PS, polymer chain length decreases at the temperatures below 300°C. At the higher temperatures than 300°C molecular weight decreases due to formation of monomer and oligomeric fragments, and other low molecular weight compounds (Guaita, 1986). The initial decomposition temperature of the commercial PS was the highest among all the other synthesized samples. The absence of potential additives available in commercial PS and impurities in the synthesized PS may be the possible reasons for this early decomposition. There was no significant difference between the decomposition temperature of the sPS-4 sample and the masterbatch samples produced with in-situ polymerization of PS and CNTs.

The temperatures at 5 wt.% weight loss of the sample increased with decreasing the initiator concentration to 0.005 mol/L from 0.01 mol/L. According to these results, decreasing the initiator concentration led to an increase in the thermal stability of the samples due to the increase in the average molecular weights with decreasing initiator concentration.

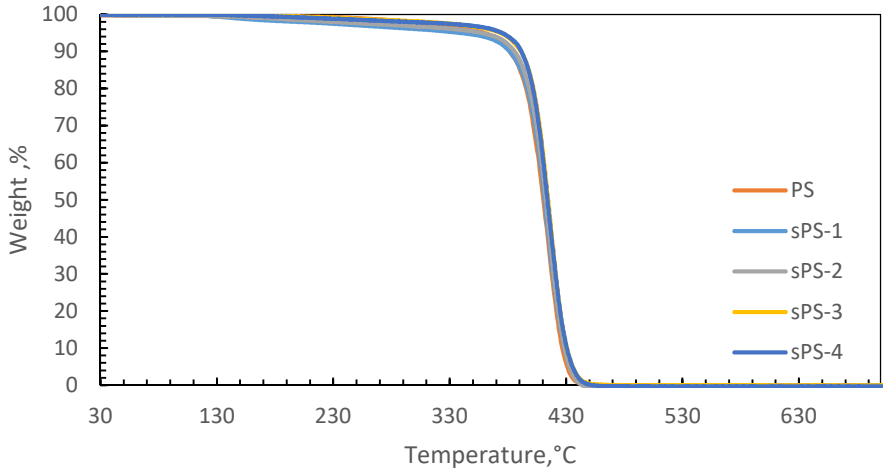

Figure 4.22. TGA plots of commercial PS and sPS samples prepared with different initiator concentrations.

Table 4.4 TGA analysis results of the commercial and synthesized PS samples.

Sample Code	Initial decomposition temperature, °C	T_{max}, °C	Temperature at 5 wt.% weight loss, °C
PS	250	416	359
sPS-1	146	414	334
sPS-2	174	416	359
sPS-3	240	419	374
sPS-4	219	419	375

Glass transition temperatures of commercial and synthesized PS samples are given in Table 4.5. T_g of commercial PS was determined as 89.0°C and this value increased up to 99.7°C with decreasing initiator concentration. For sPS-1, sPS-2 and sPS-3 samples the increase of the T_g can be explained by the increase in molecular weight with decreasing the initiator concentration. Longer chains and more entanglements that present in the structure of polymers with high molecular weight led to an increase in the glass transition temperature of the polymer.

Table 4.5 Glass transition temperatures of commercial PS and synthesized PS.

Sample	T_g, °C
PS	89.0
sPS-1	91.8
sPS-2	96.8
sPS-3	97.0
sPS-4	99.7

4.3 Characterization of PS-CNT Masterbatches

In this section, the characterization test results of PS-CNT masterbatch samples produced with in-situ polymerization technique were given in terms of their FTIR spectra and thermal properties obtained from TGA and DSC analyses.

4.3.1 Fourier Transform Infrared Spectroscopy (FTIR)

The FTIR spectra of sPS-4 sample, in-situ polymerized PS-CNT masterbatches and the CNT samples are illustrated in Figure 4.23. Aromatic C-H bond stretching mode was observed at 3022 cm^{-1}. Symmetric and asymmetric CH_2 stretching modes were detected at 2846 and 2914 cm^{-1}. The peaks that appeared at the wavenumbers of 1452 cm^{-1}, 1492 cm^{-1} and 1600 cm^{-1} were related with aromatic C-C bond stretching vibrations of the benzene ring in the chemical structure of PS. The in-plane C-H bending of the phenyl ring was represented by the peak at 1026 cm^{-1} (Olmos et al., 2014). The out-of-plane C-H bending was observed at 694 cm^{-1} and 748 cm^{-1} represented the characteristics of aromatic substitution pattern. These peaks were obtained in the spectra of sPS-CNT, sPS-A-CNT, and sPS-MSPM-A-CNT samples with different intensities.

There was no clear signal in the spectrum of the CNT sample, except for a wide and a weak band at 3440 cm^{-1} which represent the OH functional group. The OH band

intensity increased in the A-CNT sample due to the treatment with HNO_3 and H_2SO_4. With silane coupling agent treatment this band became apparent in the spectra of MSPM-A-CNT sample.

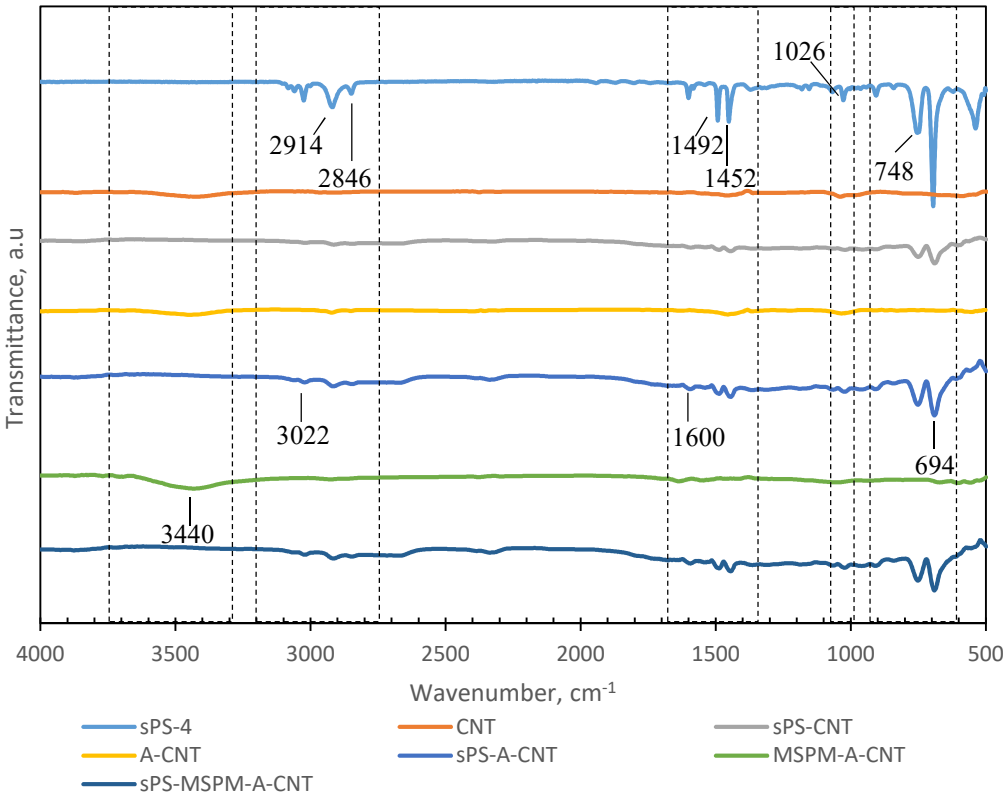

Figure 4.23. FTIR spectra of in-situ polymerized PS-CNT masterbatches and CNT samples.

4.3.2 Thermal Analysis

TGA curves of synthesized PS and PS-CNT masterbatches are given in Figure 4.24 and the initial decomposition temperature (approximately the temperature at 1 wt.% weight loss), the temperature at maximum degradation (T_{max}) and the temperature at 5 wt.% weight loss are given in Table 4.6. The decomposition of the sPS-4 was observed in the range of 219 to 419°C. This range was 150 to 418°C for sPS-CNT,

106 to 423°C for sPS-A-CNT and 132 to 421°C for sPS-MSPM-A-CNT. The degradation observed in the range of 200-300°C represented the release of carbonyl groups related to the acid modification applied to the CNTs (Thaher et al., 2011). The decomposition temperature of samples did not show a significant difference. The temperature at 5 wt.% weight loss of the sPS-CNT, sPS-A-CNT and sPS-MSPM-A-CNT samples were lower than the sPS-4 sample which indicated lower thermal stability of the masterbatches than neat PS. This can be explained with the formation of the agglomerates in the sPS-CNT and the behavior of CNTs as heat dissipating agents, leading to a decrease in temperature values (S. Choi, Im, & Kim, 2012). In the modified CNT added samples, surface modifications with acid and silane coupling agent (MSPM) may damage the perfect wall structure of the CNTs and decrease the thermal conductivity of the CNTs (Valesco-Santos, Martinez-Hernandez, & Castano, 2011).

In the sPS-A-CNT sample, approximately 20% weight loss was observed between 140 to 270°C. The boiling point of styrene is 145°C. The weight loss in this range may be resulted from the evaporation of the styrene remained after the polymerization completed. This sample was not rigid when the polymerization completed. This may be resulted from non-polymerizing styrene remained in the structure.

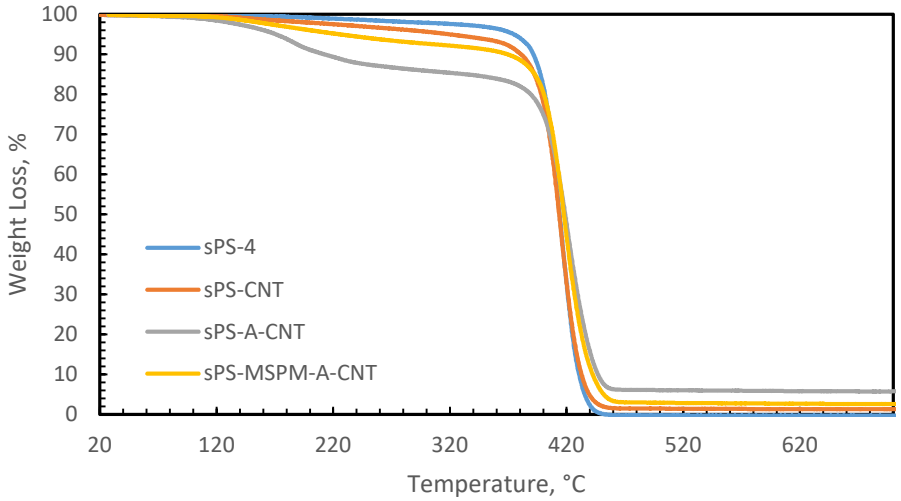

Figure 4.24. TGA plots of PS-CNT masterbatches.

Table 4.6 TGA analysis results of the sPS-4 and sPS-CNT masterbatch samples.

Sample Code	Initial decomposition temperature, °C	$T_{max,}$ °C	Temperature at 5 wt.% weight loss, °C
sPS-4	219	419	375
sPS-CNT	150	418	321
sPS-A-CNT	106	423	171
sPS-MSPM-A-CNT	132	421	227

Glass transition temperatures of sPS-CNT masterbatches are given in Table 4.7. According to the results, glass transition temperature slightly decreased with CNT addition. This can be explained with the imperfect dispersion of nanotubes and the generation of free voids in the matrix (Şengör, 2013). For modified CNTs added masterbatches, the plasticizing effect of the surface modifiers applied on the CNT surfaces may cause a decrease in the glass transition temperature (Yesil, 2010).

Table 4.7 Glass transition temperatures of sPS-CNT masterbatches.

Sample	T_g, °C
sPS-4	99.7
sPS-CNT	92.7
sPS-A-CNT	96.2
sPS-MSPM-A-CNT	96.2

4.4 Comparison of Masterbatch Dilution and Direct Melt Mixing Methods in the Characterization of Multilayer Composites

Amongst the PS-E-CNT ternary composites, PS-E-MSPM-A-CNT sample was selected as the composite formulation produced with modified CNTs due to the slightly higher electrical conductivity and much higher impact strength values which were achieved owing to relatively homogeneous dispersion. The multilayer composites were fabricated with polymer layers produced with PS-E, PS-E-CNT and PS-E-MSPM-A-CNT samples.

In this section, the effects of the masterbatch dilution and direct melt mixing methods on the properties of multilayer composites were discussed. The comparison of these methods were performed with SEM analysis, two-point probe measurements, tensile test and bending tests triggered by heat and electricity.

4.4.1 Scanning Electron Microscopy (SEM) Analysis

SEM images of the cross-section of the multilayer composites after the tensile test are given in Figure 4.25 (a-c) for method 1 (masterbatch dilution), and Figure 4.25 (d-f) for method 2 (direct melt mixing). These micrographs provided information about the interfacial adhesion between the polymer and CF layers and the wetting of

the fibers by the matrix. There were no traces of fiber pull-outs, holes or cavities for all the images.

In the samples prepared with method 1, it can be seen that fibers were wetted thoroughly with polymer layer as seen in the sub-images of Figures 4.25 (b) and (c). This indicated the improved adhesion between the polymer layer and the fibers of the CF, resulting in better mechanical properties of the multilayer composites by applying masterbatch dilution method. On the contrary, in the samples produced with the direct melt mixing method, bare surfaces of the fibers were observed in the images and a close look was given in the sub-image of Figure 4.25 (f) for PS-E-MSPM-A-CNT-CF sample. These non-wetted fibers may form weak points and resulted in the low mechanical performance of the multilayer composites.

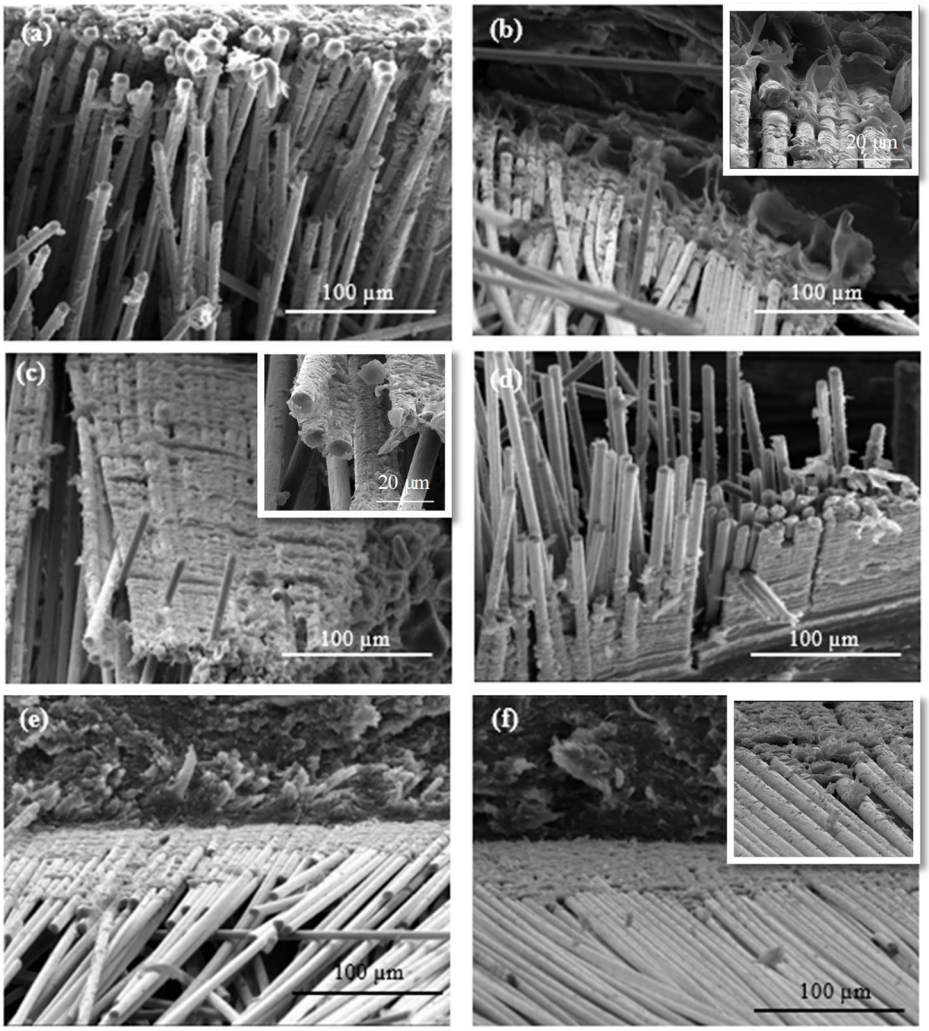

Figure 4.25. SEM images of the fractured surfaces of (a) PS-E-CF, (b) PS-E-CNT-CF and (c) PS-E-MSPM-A-CNT-CF multilayer composites prepared with method 1 and (d) PS-E-CF, (e) PS-E-CNT-CF, and (f) PS-E-MSPM-A-CNT-CF multilayer composites prepared with method 2 at 1000x.

4.4.2 Electrical Resistivity Measurements

The electrical resistivities of the multilayer composites measured with two-point probe method are given in Figure 4.26. The detailed results are given in Appendix B. In the PS-E-CF and PS-E-CNT-CF composites prepared with method 1 (masterbatch dilution); resistivity values were lower than the same composites

prepared with method 2 (direct melt mixing). Masterbatch production before extrusion improved the dispersion of CNTs in the polymer phase and a better conductive pathway was formed in polymeric layers and this behavior increased conductivity in the samples.

The electrical resistivity values of the composites including modified CNTs were higher than as-received CNT added samples. Carboxyl and hydroxyl groups were formed on the CNT surface after acid modification. The crystalline structure of CNTs was damaged with strong acids. This changes on the CNT walls might increase the intrinsic electrical resistivity of the CNTs, due to the electrical insulating oxide layer, resulted from the oxidation of carbon-based structures (Y. J. Kim et al., 2005). Similar behavior was observed in composites prepared with silane coupling agent modified CNTs (Gojny et al., 2006). Insulating modifier layer coated on CF surfaces did not allow the transportation of electrons effectively which decreased the electrical conductivity of the CNT aggregates. The conductivity values of all the composites were in the semiconductor region.

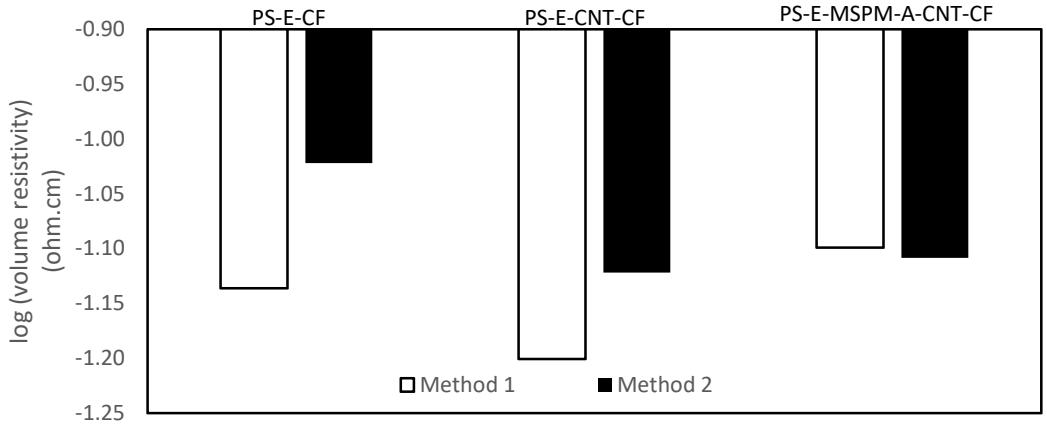

Figure 4.26. Electrical resistivities of the multilayer composites.

4.4.3 Tensile Test Results

The tensile strength results of the multilayer composites, which were produced with two layers of polymers reinforced with and without CNTs and a layer of CF, are given in Figure 4.27. The polymer composites used to prepare the polymer layers, were produced with masterbatch dilution (method 1) and direct melt mixing (method 2). Tensile properties of the multilayer composites with average values of five data and their standard deviations are given in Appendix C. The tensile strength of the multilayer composites produced with method 1 were higher than the ones prepared with method 2. Usage of nano-sized fillers are resulted in small particles dispersed in the polymer matrix and these particles possess a high total surface area. This shows that the rupture tension improves with increasing surface area of the fillers through a more successful stress transfer mechanism (García, Marchese, & Ochoa, 2010). CNTs have a strong tendency to agglomerate due to van der Waals forces. Agglomerates act as large particles and form weak points of composites and tensile strength decreases due to the increase in particle size. With masterbatch preparation and then dilution process, formation of agglomerations may be prevented to some extent and resulted in an increase of tensile strength.

Nanoscale defects formed on the CNT surface due to the acidic treatment may increase the mechanical interlocking. With this treatment, negatively charged –OH and –COOH functional groups were generated on the CNTs walls through oxidation or reduction processes (Gómez, Rendtorff, Aglietti, Sakka, & Suárez, 2016). These groups formed hydrogen bonds with trisilanol that hydrolyzed from trimethoxy ($(OCH_3)_3$) of MSPM in silane coupling agent modification (Kathi & Rhee, 2008). The acrylate based organofunctional group was responsible for forming interaction between the polymer matrix and CNTs modified with the silane coupling agent. This enhanced interaction resulted in higher tensile strength of the multilayer composites reinforced with MSPM-A-CNTs in both methods than the tensile strengths of PS-E-CF and PS-E-CNT-CF samples.

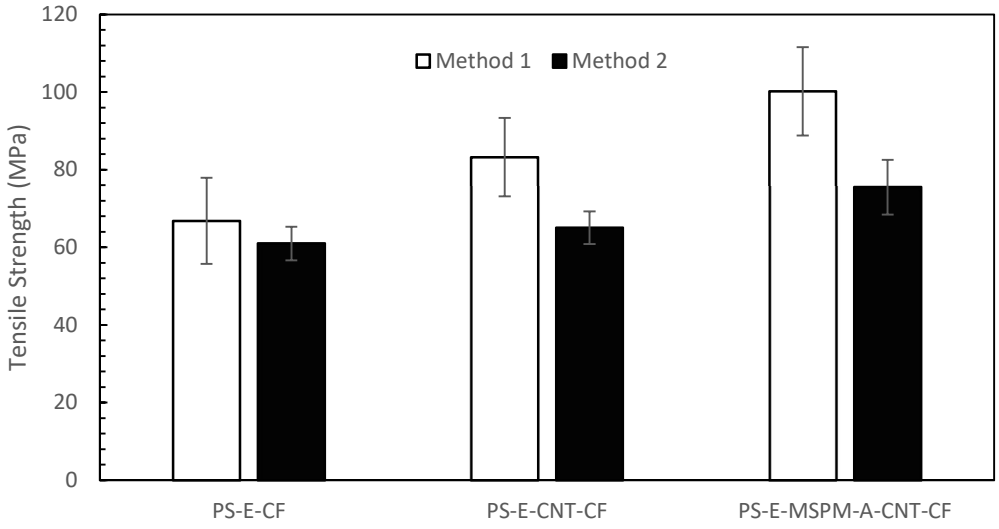

Figure 4.27. Tensile strengths of the multilayer composites.

The tensile moduli of the multilayer composites are given in Figure 4.28. A decrease was observed in tensile modulus with CNT addition (PS-E-CNT-CF) to 4333 MPa from 6321 MPa (PS-E-CF) in samples produced with the masterbatch dilution method. For the PS-E-CNT-CF sample prepared with direct melt mixing, the CNT addition had no significant effect on the tensile modulus than the PS-E-CF sample produced with the same method. This may be due to the non-functional surface of CNTs resulted in agglomerations in both methods. Functionalized CNTs, favor the dispersion of CNTs by promoting the stress transfer between the CNTs and the matrix as seen for the PS-E-MSPM-A-CNT-CF samples. The tensile modulus of the sample prepared with silane treated CNTs was 52.7% higher than the tensile modulus of the sample prepared with as-received CNTs in method 1. This indicated the better dispersion of CNTs in the polymer matrix with MSPM treatment and masterbatch dilution techniques.

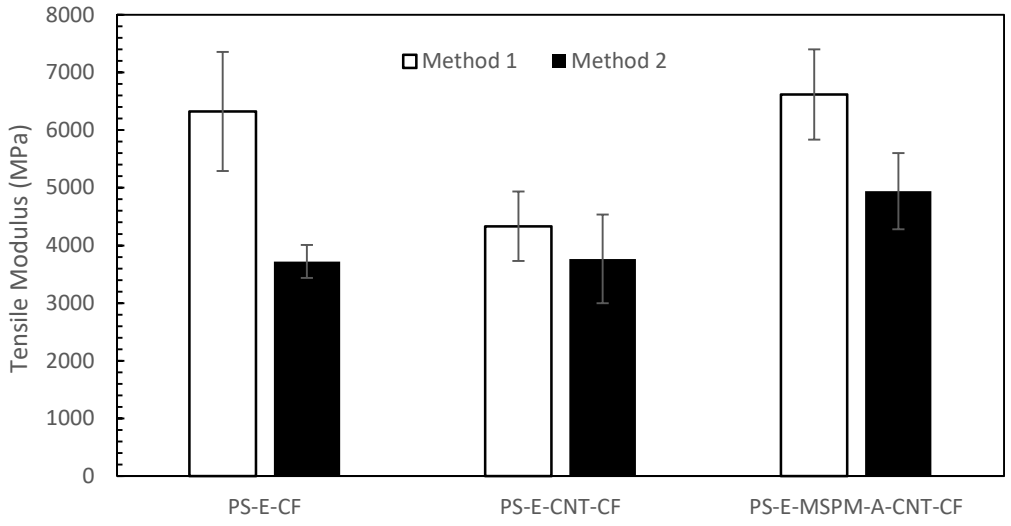

Figure 4.28. Tensile moduli of the multilayer composites.

The elongation at break values of multilayer composites are given in Figure 4.29. CF in the composite system made composites difficult to elongate due to the limited elongation of CFs and restriction of the mobility of the composite structure, resulting in low elongation at break values of the composites. The elongation of break of the PS-E sample was 8.4% and reinforcing with CF led the elongation at break value of PS-E-CF sample reduced to 2.0% for method 1 and 2.2% for method 2. This may be resulted from the better adhesion between the CF and the polymer layers resulted in stiffer composites. For the samples reinforced with CNTs, elongation at break values were slightly higher for the samples produced with masterbatch dilution method. The increase in elongation at break with the addition of CNTs can be explained with CNTs in the elastomeric domains resulting in the higher elastomer phase coalescence rate and enlarged domains, which led to enhanced elongation at break values of the composites. (Yeniova et al., 2010).

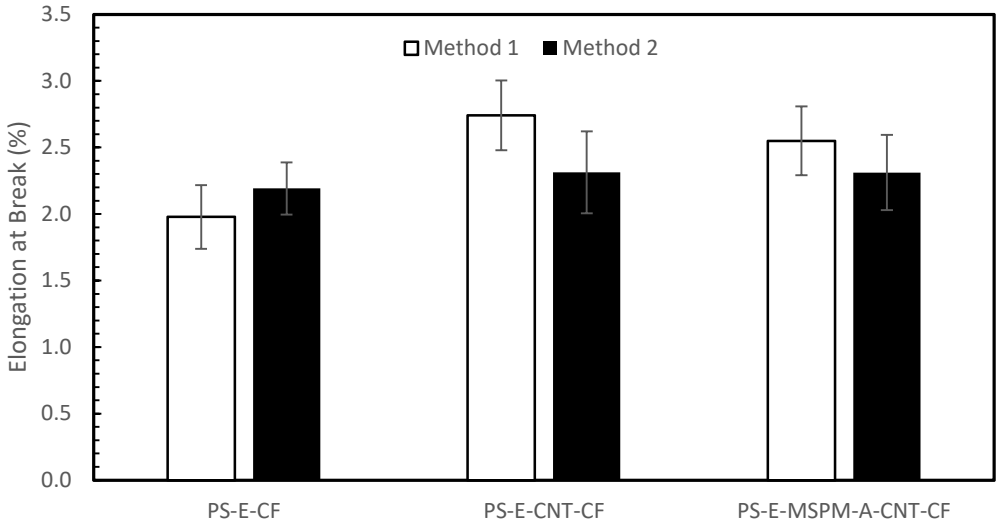

Figure 4.29. Elongation at breaks of the multilayer composites.

4.4.4 Shape Memory Behavior Analysis with Bending Test Actuated by Heat and Electricity

The thermally and electrically triggered bending test images of PS-E-MSPM-A-CNT-CF-M1 sample which was produced with the masterbatch prepared with MSPM treated CNTs are shown in Figure 4.30 as representative samples. The temporary bent shape and the sample state after the shape recovery are displayed in these images. The detailed results are given in Appendix D. Recovery ratio and recovery time values are given in Table 4.8. Higher than 90% recovery was achieved in all the multilayer composites.

For the thermal shape recovery performance of the samples, the shape recovery time of the PS-E-CF-M2 composite prepared with direct melt mixing was lower than the same sample produced with masterbatch dilution. The masterbatches were produced with in-situ polymerization of styrene (sPS) in the presence of CNTs (sPS-CNTs). T_g values of sPS and sPS-CNT masterbatches, which were given in Table 4.7, were higher than the commercial PS. This indicated the decrease in chain mobility of polystyrene after in-situ polymerization. In thermally triggered bending test, the

shape recovery time values of the PS-E-CF-M2, PS-E-CNT-CF-M2, and PS-E-MSPM-A-CNT-CF-M2 samples which were produced with direct melt mixing were lower than the multilayer composites prepared with the masterbatch dilution method due to the low mobility of the polymer chains.

The highest shape recovery time and the lowest shape recovery ratio with thermal triggering were reached in the PS-E-CNT-CF-M1 composite than PS-E-CF-M1 and PS-E-MSPM-A-CNT-CF-M1 samples. It was caused by the limiting effect of agglomerations of the CNTs on chain mobility of the polymer matrix and restricting the shape recovery of the samples (Azam, Jumahat, Rosli, & Frormann, 2012). With silane coupling agent modification, dispersion of the CNTs were enhanced in the masterbatch and in the dilution step, CNTs were dispersed again during the extrusion. The conduction of the heat was better in this sample due to the formation of conductive pathway of the fillers. For the composites produced with direct melt mixing, shape recovery time decreased and the shape recovery ratio increased with CNT addition due to the increase in the conductivity of the samples.

The multilayer composites recovered to their original shapes under electricity lower than 30 seconds with 100% recovery ratio. This behavior can be explained with the control and ability of the CF to form a straight conductive pathway. The PS-E-CNT-CF multilayer composites heated more rapidly than surface modified CNT added multilayer composites due to the insulating modifier layer coated on CF surfaces which did not allow the transportation of electrons effectively (Gojny et al., 2006). Thus, shape recovery was faster in PS-E-CNT-CF samples than PS-E-MSPM-A-CNT-CF composites.

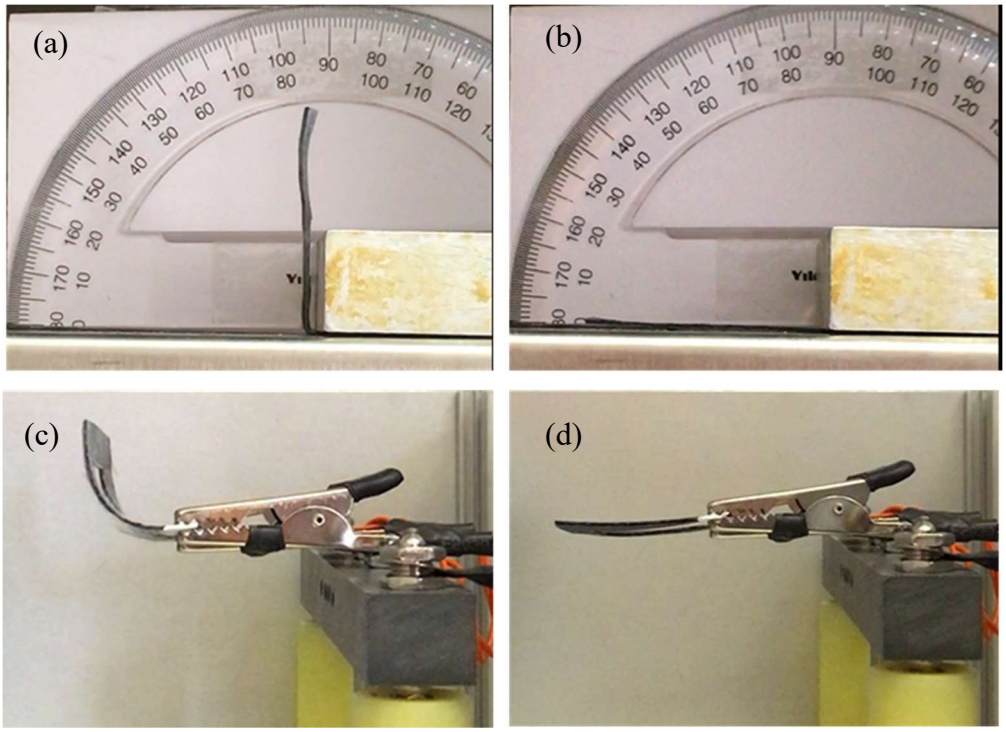

Figure 4.30. Thermally bending test images for masterbatch diluted PS-E-MSPM-A-CNT-CF samples (a) t=0, (b) t=25 s, electrically bending test images for masterbatch diluted PS-E-MSPM-A-CNT-CF samples (c) t=0, (d) t=20 s.

Table 4.8 Bending test results of multilayer composite samples.

Sample	Thermally		Electrically	
	Recovery Time, min:sec	Recovery Ratio, %	Recovery Time, sec	Recovery Ratio, %
PS-E-CF-M1	01:46 ± 44	97.3 ± 2	00:28 ± 7	100
PS-E-CF-M2	00:25 ± 13	100	00:23 ± 6	100
PS-E-CNT-CF-M1	02:54 ± 66	90.8 ±7	00:14 ± 6	100
PS-E-CNT-CF-M2	00:18 ± 5	100	00:18 ± 4	100
PS-E-MSPM-A-CNT-CF-M1	00:39 ± 20	100	00:27 ± 11	100
PS-E-MSPM-A-CNT-CF-M2	00:25 ± 5	100	00:20 ± 6	100

4.5 Surface Modification of CF Layers

Surface modifications were applied directly on the as-received CF surfaces to improve the interaction between the layers of the multilayer composites. The effect of the modifications were characterized by contact angle measurements, optical microscope and FTIR analyses, and T-peel test. Desizing of the CF before its modification was also studied and discussed in the last part of this section.

4.5.1 Contact Angle Measurements

The contact angles measured from the polymer layer and CF surfaces and the calculated values of surface free energy components and total surface free energy of the composites are given in Table 4.9. A sample calculation for surface free energy and work of adhesion is given in Appendix F.

Table 4.9 Contact angles, surface free energy components and total surface free energy of the polymer layer and CF surfaces.

Sample	θ_{Water}, Deg.	θ_{DIM}, Deg.	$\boldsymbol{\gamma_s^p}$, mJ/m^2	$\boldsymbol{\gamma_s^d}$, mJ/m^2	$\boldsymbol{\gamma_s^{total}}$, mJ/m^2
PS-E-MSPM-A-CNT	99.68	47.99	0.11	35.73	35.84
CF	90.00	41.39	1.16	37.81	38. 96
MSPM-CF	99.98	38.03	0.0001	41.30	41.30
PSMA-CF	101.80	38.48	0.03	35.20	35.23
sPS-CF	106.83	32.67	0.67	18.39	19.06
sPS-E-CF	105.62	42.28	0.186	25.36	25.55
sPS-E-MSPM-CF	94.41	50.80	0.90	32.97	33.87
PA6-ES-CF	43.54	43.96	27.99	28.69	56.68
PA6-ES-APTES-CF	65.12	41.67	12.14	33.03	45.17

In our composite system, surface modifications were applied to the CF surface in order to increase the surface energy of CF. The total surface free energy of the polymer layer was calculated as 35.84 mJ/m^2. This value was lower than the total surface free energy of CF surface which was calculated as 38.96 mJ/m^2. With MSPM modification, the surface energy of CF was increased further due to the interaction of the silane coupling agent with both substrate (CF) and the polymer layer acting as an adhesive (PS-E-MSPM-A-CNT), and formation of a chemical bridge at the interface. There was no significant difference between the surface free energy of the polymer layer and PSMA-CF. Lower contact angles (<< 90°) are resulted in good wettability and high energy surfaces but higher contact angles (>> 90°) correspond to low wettability between adhesive and adherent (Yuan et al., 2013). For strong adhesion, lower surface tension of the adhesive than the adherent is needed. According to these information, it can be expected that the adhesion between the polymer layer and PSMA-CF sample is not sufficient due to their incompatibilities with each other.

The sPS-CF sample was prepared by coating the surface with PS synthesized using bulk polymerization. Non-polar characteristics of PS led to a decrease in the polarity of the CF surface. The polar component of the surface energy decreased to 0.67 mJ/m^2. Another approach to enhance the compatibility between the layers was the elastomer addition during the PS synthesis and then coating the CF surface with this polymer blend (sPS-E-CF). The total surface free energy was increased to 25.55 mJ/m^2 from 19.06 mJ/m^2 with the elastomer addition. For further improvement in the surface energy, sPS-E blend produced with bulk polymerization and then coated on the MSPM-CF. With the effect of silane treatment on the compatibility between the polymer and CF layer, total surface free energy was improved to 33.87 mJ/m^2.

Electrospun PA6 nanofibrous mat was also coated on the CF surface (PA6-ES-CF) to provide interfacial interlocking and increase the polarity of the CF surface. Interfacial interlocking is one of the adhesion theories. Lower water contact angles and higher polar components of surface free energy in PA6-ES-CF and PA6-ES-

APTES-CF samples indicated the increase of polarity of the CF and resulted in high total surface free energy compared to CF surface.

According to these results, when as-received CF, MSPM-CF, PA6-ES-CF and PA6-ES-APTES-CF samples were chosen as the CF layer in the composite structure, the adhesion between the layers of the composite was expected to be strong due to the higher total surface free energy of these fabrics than the polymer layer.

The work of adhesion (W_a) values calculated between the polymer layer and CFs using Young-Dupre Eqn. are represented in Figure 4.31. W_a results revealed that strength of the adhesion between PS-E-MSPM-A-CNT polymer layer and sPS-CF and sPS-E-CF samples was lower than the other surface modifications due to the low surface free energy of these fabrics. There was no significant differences between the W_a values of PSMA-CF, sPS-E-MSPM-CF, PA6-ES-CF and PA6-ES-APTES-CF samples. MSPM-CF sample had the highest W_a with 76.83 mJ/m^2 and this value was 71.04 mJ/m^2 for the as-received CF. The W_a is the extent of the strength of the adhesion between the adhesive and substrate. Higher W_a values corresponds to easy wetting of adhesive on the substrate and strong bond formation at the interface of the adhesive and substrate (J. Zhang, 2013).

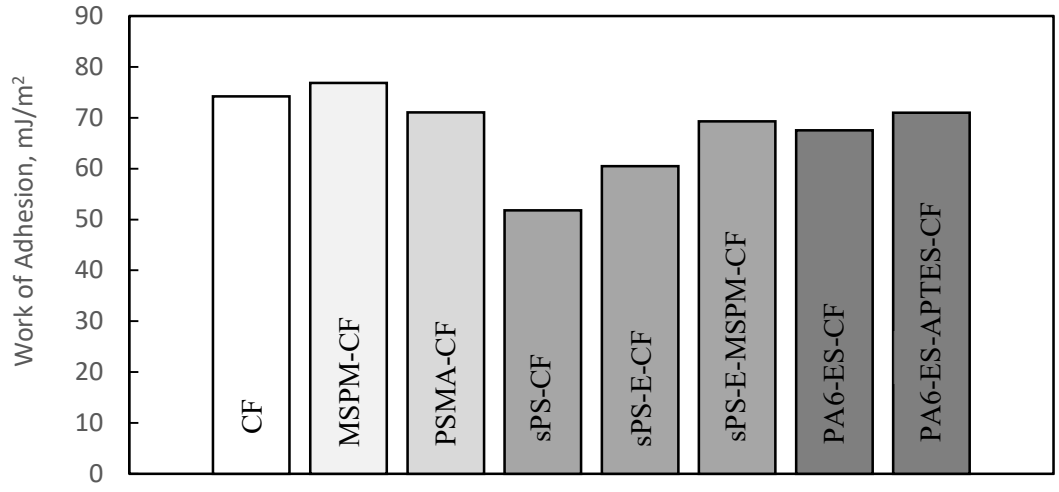

Figure 4.31. Work of adhesion between polymer layer and CF surfaces.

4.5.2 Optical Microscope Analysis

The images of CF and PS-E-MSPM-A-CNT polymeric layer surfaces are shown in Figure 4.32. Smooth surfaces of the CF layer and the polymer layer were observed from these images, respectively.

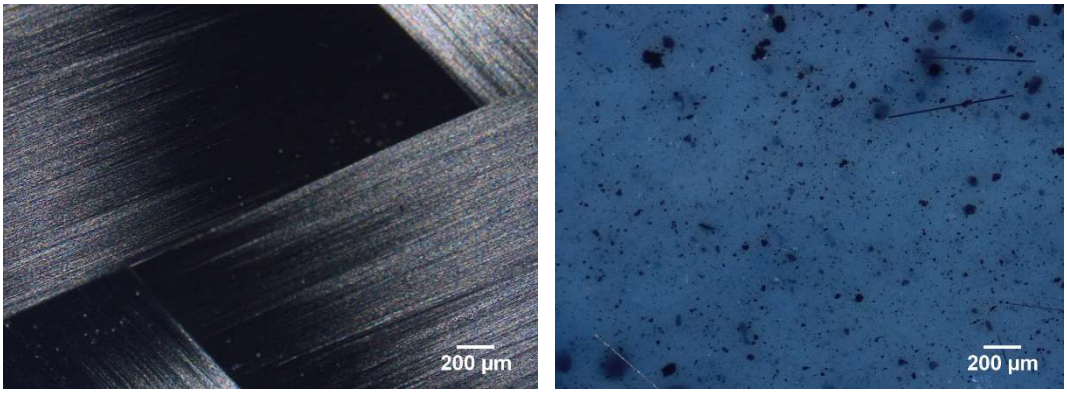

Figure 4.32. Micrographs of CF and PS-E-MSPM-A-CNT surfaces before multilayer composite preparation.

The surfaces of the T-peel test specimen are represented in Figure 3.12. Micrographs of unbonded surfaces of the T-peel test specimens, which are the CF side of the sample that clamped to the grips during the test, are given in Figure 4.33. When the images of as-received and MSPM modified CF surfaces were examined, impregnation of fabric surfaces with polymer composite (blue regions) was observed. This was the reason for better adhesion between the composite constituents. The peel strength of the MSPM modified CF composite was higher than the unmodified one due to the better impregnation of CF surface. In PSMA-CF and sPS-CF samples, the polymeric modification layer coated onto the CF surface prevented the impregnation of PS-E-MSPM-A-CNT through CF fibers. This led to a decrease in the peel strength of this composites. sPS-E-CF surface was also coated with the polymeric modification layer, but compatibilities between the layers upon the modification were more effective in these composites. When electrospun PA6 nanofibers were coated directly on CF surface, a smooth polymeric layer was

observed on the CF surface. With silane coupling agent treatment applied before electrospinning process (PA6-ES-APTES-CF); compatibility and impregnation were improved and nanofibers that increased the contact area may be the reason of the increase in peel strength of this composite. The magnified image of the nanofibers formed with electrospinning technique was shown in the sub-image of the PA6-ES-APTES-CF sample in Figure 4.33.

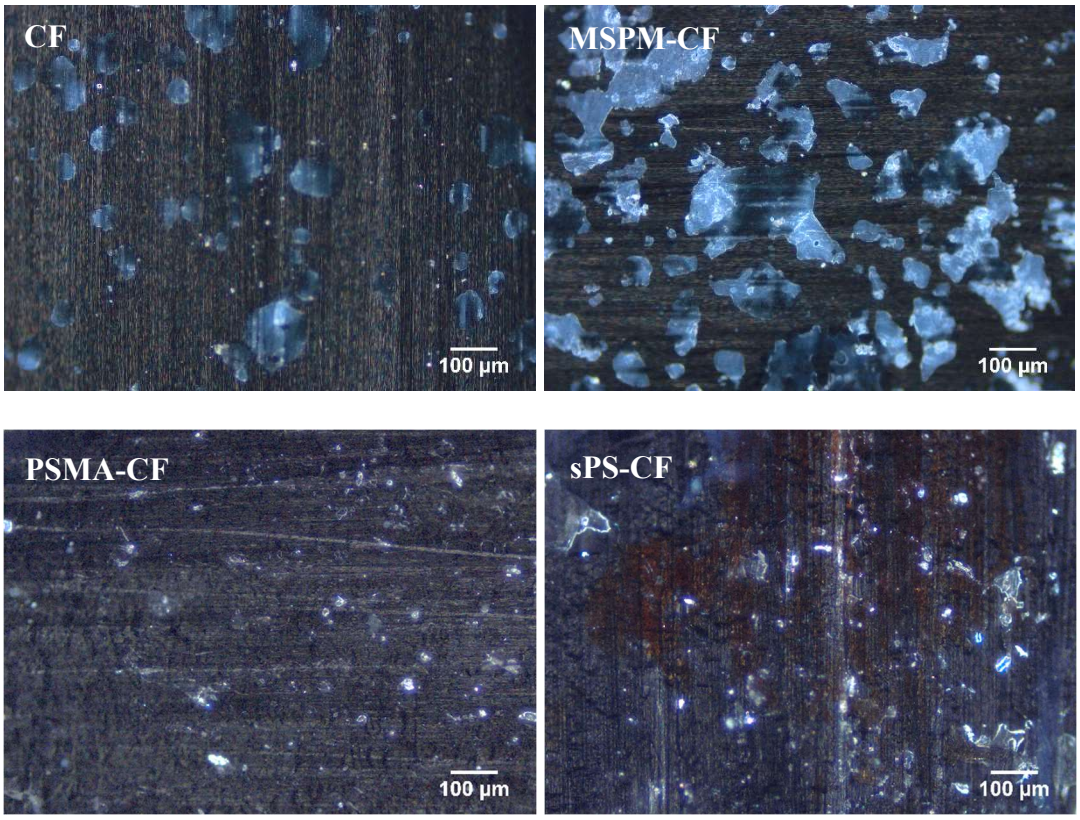

Figure 4.33. Micrographs of unbonded surfaces of T-peel test specimens.

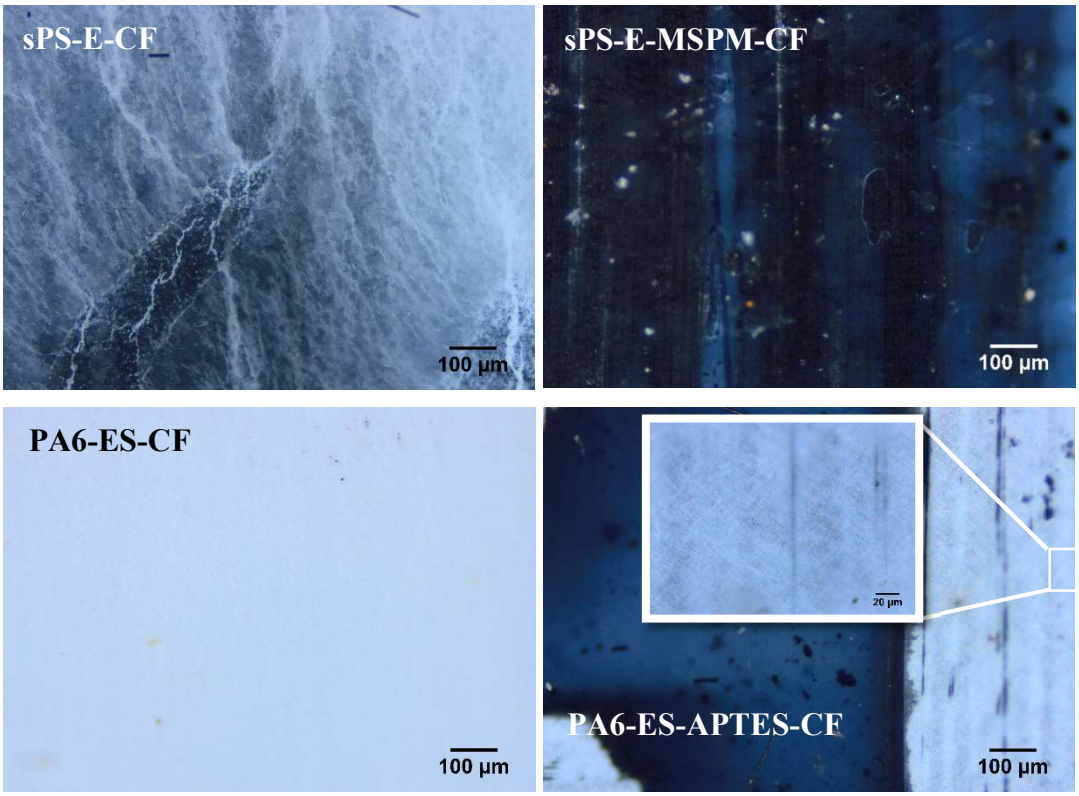

Figure 4.33. (cont'd) Micrographs of unbonded surfaces of T-peel test specimens.

The morphology of peeled surfaces of the composites after T-peel test is shown in Figure 4.34. '–CF' abbreviation at the end of the sample code indicates the CF side and '–P' abbreviation represents the polymer layer side of the peeled surfaces. CF side of the peeled surfaces of CF, MSPM-CF, PSMA-CF, sPS-E-CF, sPS-E-MSPM-CF samples were coated with polymer composite and also rough surfaces were observed on the polymeric layer side. For sPS-CF sample, smooth regions were detected on CF surface and adhesion was weak in this sample. There was no roughness on the polymeric side of this sample which indicated no interaction between modified CF and the polymer layer. In the electrospun PA6 nanofibers coated sample, the polymer side of this sample was coated with PA6 nanofibers as can be seen from the image in white color. On the CF side, there was no trace of nanofibers and they were transferred to the polymeric layer after compression molding due to the lack of chemical bonding with as-recieved CF. By applying silane coupling agent treatment with APTES and coating with electrospun nanofibers

(PA6-ES-APTES-CF), a more compatible composite system was achieved, and adhesion between layers was improved due to the enhanced bonding with the application of the silane treatment.

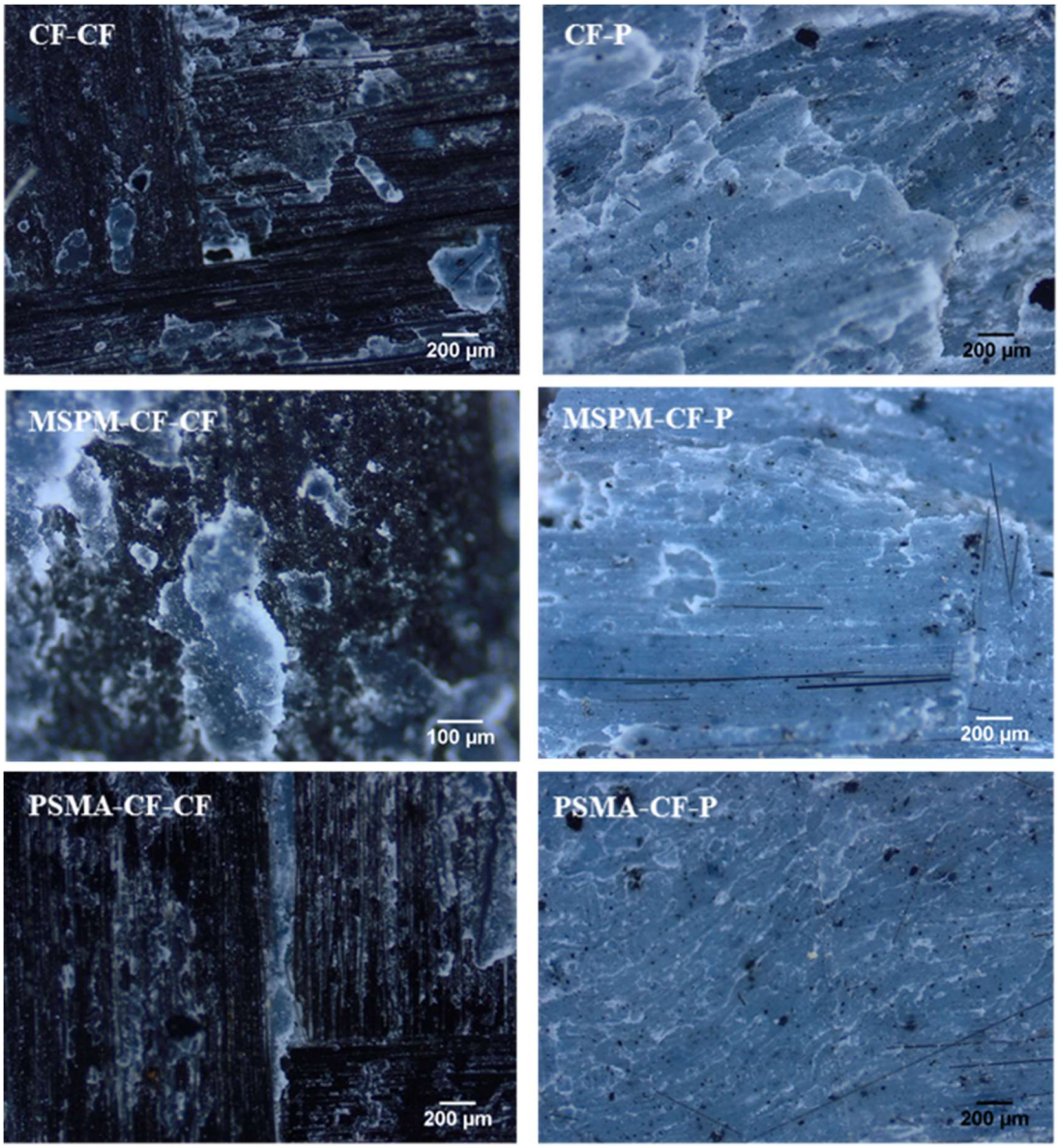

Figure 4.34. Micrographs of peeled surfaces of T-peel test specimens.

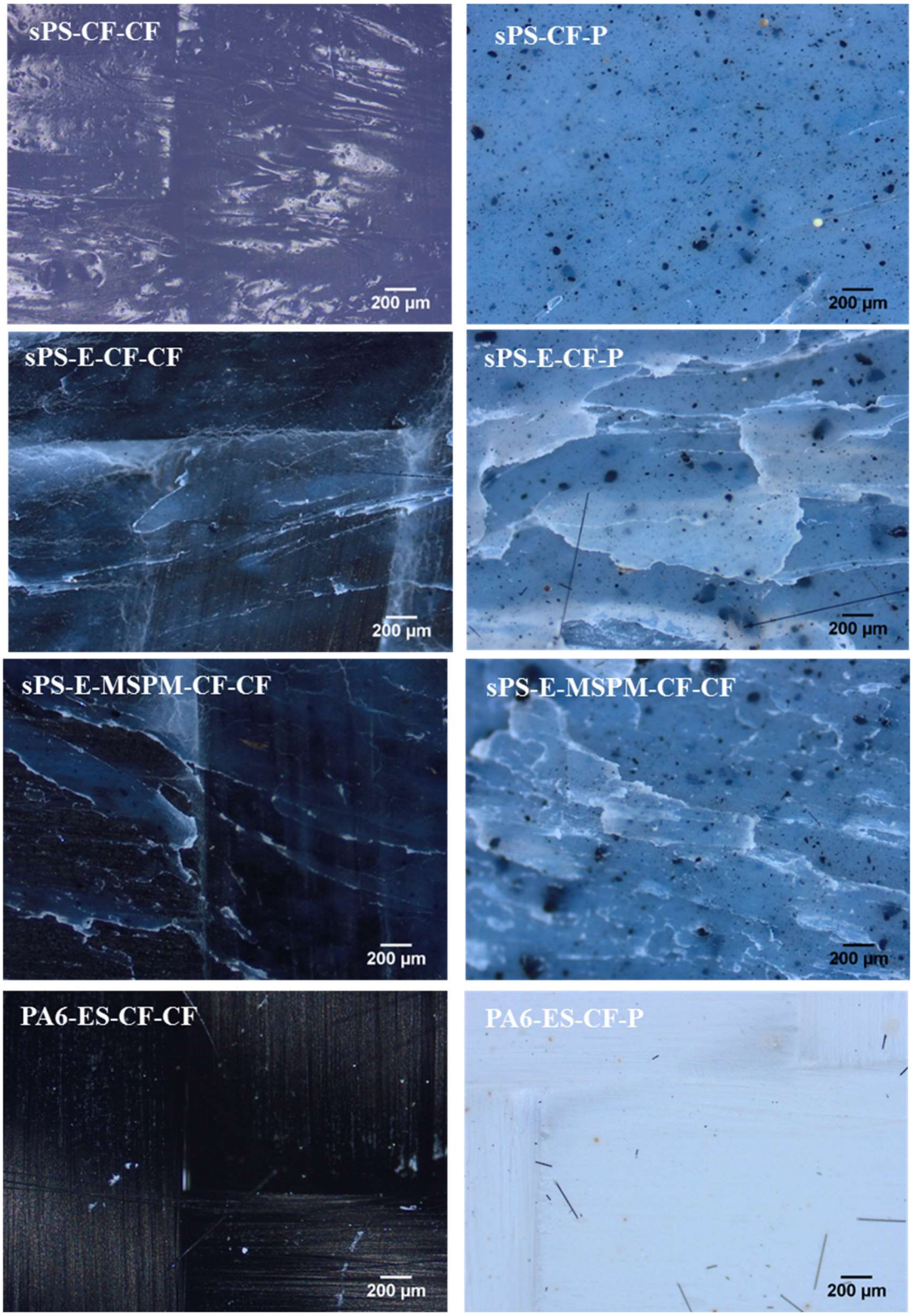

Figure 4.34 (cont'd). Micrographs of peeled surfaces of T-peel test specimens.

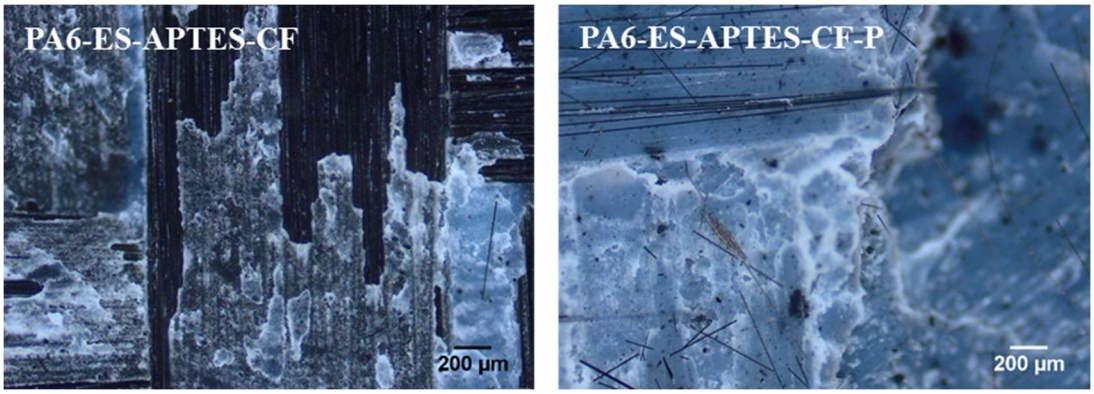

Figure 4.34 (cont'd). Micrographs of peeled surfaces of T-peel test specimens.

4.5.3 Fourier Transformed Infrared (FTIR) Spectroscopy

FTIR spectra of neat PS (sPS) and PS-E blend synthesized with bulk polymerization method (sPS-E) and the commercial SEBS-gMA are shown in Figure 4.35. Characteristic peaks of PS was obtained in the sPS and the sPS-E samples in the spectra, as discussed in Section 4.2.1 and 4.3.1. The aromatic C-H stretching vibration at 3022 cm^{-1}, and CH_2 symmetric and asymmetric stretching at 2848 and 2914 cm^{-1}, respectively, the aromatic C-C bond stretching vibrations in the ring structure at 1600 cm^{-1}, 1492 cm^{-1}, and 1452 cm^{-1}, in-plane C-H bending of the phenyl ring at 1026 cm^{-1} and out-of-plane C-H bending bands at 694 cm^{-1} and 748 cm^{-1} were observed in the spectra of the samples containing polystyrene. In the SEBS-gMA sample, the free carboxyl group in maleic anhydride appeared at 1713 cm^{-1} wavenumber (Zhan et al., 2019).

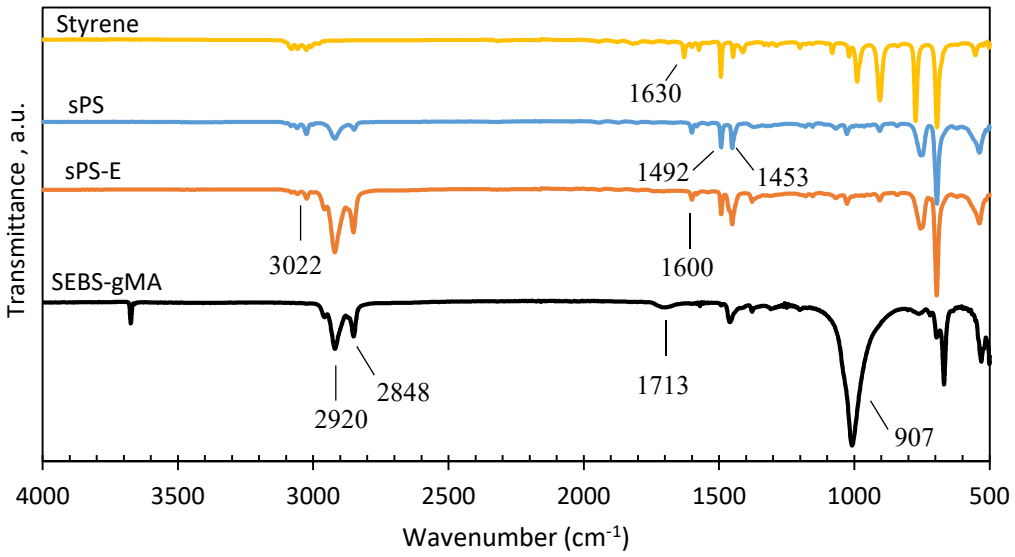

Figure 4.35. FTIR spectra of in-situ polymerized PS (sPS), in-situ polymerized PS-E (sPS-E) and SEBS-gMA.

To understand the most successful surface treatment method applied to the CF surfaces, a T-peel test was applied to the multilayer composites. The configuration of the test specimen is given in Figure 3.12. Figure 4.36 displays the FTIR spectra of the unbonded surfaces of the test specimens which are the CF side of the sample that clamped to the grips during the test. The peaks at 2850 and 2920 cm^{-1} that are related with CH_2 symmetric and asymmetric stretching, respectively were obtained on the surfaces which was wetted with the polymeric layer. PSMA-CF showed a peak at 1713 cm^{-1} which is related with free carboxyl group and at 1780 cm^{-1} stretching vibration of the carbonyl group in maleic anhydride (Zhan et al., 2019). For the samples coated with electrospun PA6 nanofibers, peaks were observed at 3296 cm^{-1}, which represented the valence stretch vibrations of hydrogen atoms bonded as –NH. Amide I in the α- and β-crystalline phases at 1640 cm^{-1} and α- and β-crystalline phases with an unassociated amide at 1540 cm^{-1} were observed (Porubská et al., 2012). In silane coupling agent modified samples, traces of modifiers cannot be observed in the spectrum.

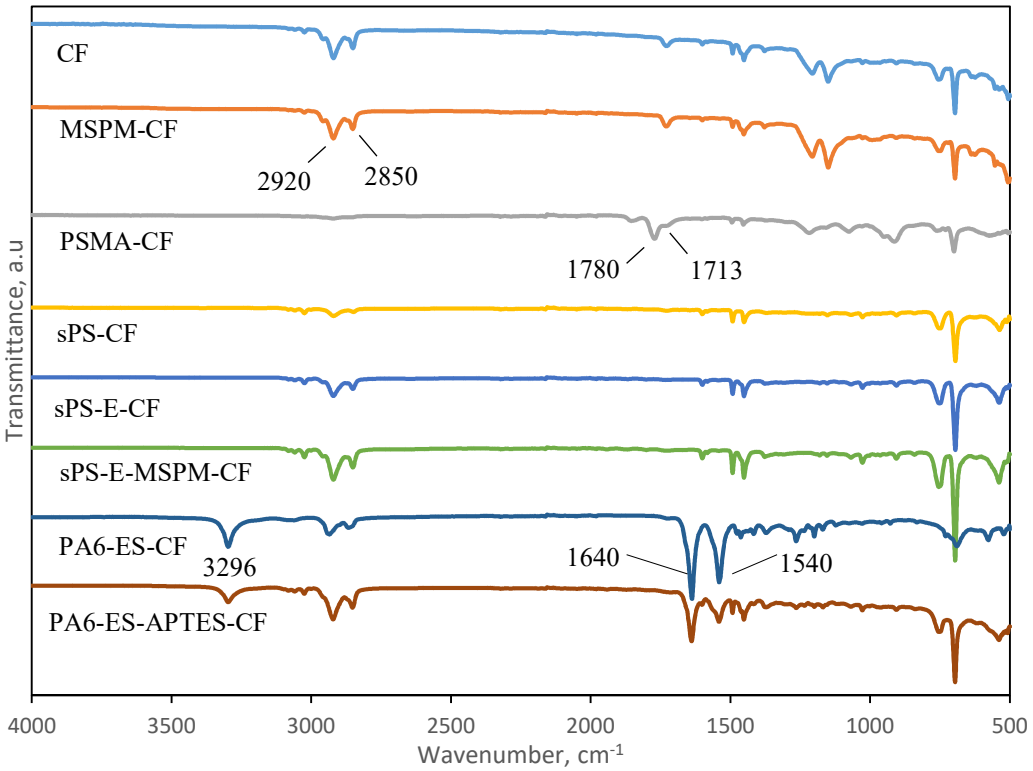

Figure 4.36. FTIR spectra of un-bonded surfaces of T-peel test specimens.

FTIR spectra of the polymer layer side of peeled surfaces after the T-peel test are shown in Figure 4.37. The spectrum of the polymer layer named PS-E-MSPM-A-CNT was given on top. In the spectra of the CF, MSPM-CF, PSMA-CF, sPS-CF, sPS-E-CF, sPS-E-MSPM-CF and PA6-ES-APTES-CF samples, the same peaks were detected on the polymer layer side of the specimens with the polymer layer. In the spectrum of the PA6-ES-CF sample, peaks belonging to PA6 were observed (1640 and 1540 cm^{-1}) on the polymer side due to the peeling of PA6 nanofibrous mat coated on the CF and adhered on to the polymer surface after compression molding. In the optical microscope images of this sample (Figure 4.34), the white colored PA6 nanofibrous mat was seen on the polymer side.

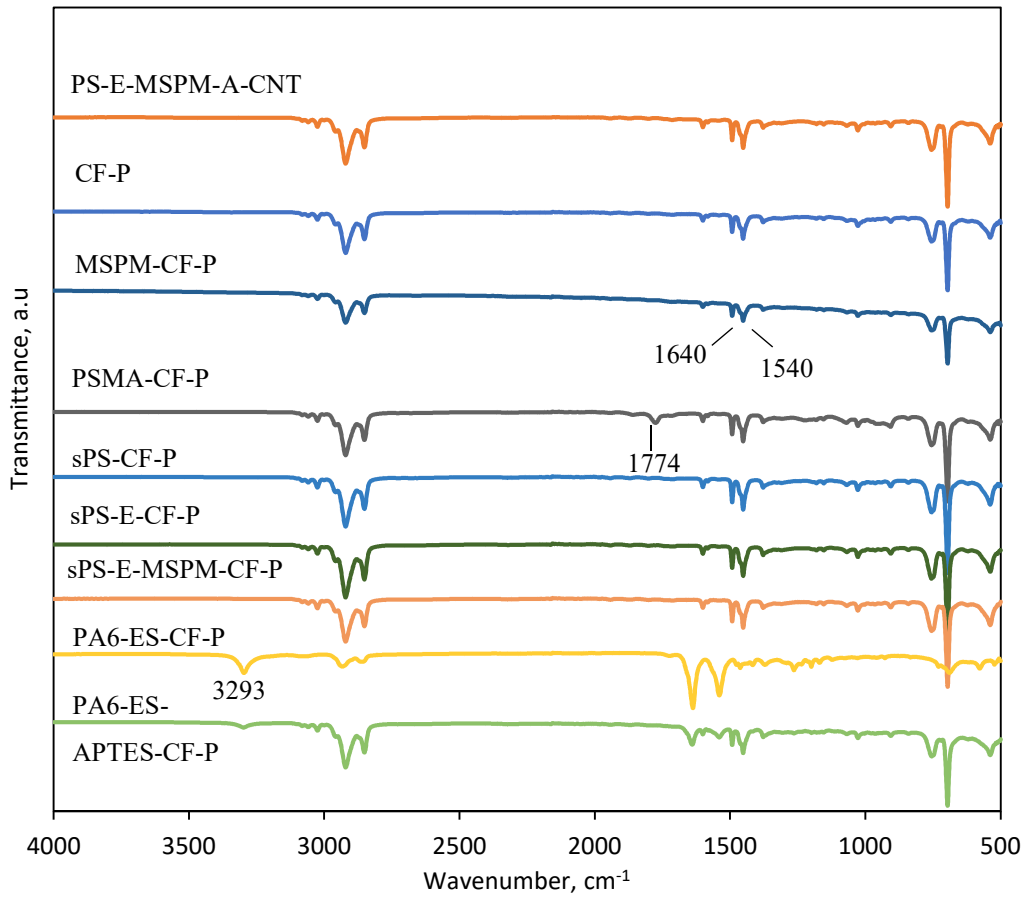

Figure 4.37. FTIR spectra of the polymer side of peeled surfaces after T-peel test.

The FTIR spectra of the CF side of the peeled surfaces after T-peel test are given in Figure 4.38. In the CF, MSPM-CF, PSMA-CF, sPS-CF, sPS-E-CF, sPS-E-MSPM-CF and PA6-ES-APTES-CF samples, the characteristic peaks of the polymer layer with different intensities were detected due to the polymer traces on the CF side of the specimens which adhered to the CF surface after peeling. In the spectrum of the PA6-ES-CF sample, there were no peaks represented the polymer layer and PA6; as discussed above, the nanofibrous layer was peeled from the CF surface and adhered to the polymer layer surface.

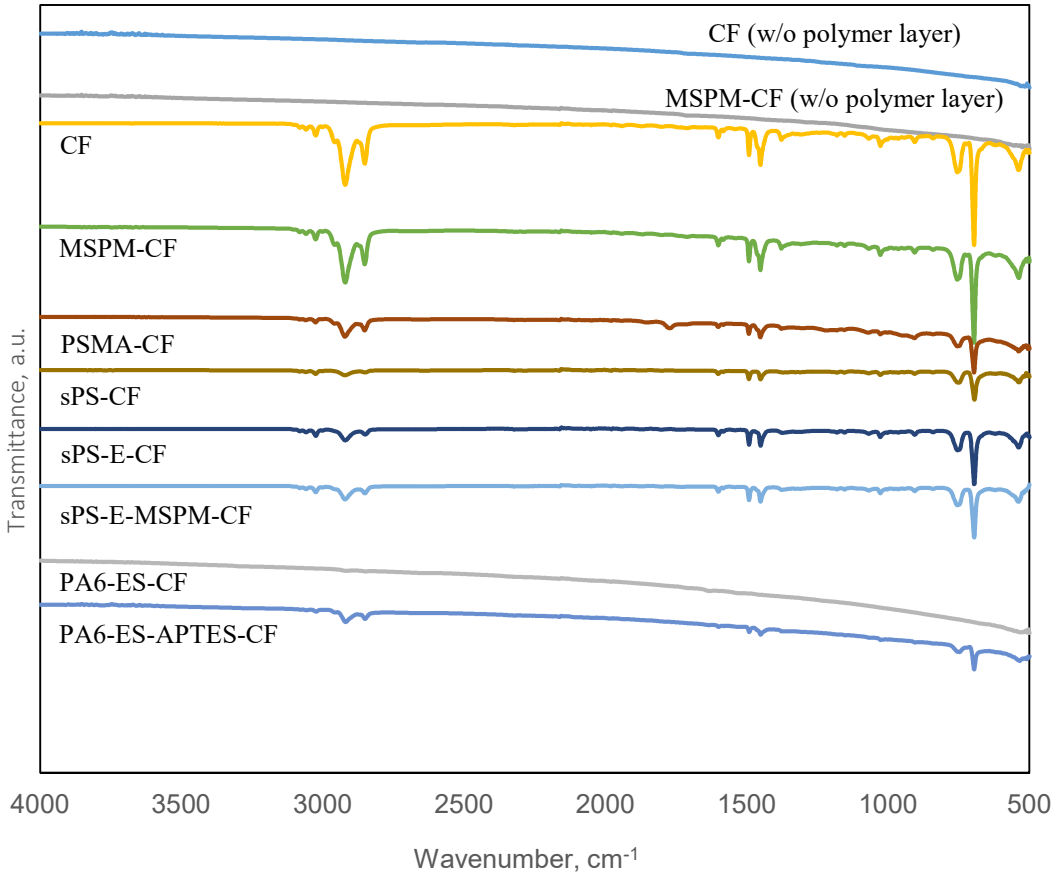

Figure 4.38. FTIR spectra of CF side of the peeled surfaces after T-peel test.

4.5.4 Desizing of CF

Sizing with a silane coupling agent was present on the as-received CFs. In order to investigate the effect of the presence of this sizing, desizing was performed by heating the as-received CFs in an oven. SEM images of the as-received CF, desized CF and first desized and then MSPM treated samples (MSPM-CF) are given in Figure 4.39. Surface of the fibers were not affected from the removal of the sizing by applying heat. There were no significant differences in the surface roughness of the fibers.

EDX analysis was also conducted during SEM imaging and elemental analyses results containing carbon (C), oxygen (O) and silicon (Si) are given in Table 4.10. The oxygen concentration was increased with desizing on the air atmosphere in the oven. This may be explained with the possible oxidations on the CF surface. The oxygen content increased further with silane treatment due to the formation of silonol groups between silane coupling agent and the substrate. Si content of the CF was decreased to 0.54% from 1.13% with desizing. With MSPM application on the desized CF surface, Si content was increased to 2.05%. The difference in Si content between the Desized-CF and Desized-MSPM-CF was approximately 2% which was the amount of silane coupling agent in the treatment solution.

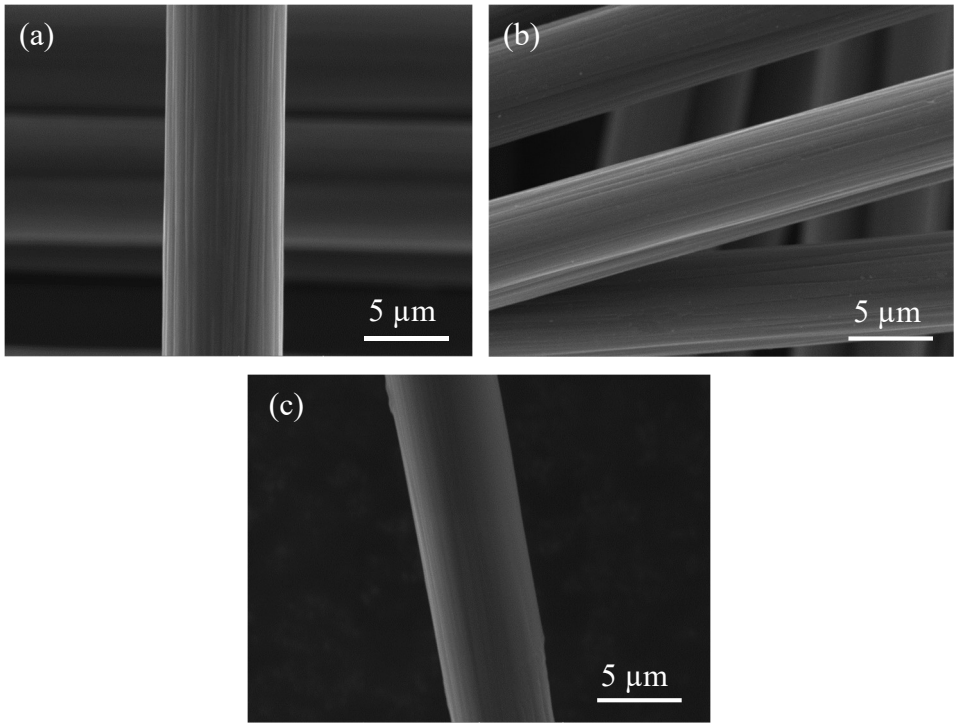

Figure 4.39. SEM images of (a) CF, (b) Desized-CF and (c) Desized-MSPM-CF samples.

Table 4.10 EDX results of CF and desized CF samples.

Sample	Carbon, wt. %	Oxygen, wt.%	Silicium, wt.%
CF	95.38 ± 2.3	3.50 ± 1.9	1.13 ± 0.5
Desized-CF	92.75 ± 0.6	6.72 ± 0.5	0.54 ± 0.1
Desized-MSPM-CF	83.29 ± 4.4	14.66 ± 3.7	2.05 ± 0.7

4.5.5 T-Peel Test Results

Representative peel curves of as-received and MSPM modified CF samples are given in Figure 4.40. The force required to peel the layers of the composites versus displacement which was the peeled distance of the films was recorded in the peel curves. The differences between the magnitudes of force required to peel the multilayer films were observed.

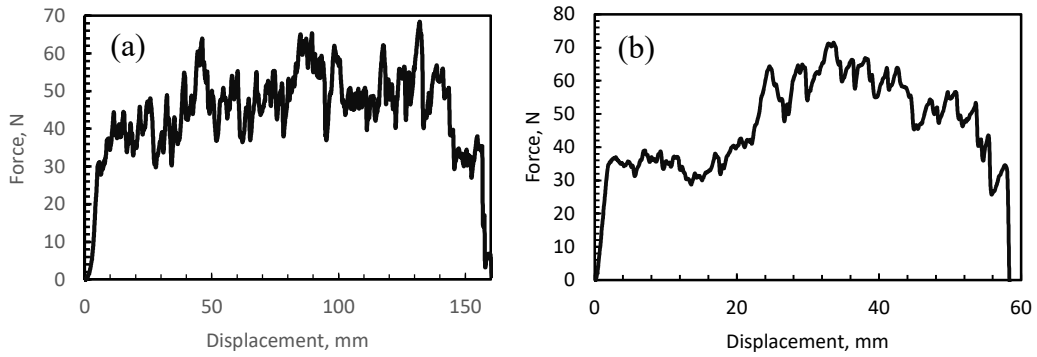

Figure 4.40. Force vs. displacement plot of the multilayer composite with (a) CF and (b) MSPM-CF.

The peel strengths of the as-recieved and modified multilayer composites are shown in Figure 4.41. The detailed results are given in Appendix G. When the present sizing was removed from the CF surface, peel strength was decreased to 1471 N/m from 1627 N/m. MSPM modification to the bare surface of CF was led to an increase up to 1625 N/m, which was close to the peel strength of as-received CF, due to the

possible hydrogen bond formation after the hydrolysis and condensation steps of the deposition of silane coupling agents (Arkles, 2014). With silane coupling agent modification applied to the as-received CF, we observed an increase in peel strength. The possible synergistic effect of the present silane coupling agent and MSPM may be the reason of this improvement.

PSMA molecule contains PS and reactive maleic anhydride group. During the PSMA modification of CF, non-homogeneous surface coating was observed after the evaporation of acetone from the CF surface. This may have resulted from the surface treatment application technique in this study. As understood from the peel strength of this composite, non-homogeneous coating of PSMA resulted in a high standard deviation in peel strength and also poor adhesion between the polymer layer and the CF modified with PSMA. In the optical microscope image of unbonded surface of this sample, polymer layer impregnation was weak compared to other composite surfaces. In the image of peeled surfaces, the areas impregnated with the polymer layer may be resulted from the regions which were not coated with PSMA solution.

When the T-peel test was performed with sPS-CF, the PS layer was acted as a separate layer and did not contribute to the adhesion. In order to increase the adhesion further, in-situ polymerization of PS and SEBS-gMA was conducted. The peel strength of this composite increased due to the introduction of polar groups to the interface with the addition of elastomer. The interaction between the CF and PS-E-based polymeric layers was improved with silane coupling agent treatment which was applied before coating the surface with sPS-E. There was a significant improvement in peel strength with MSPM treatment of CF due to the enhancement of the interaction resulting from the high possibility of forming chemical bonds with silane treatment.

Electrospinning of PA6 on the CF was performed to increase the contact area and mechanical interlocking between the polymeric layer and CF. The nanofibrous layer was easily peeled from CF during the T-peel test due to the lack of chemical interaction between the thick PA6 layer and CF in PA6-ES-CF sample. In order to

form chemical bonding between PA6 and CF, PA6 compatible silane coupling agent (APTES) modification was performed and PA6 layer was formed on the CF surface. Peel strength of this composite was approximately eight times higher than PA6-ES-CF sample. This increase can be explained with the improved interaction between the polymer layer and CF, and the potential functional groups formed between the PA6 nanofibers and APTES.

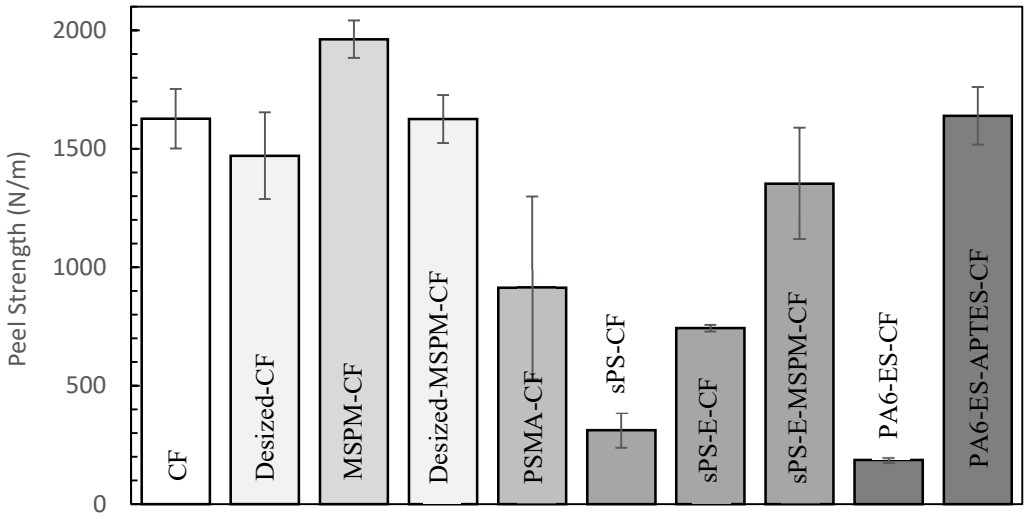

Figure 4.41. Peel strength dependence on different surface modifications applied to CF.

4.6 Effect of Increasing Number of CF Layers and Surface Modification on the Properties of Multilayer Composites

In this section, the characterization test results of the multilayer composites prepared with one, three, and five layers of CFs were discussed. Firstly, the results of ash content and TGA analyses were given in terms of the CF content of the multilayer composites. Then, the morphology of the samples was explained with SEM analysis, and the mechanical properties of the samples were investigated with the tensile test.

Finally, electrical resistivity measurements were discussed, and the shape memory behavior of the multilayer composites triggered with electricity was explained.

4.6.1 Ash Content and TGA Analyses

CF amount of the multilayer composites were determined applying ash content and TGA analyses. CF amount due to ash, total weight loss at 650°C from TGA analysis, temperatures at 5% weight loss and temperatures at the maximum weight loss (T_{max}) are given in Table 4.11.

According to the results, CF content in the multilayer composites increased from 10.3 wt.% to 47.5 wt.% with increasing number of CF plies. CF amount was also determined with TGA analysis and similar results were obtained with ash content analysis. The higher the number of CF layers in the multilayer composites, the lower the temperature at which 5% weight loss was observed. This can be explained by the fact that the CF layers and CNTs in the composites with higher thermal conductivities than the polymer act as heat dissipating agents, leading to a decrease in temperature values. The network structure formed by the carbonaceous fillers enhances the heat transfer and dominates the thermal conductivity of the composites (S. Choi et al., 2012).

Table 4.11 Ash content and TGA analyses results of multilayer composites.

Sample codes	CF amount, wt.%	Weight loss at 650°C, wt.%	Temperature at 5% weight loss, °C	T_{max}, °C
PS-1-CF	10.3 ± 0.4	11.1 ± 0.6	338 ± 7.5	418 ± 8.5
PS-3-CFs	28.5 ± 0.6	31.1 ± 0.8	323 ± 11.2	412 ± 2.8
PS-5-CFs	47.5 ± 1.9	46.1 ± 1.1	317 ± 12.0	408 ± 5.7
PS-5-MSPM-CFs	44.6 ± 0.6	46.1 ± 4.1	314 ± 7.6	402 ± 1.4

4.6.2 Scanning Electron Microscopy (SEM) Analysis

SEM images of the multilayer composites with respect to the increasing number of CF layers and the CF surface modification are shown in Figure 4.42. In PS-1-CF, PS-3-CFs and PS-5-CFs samples, which were produced with as-received PS-CFs, the fibers of the fabric were wetted non-homogeneously with the polymer layer. It was observed in the images of the PS-1-CF and PS-3-CFs composites that some of the fibers were separated from the polymer layer after the tensile test due to the weak impregnation. As seen in Figure 4.42 (d) and Figure 4.42 (f), the surface of the fibers were smooth. Even though there exists sizing on the as-received CFs and also potential compatibility between the layers, this did not lead to sufficient impregnation of the fibers by the polymeric material.

The surface modification applied on the CFs was resulted in an enhancement in the coverage of the fibers with polymer layer as can be seen in Figure 4.42 (g) and (h) which represent PS-5-MSPM-CFs composite. This can be based on the potential interactions between maleic anhydride groups which present in SEBS-gMA in the polymer matrix and the functional groups available on the CF surface with MSPM modification. Therefore, more homogeneous impregnation of polymeric material through the fibers was obtained. Also, the rough surfaces observed in Figure 4.42 (g) and (h) may contribute to the adhesion between the CF and polymer layers due to the mechanical interlocking. On the other hand, bundles of fibers were also observed in Figure 4.42 (g). This can be resulted in weak points in the multilayer composite. During surface modification, these weak points were formed in some regions due to the excess amount of silane coupling agent which was coated as a second layer on the present sizing. The relatively high concentration of silane coupling agent may cause a thick boundary layer and result in a decrease in modulus (T. Yang et al., 2019).

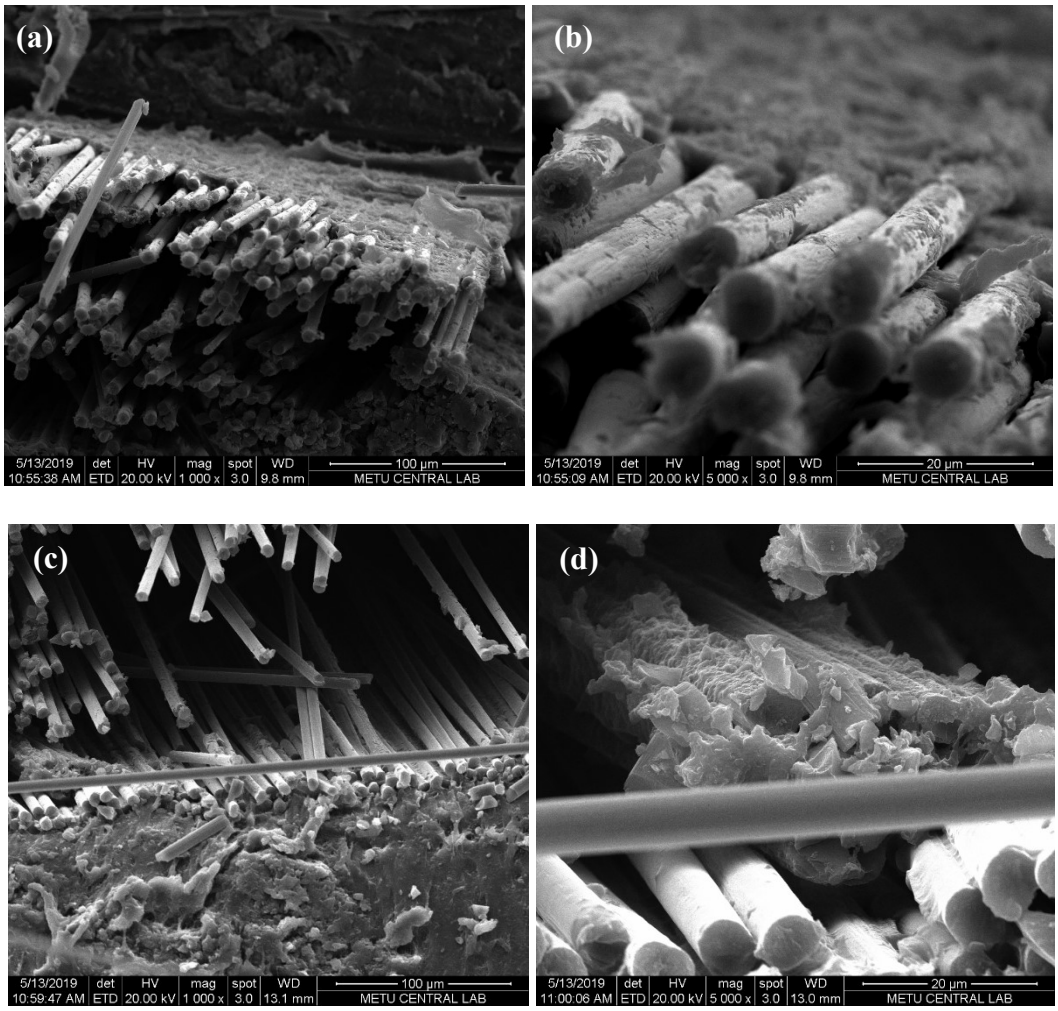

Figure 4.42. SEM images of the fracture surfaces of the multilayer composites; (a), (b) PS-1-CF, (c), (d) PS-3-CFs, (e), (f) PS-5-CFs and (g), (h) PS-5-MSPM-CFs at 1000x and at 5000x magnification, respectively.

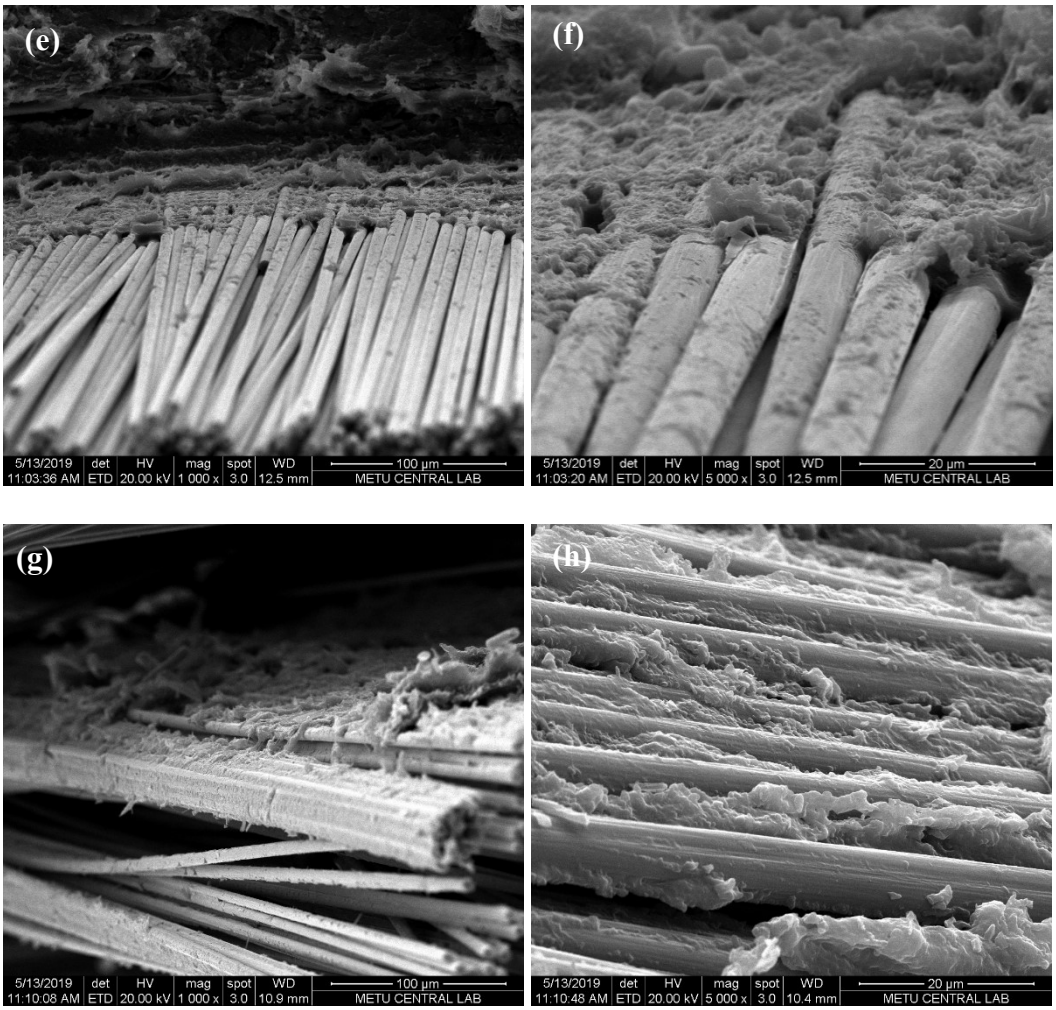

Figure 4.42. (cont'd) SEM images of the fracture surfaces of the multilayer composites; (a), (b) PS-1-CF, (c), (d) PS-3-CFs, (e), (f) PS-5-CFs and (g), (h) PS-5-MSPM-CFs at 1000x and at 5000x magnification, respectively.

4.6.3 Tensile Test Results

The representative stress versus strain plots of the multilayer composites with increasing number of CF layers and the one modified with MSPM are shown in Figure 4.43. The largest area under the curve among all the graphs was obtained with the PS-5-MSPM-CFs composite. The amount of the energy adsorbed and plastic deformation without fracture of the composite with MSPM treated CFs were higher

than the other samples. Moreover, the highest tensile strength of this composite indicated the use of an efficient modification technique which led to enhanced interactions between the layers.

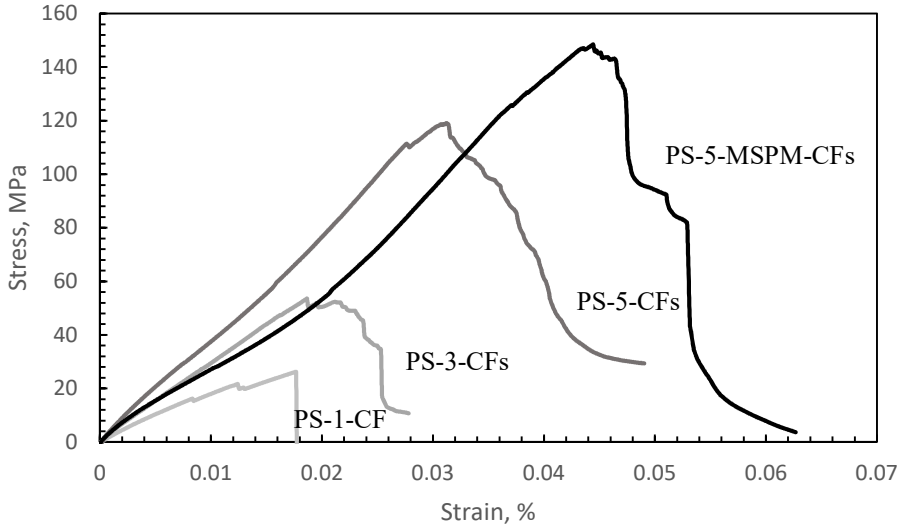

Figure 4.43. Stress-strain plots of the multilayer composites.

Tensile properties of the multilayer composites calculated for at least five samples are given in Appendix C with average values and standard deviations. The tensile strength results of the multilayer composites are illustrated in Figure 4.44. An increase in tensile strength was observed with increasing the CF amount. The tensile strength value of PS-1-CF sample was 18.8 MPa and this value was 117.6 MPa for the sample that contained five plies of as-received CF. The tensile strength of the sample produced with five plies of CFs modified with MSPM was 26% higher than the sample prepared without MSPM modification due to the improved interfacial adhesion between the layers of the composites. Silane coupling agent treatment is the most effective and common method to promote interfacial adhesion and provides an efficient stress transfer from thermoplastic matrix to fibers (Sang et al., 2016).

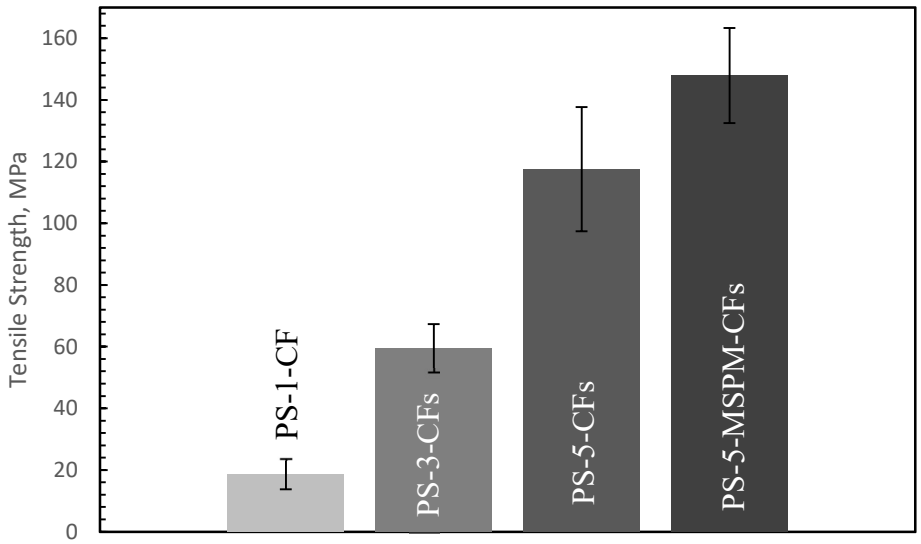

Figure 4.44. Tensile strengths of the multilayer composites.

The tensile moduli of the multilayer composites are shown in Figure 4.45. The increase in the amount of CF led to an increase in tensile modulus due to the higher modulus of CF. While the modulus of the multilayer composites containing one layer of as-received CF was 2091 MPa, the sample produced by using five plies of CFs was 4712 MPa. When MSPM modification was applied on the CF surfaces it was observed that tensile modulus of PS-5-MSPM-CFs was lower than the composite without MSPM modification. This can be due to the excess amount of sizing on some parts of the fibers causing them to adhere together and insufficient impregnation of the polymer through bundles of the fibers, which may create weak points in the multilayer composite as observed in the SEM analyses (Sun et al., 2020).

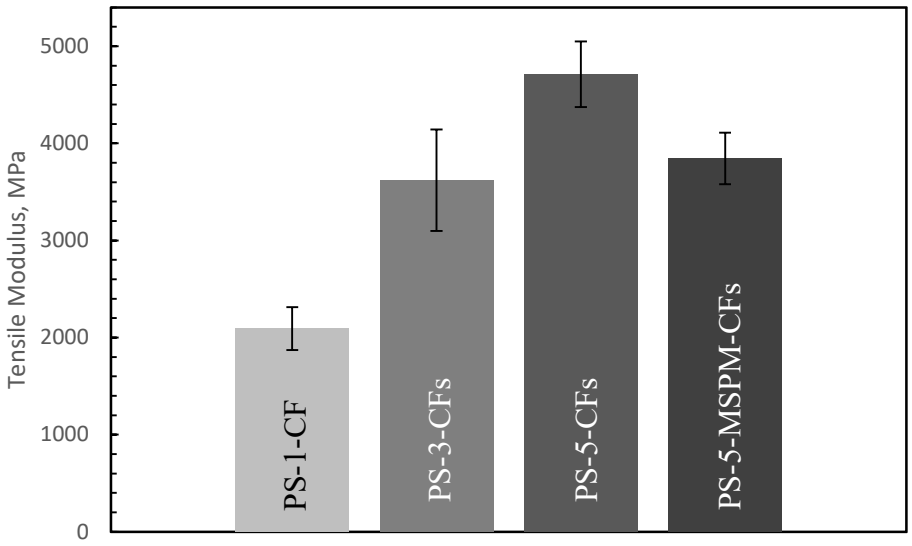

Figure 4.45. Tensile moduli of the multilayer composites.

The elongation at break values of the multilayer composites are illustrated in Figure 4.46. When the number of CF layers increased, elongation at break values of the samples also increased. The percent elongation was further improved with MSPM modification. It is known from the manufacturer that the existing silane coupling agent on the as-received CFs is compatible with epoxy resins. In the present study, CF surfaces were modified on top of this available sizing. Therefore the excess amount of silane coupling agent may form a weak boundary layer by physical adsorption and may increase the thickness of the sizing layer which may reduce the efficiency of load transfer at the interface. This is explained in the literature as the lubrication effect of the boundary layer (Cho et al., 2005; Qi et al., 2016).This may also be responsible for decrease in the tensile modulus of the MSPM modified CF-reinforced multilayer composites.

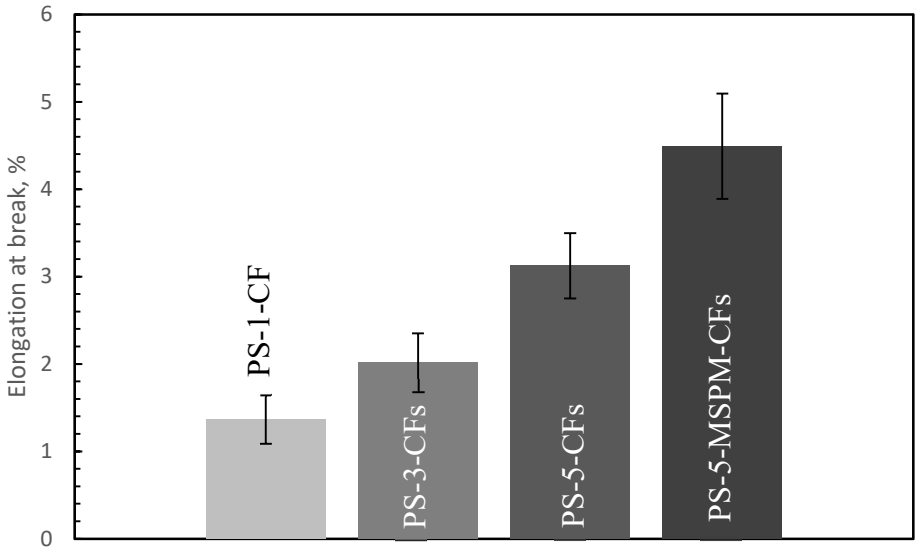

Figure 4.46. Elongation at breaks of the multilayer composites.

4.6.4 Electrical Resistivity Measurements

The electrical resistivities of the multilayer composites prepared with different number of CF plies were measured with two-point probe method (Figure 4.47). The lowest electrical resistivity with $10^{-1.3}$ ohm.cm was reached in the sample that containing five plies of as-received CF and this value was $10^{-0.8}$ ohm.cm for PS-1-CF sample. With silane coupling agent treatment, an increase was observed in the resistivity value to $10^{-1.2}$ ohm.cm. This can be explained with the insulating modifier layer coated on CF surfaces which did not allow the transportation of electrons effectively, therefore decreased the electrical conductivity (Gojny et al., 2006). The conductivity values of all of the composites were in the semiconductor region.

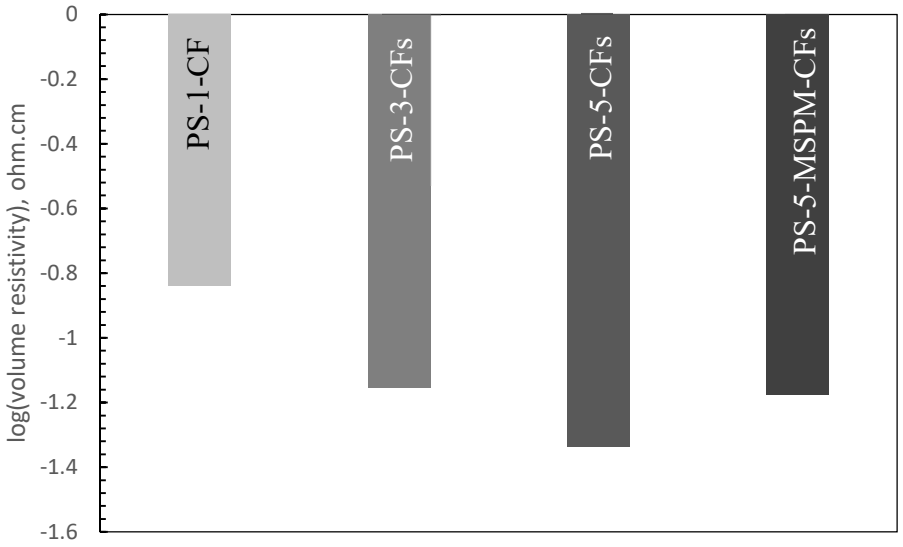

Figure 4.47. Electrical resistivities of the multilayer composites.

4.6.5 Shape Memory Behavior Analysis with Bending Test Actuated by Electricity

The electrically triggered bending test images of the samples at the beginning of the test and after recovery are shown in Figure 4.48. While giving the temporary shape to the samples containing three and five plies of CFs (Figure 4.48 (c) and (e)), shape deformations in the form of folded regions were observed, which are also seen in Figure 4.48 (g) for the composite with MSPM modified CFs. These folded regions can be considered as defects which are considered to be resulted from non-homogeneous wetting of the fibers, in other words, the bundles of CFs without any impregnation so that they do not interact sufficiently with the polymer layers. They are expected to make the shape recovery difficult due to the weak bonding through these points, therefore, they prevent the samples from regaining their permanent shape in a shorter time.

Recovery ratio and recovery time values are given in Table 4.12. The detailed results with average values of five data and their standard deviations are given in Appendix D. 100% shape recovery values as calculated from the reference plane and average

recovery times less than one minute were obtained in all the multilayer composites depending on the existence of both hard and soft segments in the composite structure. PS, CFs, and CNTs contributed to the hard segments of the composites, whereas SEBS-g-MA formed the soft segment of the structure. Hard segments are responsible for the recovery of the permanent shape, and soft segments generate the switching mechanism between the temporary shape and the permanent one (Behl & Lendlein, 2007; Yasar, 2014). Shape recovery times of the multilayer composites were slightly decreased with the increasing number of CF layers. This was attributed to the increase in the electrical conductivities of the samples. A slight increase in the recovery time of the sample which was fabricated with five plies of MSPM modified CFs, was observed due to the decrease in conductivity resulting from the surface modification.

Polymers with shape memory property determined by triggering with electricity are required to possess the characteristic of electrically conductive materials, in which resistive heating is generated by electrical current passage through conductive points and this contributes to the occurrence of the shape recovery. Thus, not only the chemical structure of the composite layers consisting of aforementioned both hard and soft segments but also the electrical conductivities of the composites resulting from CFs and CNTs are effective on the shape recovery ratio and recovery times of the multilayer composites determined with electrical actuation.

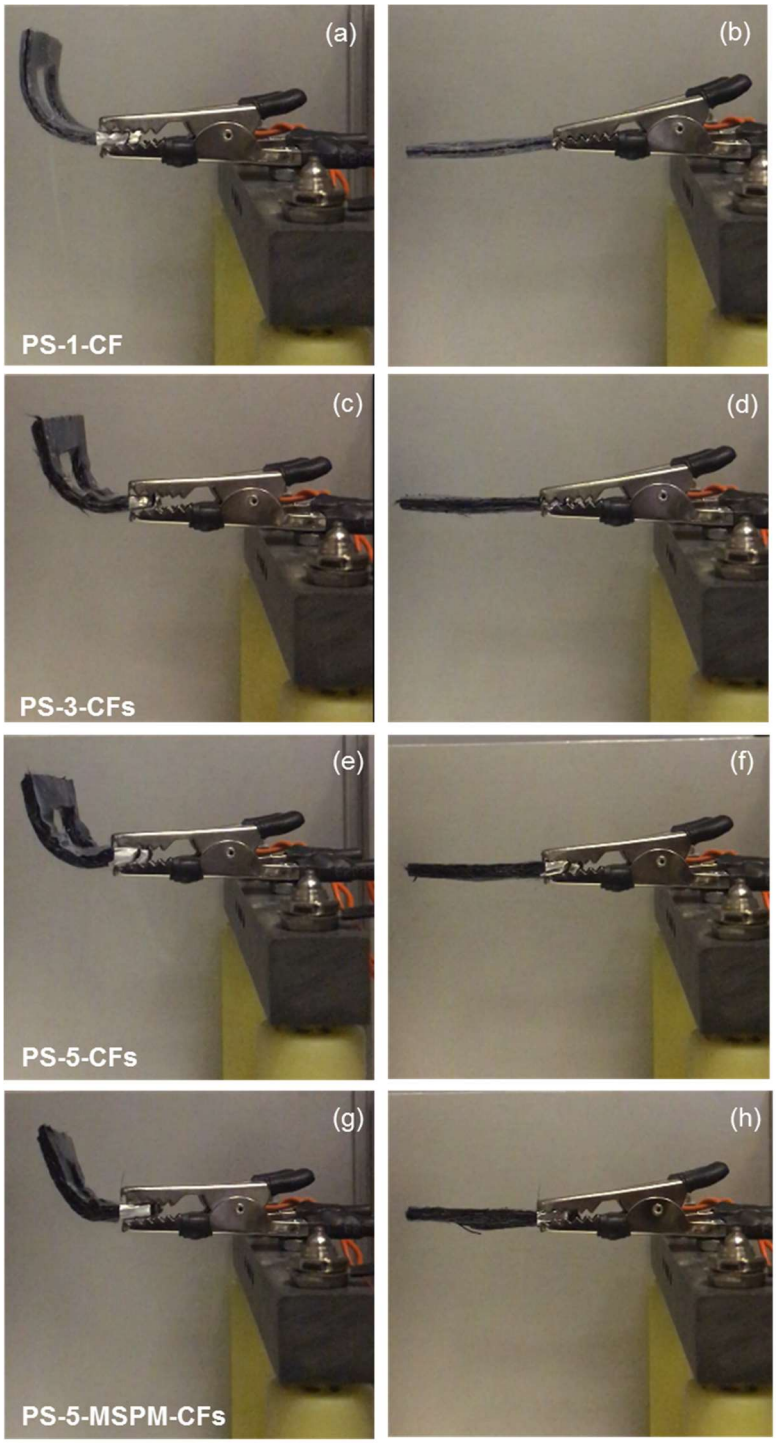

Figure 4.48. Electrically bending test images of the multilayer composites at the beginning of the test and after the recovery; (a), (b) PS-1-CF, (c), (d) PS-3-CFs, (e), (f) PS-5-CFs and (g),(h) PS-5-MSPM-CFs.

Table 4.12 Electrically bending test results of the multilayer composite samples.

Sample	Shape Recovery Time, sec.	Shape Recovery Ratio, %
PS-1-CF	58.4 ± 3.8 sec	100
PS-3-CFs	55.8 ± 6.0 sec	100
PS-5-CFs	49.4 ± 5.3 sec	100
PS-5-MSPM-CFs	51.4 ± 4.7 sec	100

CHAPTER 5

CONCLUSIONS

PS-based and CF-reinforced multilayer composites containing CNTs and SEBS-gMA were successfully prepared with compression molding method. In order to improve the dispersion of CNTs in the polymer matrix and enhance the interfacial adhesion between the layers of multilayer composites, surface modifications were applied to CNTs and CFs, respectively. To investigate the performance of thermoplastic-based CFRPs, the number of CF layers was increased from one to five layers at the end of the study. When all the experiments conducted within the scope of the thesis were evaluated, the following results were obtained.

5.1 Surface Treatment and Modification of CNTs

In the first part of the thesis, CNTs were modified with different materials in order to achieve homogeneous dispersion in the PS matrix. Before the surface modification, CNTs were treated with 1:1 H_2SO_4 and HNO_3 solution and then modified with two silane coupling agents (MSPM, GLYMO), three surfactants (SDS, SDBS, TX100) and a copolymer (PSMA).

Stability of the suspensions of CNTs in PS-Toluene solutions was ranged as MSPM-A-CNT> SDBS-A-CNT> TX100-A-CNT> SDS-A-CNT> CNT> PSMA-A-CNT> GLYMO-A-CNT. Thin film samples were fabricated with compressing molding from melt blended PS-CNT binary nanocomposites. According to the measurements performed on optical microscope images of the thin films, the areas that covered by the agglomerates were decreased with surface modifications applied to the CNTs. PSMA-A-CNT and GLYMO-A-CNT samples were not compatible with PS, and SDS-A-CNT were not stable enough in the PS-Toluene solution.

Also, to prevent the formation of agglomerations during extrusion, three different parametric approaches in terms of feeding point (main feeder and hopper), feed rate (25 and 15 g/min), and screw speed (150 and 100 rpm) were investigated in melt mixing process. PS-CNT composites were produced with 1 wt% of SDBS-A-CNT, TX100-A-CNT, and MSPM-A-CNT. The highest tensile and impact properties, the lowest electrical resistivities were achieved with feeding from the hopper, a feed rate of 15 g/min, and a screw speed of 100 rpm, and melt blending of ternary nanocomposites were conducted with these conditions throughout the study.

For PS modification, a compatible elastomer (SEBS-gMA) was also added in order to form soft segments of the composite structure in the present study. Ternary composites containing PS, SEBS-gMA, unmodified, and modified CNTs were characterized in terms of electrical resistivity, tensile and impact properties, morphology, and shape memory behavior. Electrical resistivity decreased to $10^{8.2}$ ohm.cm from $10^{8.9}$ ohm.cm with MSPM modified CNT addition to the PS-E sample. Impact strength increased to 61.7 kJ/m^2 for PS-E-MSPM-A-CNT from 37.1 kJ/m^2 for PS-E. Homogeneously dispersed CNTs were observed in the SEM images of PS-E-MSPM-A-CNT sample. The fastest shape recovery behavior was recorded in PS-E-MSPM-A-CNT sample with 1 minute and 9 seconds compared to other CNT added ternary composites. MSPM modification was chosen as the most suitable surface modification method for the dispersion of CNTs in the composite systems of this study.

5.2 Characterization of Synthesized PS (sPS)

Bulk polymerization of styrene was conducted with 0.01, 0.008, and 0.005 mol/L initiator concentrations in the second part of the thesis. The success of the synthesis was checked with FTIR analyses, and characteristic peaks for PS were observed. The MFI and molecular weight values of commercial PS used in dilution and melt blending methods were obtained in the PS sample prepared by using 0.005 mol/L initiator concentration.

5.3 Characterization of PS-CNT Masterbatches

sPS-CNT, and sPS-MSPM-A-CNT masterbatches were successfully prepared with in-situ polymerization containing 3.2 wt.% CNTs, and were diluted with commercial PS and SEBS-gMA with melt mixing method to have 1 wt.% CNTs in the composites.

5.4 Comparison of Masterbatch Dilution and Direct Melt Mixing Methods in the Characterization of Multilayer Composites

To investigate the effect of alternative preparation techniques on the mechanical, electrical, and shape memory properties of multilayer composites, polymer layers were prepared with nanocomposites produced with both the masterbatch dilution and direct melt mixing.

The masterbatch dilution method improved the strength, stiffness, and electrical conductivity of the multilayer composites. In this part of the thesis, it has been proven that the in-situ polymerization method provided a more uniform distribution of CNTs in the polymer matrix than the direct melt mixing method. However, the in-situ polymerization followed by masterbatch dilution method is not a practical technique for large scale production of the multilayer composites. Therefore, the direct melt mixing method was preferred in the preparation of ternary composites.

5.5 Surface Modification of CF Layers

To improve the adhesion between polymeric layers and CF plies of the multilayer composites, seven different surface modification techniques were applied to CFs.

Traces of surface modifications were detected from un-bonded and peeled surfaces from T-peel test specimens. The theoretical work of adhesion (W_a) was calculated from contact angles measured with the sessile drop method. W_a values varied

between 76.83 mJ/m^2 and 51.80 mJ/m^2 and indicated that MSPM modification was a promising method to enhance the interaction between the layers.

The highest peel strength was reached in MSPM treated CF, which was 1962 N/m. Desizing of CF was also studied. After desizing, the peel strength was decreased to 1471 N/m from 1627 N/m. When the second silanization was applied with MSPM to the bare surface of CF, peel strength increased to 1625 N/m, which was similar to the peel strength of the composite with as-received CF. The results showed that present sizing on the CF surface had no adverse effect through second silanization with MSPM.

5.6 Effect of Increasing Number of CF Layers and Surface Modification on the Properties of Multilayer Composites

Finally, multilayer composites with one, three, and five layers of as-received and five layers of MSPM-CF were prepared. The nanocomposite consisting of PS, SEBS-gMA and MSPM treated CNTs was used as polymer layer configuration in these multilayer composites due to the slightly higher electrical conductivity and much higher impact strength values, which were achieved owing to relatively homogeneous dispersion amongst the ternary composites produced.

The CF content of the multilayer composites increased to 47.5 wt.% from 10.3 wt.% when the number CF layers increased from one to five. To observe the effect of silane modification in multilayer composites, a PS-5-MSPM-CFs sample was prepared with five CF plies modified with MSPM. The tensile strength value of PS-1-CF was 18.8 MPa, and this value was 148 MPa for PS-5-MSPM-CFs. While the modulus of PS-1-CF was 2091 MPa, the sample produced by using five plies of CFs had the tensile modulus of 4712 MPa. The modulus of PS-5-MSPM-CFs was lower than the sample without MSPM modification.

The lowest electrical resistivity with $10^{-1.3}$ ohm.cm was reached in PS-5-CFs, and this value was $10^{-0.8}$ ohm.cm for PS-1-CF. According to the bending test results, all the multilayer composites showed shape recovery ratio of 100% within one minute.

CHAPTER 6

RECOMMENDATIONS

It was aimed to produce thermoplastic-based CFRPs, which can be a potential material to be applied in the aerospace and automotive industries instead of thermoset-based CFRPs due to environmental concerns. Mechanical, electrical, and shape memory properties of PS-based multilayer composites were enhanced to a certain extent, with the addition of CNTs treated with a silane coupling agent and the surface modified CFs.

Purification of CNTs can be performed with a nondestructive method in order to enhance the dispersion of CNTs in the polymer matrix without forming defects on the CNTs walls. For achieving more homogeneous dispersion, vinyltrimethoxysilane which is compatible with polystyrene, can be used as silane coupling agent instead of MSPM applied in this study.

To improve the performance of multilayer composites further, the concentration of CF in the composites can be increased. This can be achieved by applying different process techniques explained as follows. For better impregnation, firstly, thermoplastic polymers may be dissolved in suitable solvents, and then hand lay-up method can be used to prepare multilayer composites. Thermoplastic prepregs can also be used as layers of multilayer composites.

In this study, PS was chosen due to recyclability and economic considerations. Another approach to enhance the properties of CFRPs is the usage of advanced engineering plastics such as polyether ether ketone and polyphenylene sulfide, which have higher mechanical properties than PS.

REFERENCES

A350 XWB. (2019). Retrieved from https://www.airbus.com/aircraft/passenger-aircraft/a350xwb-family.html#smartchoice

Ahmad, M., Singh, D., Fu, Y. Q., Miraftab, M., & Luo, J. K. (2011). Stability and deterioration of a shape memory polymer fabric composite under thermomechanical stress. *Polymer Degradation and Stability*, *96*, 1470–1477. https://doi.org/10.1016/j.polymdegradstab.2011.05.009

Akkaoui, W., & Bayram, G. (2004). Effects of processing parameters on mechanical and thermal properties of glass mat reinforced nylon 6 composites. *Journal of Reinforced Plastics and Composites*, *23*, 881–892. https://doi.org/10.1177/0731684404033376

Annala, M., Lahelin, M., & Seppälä, J. (2012). The effect of MWCNTs on molar mass in in situ polymerization of styrene and methyl methacrylate. *European Polymer Journal*, *48*, 1516–1524. https://doi.org/10.1016/j.eurpolymj.2012.05.016

Arao, Y., Yumitori, S., Suzuki, H., Tanaka, T., Tanaka, K., & Katayama, T. (2013). Mechanical properties of injection-molded carbon fiber/polypropylene composites hybridized with nanofillers. *Composites Part A: Applied Science and Manufacturing*, *55*, 19–26. https://doi.org/10.1016/j.compositesa.2013.08.002

Arkles, B. (2014). *Silane Coupling Agents: Connecting Across Boundaries*.

ASTM D7490-08, Standard Test Method for Measurement of the Surface Tension of Solid Coatings, Substrates and Pigments using Contact Angle Measurements. (2008). https://doi.org/10.1520/D7490-08.2

Ávila-Orta, C. A., González-Morones, P., Espinoza-González, C. J., Martínez-Colunga, J. G., Neira-Velázquez, M. G., Sáenz-Galindo, A., & López-López, L. I. (2013). Toward Greener Chemistry Methods for Preparation of Hybrid Polymer Materials Based on Carbon Nanotubes. In *Syntheses and Applications of Carbon Nanotubes and Their Composites* (pp. 167–192). https://doi.org/10.1016/j.colsurfa.2011.12.014

Avilés, F., Cauich-Rodríguez, J. V., Toro-Estay, P., Yazdani-Pedram, M., & Aguilar-Bolados, H. (2018). Improving carbon nanotube/polymer interactions in nanocomposites. In *Carbon Nanotube-Reinforced Polymers: From Nanoscale to Macroscale* (pp. 83–115). https://doi.org/10.1016/B978-0-323-48221-9.00005-4

Ayatollahi, M. R., Barbaz Isfahani, R., & Moghimi Monfared, R. (2017). Effects of multi-walled carbon nanotube and nanosilica on tensile properties of woven carbon fabric-reinforced epoxy composites fabricated using VARIM. *Journal of Composite Materials*, *51*(30), 4177–4188. https://doi.org/10.1177/0021998317699982

Ayewah, D. O. O., Davis, D. C., Krishnamoorti, R., Lagoudas, D. C., Sue, H., & Willson, M. (2010). A surfactant dispersed SWCNT-polystyrene composite characterized for electrical and mechanical properties. *Composites: Part A*, *41*, 842–849. https://doi.org/10.1016/j.compositesa.2010.02.015

Azam, S., Jumahat, A., Rosli, N., & Frormann, L. (2012). Determination of Shape Fixity and Shape Recovery Rate of Carbon Nanotube-filled Shape Memory Polymer Nanocomposites. *Engineering Procedia*, *41*, 1641–1646. https://doi.org/10.1016/j.proeng.2012.07.362

Baldan, A. (2012). Adhesion phenomena in bonded joints. *International Journal of Adhesion and Adhesives*, *38*, 95–116. https://doi.org/10.1016/j.ijadhadh.2012.04.007

Balık, E. (2015). *Polystyrene/Boron Nitride Nanotube Composites: Synthesis, Processing and Characterization*. METU, MSc. Thesis.

Behl, M., & Lendlein, A. (2007). Shape-memory polymers. *Materials Today*, *10*(4), 20–28. https://doi.org/10.1016/S1369-7021(07)70047-0

Bekyarova, E., Thostenson, E. T., Yu, A., Kim, H., Gao, J., Tang, J., Hahn, H. T., Chou, T. W., Itkis, M. E., Haddon, R. C. (2007). Multiscale Carbon Nanotube - Carbon Fiber Reinforcement for Advanced Epoxy Composites. *Langmuir*, (23), 3970–3974.

Bhattacharya, M. (2016). Polymer nanocomposites-A comparison between carbon nanotubes, graphene, and clay as nanofillers. *Materials*, *9*(4), 1–35. https://doi.org/10.3390/ma9040262

Bhattacharya, S. N., Kamal, M. R., & Gupta, R. K. (2006). Polymeric nanocomposites: Theory and practice. In *Polymeric Nanocomposites: Theory and Practice*. https://doi.org/10.3139/9783446418523

Billmeyer, F. W. (1984). Textbook of Polymer Science. In *A Wiley-lnterscience Publication*. https://doi.org/10.1007/978-1-4614-7696-2

Boeing 787 from the Ground Up. (2019). Retrieved from http://www.boeing.com/commercial/aeromagazine/articles/qtr_4_06/article_04_2.html

Boon, Y. Di, & Joshi, S. C. (2020). A review of methods for improving interlaminar interfaces and fracture toughness of laminated composites. *Materials Today Communications*, *22*, 1–15. https://doi.org/10.1016/j.mtcomm.2019.100830

Braga, N. F., Zaggo, H. M., Montagna, L. S., & Passador, F. R. (2020). Effect of Carbon Nanotubes (CNT) Functionalization and Maleic Anhydride-Grafted Poly(trimethylene terephthalate) (PTT-g-MA) on the Preparation of Antistatic Packages of PTT/CNT Nanocomposites. *Journal of Composites Science*, *4*(44), 1–18.

Brostow, W. (2007). Mechanical Properties. In James E. Mark (Ed.), *Physical Properties of Polymers Handbook* (pp. 423–445). https://doi.org/10.1007/BF01840027

Camponeschi, E., Florkowski, B., Vance, R., Garrett, G., Garmestani, H., & Tannenbaum, R. (2006). Uniform Directional Alignment of Single-Walled Carbon Nanotubes in Viscous Polymer Flow. *Langmuir*, *22*, 1858–1862.

Chen, Z., Dai, X. J., Lamb, P. R., De Celis Leal, D. R., Fox, B. L., Chen, Y., du Plessis, J., Field, M., Wang, X. (2012). Practical amine functionalization of multi-walled carbon nanotubes for effective interfacial bonding. *Plasma Processes and Polymers*, *9*(7), 733–741. https://doi.org/10.1002/ppap.201100203

Cho, J. W., Kim, J. W., Jung, Y. C., & Goo, N. S. (2005). Electroactive shape-memory polyurethane composites incorporating carbon nanotubes. *Macromolecular Rapid Communications*, *26*, 412–416.

Choi, K. H., Yoo, D. G., Kim, G. H., & Ha, C. S. (2017). Effect of acrylic block copolymer on the fracture toughness and glass transition temperature of carbon fabric reinforced 180°C cure-epoxy composites. *Molecular Crystals and Liquid Crystals*, *659*(1), 15–22. https://doi.org/10.1080/15421406.2018.1449788

Choi, S., Im, H., & Kim, J. (2012). Flexible and high thermal conductivity thin films based on polymer: Aminated multi-walled carbon nanotubes/micro-aluminum nitride hybrid composites. *Composites Part A: Applied Science and Manufacturing*, *43*(11), 1860–1868. https://doi.org/10.1016/j.compositesa.2012.06.009

Choudhary, V., Singh, B. P., & Mathur, R. B. (2013). Carbon Nanotubes and Their Composites. In *Syntheses and Applications of Carbon Nanotubes and Their Composites* (pp. 193–222).

Chung, D. D. L. (2017). Processing-structure-property relationships of continuous carbon fiber polymer-matrix composites. *Materials Science and Engineering R: Reports*, *113*, 1–29.

Connell, M. J. O., Boul, P., Ericson, L. M., Hu, C., Wang, Y., Haroz, E., Kuper, C., Tour, J., Ausman, K. D., Smalley, R. E. (2001). Reversible water-solubilization of single-walled carbon nanotubes by polymer wrapping. *Chemical Physics Letters*, *342*(July), 265–271.

Daelemans, L., Cohades, A., Meireman, T., Beckx, J., Spronk, S., Kersemans, M., De Baere, I., Rahier, H., Michaud, V., Van Paepegem, W., De Clerck, K. (2018). Electrospun nanofibrous interleaves for improved low velocity impact resistance of glass fibre reinforced composite laminates. *Materials and Design*, *141*, 170–184. https://doi.org/10.1016/j.matdes.2017.12.045

Daelemans, L., van der Heijden, S., De Baere, I., Rahier, H., Van Paepegem, W., & De Clerck, K. (2015). Nanofibre bridging as a toughening mechanism in carbon/epoxy composite laminates interleaved with electrospun polyamide nanofibrous veils. *Composites Science and Technology*, *117*, 244–256. https://doi.org/10.1016/j.compscitech.2015.06.021

Das, T. K., Ghosh, P., & Das, N. C. (2019). Preparation, development, outcomes, and application versatility of carbon fiber-based polymer composites: a review. *Advanced Composites and Hybrid Materials*, *2*(2), 214–233. https://doi.org/10.1007/s42114-018-0072-z

Deka, H., & Karak, N. (2010). Biocompatible hyperbranched polyurethane / multi-walled carbon nanotube composites as shape memory materials. *Carbon*, *48*, 2013–2022. https://doi.org/10.1016/j.carbon.2010.02.009

Díez-pascual, A. M., Naffakh, M., Marco, C., Gómez-fatou, M. A., & Ellis, G. J. (2014). Multiscale fiber-reinforced thermoplastic composites incorporating carbon nanotubes : A review. *Current Opinion in Solid State and Materials Science*, *18*, 62–80. https://doi.org/10.1016/j.cossms.2013.06.003

Dike, A. S. (2011). *Nanocomposites Based on Blends of Polystyrene*. METU, PhD. Thesis.

Faraguna, F., Pötschke, P., & Pionteck, J. (2017). Preparation of polystyrene nanocomposites with functionalized carbon nanotubes by melt and solution mixing : Investigation of dispersion , melt rheology , electrical and thermal properties. *Polymer*, *132*, 325–341. https://doi.org/10.1016/j.polymer.2017.11.014

Fu, Q., Lu, C., & Liu, J. (2002). Selective Coating of Single Wall Carbon Nanotubes with Thin SiO_2 Layer. *Nano Letters*, *2*(4), 329–332. https://doi.org/10.1021/nl025513d

García, M. G., Marchese, J., & Ochoa, N. A. (2010). Effect of the particle size and particle agglomeration on composite membrane performance. *Journal of Applied Polymer Science*, *118*(4), 2417–2424. https://doi.org/10.1002/app.32274

Garifullin, A. R., Krasina, I. V., Skidchenko, E. A., Shaekhov, M. F., & Tikhonova, N. V. (2017). Modification of carbon fabrics by radio-frequency capacitive discharge at low pressure to regulate mechanical properties of carbon fiber reinforced plastics based on it Modification of carbon fabrics by radio-frequency capacitive discharge at low pressure. *Journal of Physics: Conference Series*, *789*, 12–15. https://doi.org/10.1088/1742-6596/755/1/011001

Gojny, F. H., Wichmann, M. H. G., Fiedler, B., Kinloch, I. A., Bauhofer, W., Windle, A. H., & Schulte, K. (2006). Evaluation and identification of electrical and thermal conduction mechanisms in carbon nanotube/epoxy composites. *Polymer*, *47*(6), 2036–2045.

Gómez, S., Rendtorff, N. M., Aglietti, E. F., Sakka, Y., & Suárez, G. (2016). Surface modification of multiwall carbon nanotubes by sulfonitric treatment. *Applied Surface Science*, *379*, 264–269. https://doi.org/10.1016/j.apsusc.2016.04.065

Gopal, N., Rana, S., Whan, J., Li, L., & Hwa, S. (2010). Polymer nanocomposites based on functionalized carbon nanotubes. *Progress in Polymer Science*, *35*(7), 837–867. https://doi.org/10.1016/j.progpolymsci.2010.03.002

Guaita, M. (1986). Thermal Degradation of Polystyrene. *British Polymer Journal*, *18*(4), 226–230. https://doi.org/10.1246/nikkashi.1975.1241

Ham, H. T., Choi, Y. S. U. K., Chee, M. U. G., & Chung, I. N. J. A. E. (2006). Singlewall Carbon Nanotubes Covered with Polystyrene Nanoparticles by In-Situ Miniemulsion Polymerization. *Journal of Polymer Science: Part A: Polymer Chemistry*, *44*, 573–584. https://doi.org/10.1002/pola.21185

Han, X. J., Dong, Z. Q., Fan, M. M., Liu, Y., Li, J. H., Wang, Y. F., Yuan, Q. J., Li, B. J., Zhang, S. (2012). pH-induced shape-memory polymers. *Macromolecular Rapid Communications*, *33*(12), 1055–1060.

Hassanzadeh-aghdam, M. K., Ansari, R., & Javad, M. (2019). Mechanics of Materials Thermo-mechanical properties of shape memory polymer nanocomposites reinforced by carbon nanotubes. *Mechanics of Materials*, *129*(November 2018), 80–98. https://doi.org/10.1016/j.mechmat.2018.11.009

Hatui, G., Bhattacharya, P., Sahoo, S., Dhibar, S., & Das, C. K. (2014). Combined effect of expanded graphite and multiwall carbon nanotubes on the thermo mechanical , morphological as well as electrical conductivity of in situ bulk polymerized polystyrene composites. *Composites Part A*, *56*, 181–191. https://doi.org/10.1016/j.compositesa.2013.10.007

Hermán, V., Takacs, H., Duclairoir, F., Renault, O., Tortai, J. H., & Viala, B. (2015). Core double-shell cobalt/graphene/polystyrene magnetic nanocomposites synthesized by in situ sonochemical polymerization. *RSC Advances*, *5*(63), 51371–51381. https://doi.org/10.1039/c5ra06847a

Hoepfner, J. C., & Pezzin, S. H. (2016). Functionalization of carbon nanotubes with (3-glycidyloxypropyl)-trimethoxysilane: Effect of wrapping on epoxy matrix nanocomposites. *Journal of Applied Polymer Science*, *133*(47), 1–10. https://doi.org/10.1002/app.44245

Hua, J., Wang, Z., Xu, L., Wang, X., Zhao, J., & Li, F. (2013). Preparation polystyrene/multiwalled carbon nanotubes nanocomposites by copolymerization of styrene and styryl-functionalized multiwalled carbon nanotubes. *Materials Chemistry and Physics*, *137*(3), 694–698. https://doi.org/10.1016/j.matchemphys.2012.10.020

Iftekhar, A. (2004). Biomedical Composites. In *Standard Handbook of Biomedical Engineering and Design* (pp. 1–17). McGraw-Hill.

Iijima, S. (1991). Helical microtubules of graphitic carbon. *Nature*, *354*, 56–58.

Islam, M. F., Rojas, E., Bergey, D. M., Johnson, A. T., & Yodh, A. G. (2003). High weight fraction surfactant solubilization of single wall carbon nanotubes in water. *Nano Letters*, *3*(2), 269–273. https://doi.org/10.1021/nl025924u

Jeon, I.-Y., Chang, D. W., Kumar, N. A., & Baek, J.-B. (2011). Functionalization of Carbon Nanotubes. In *Carbon Nanotubes – Polymer Nanocomposites* (pp. 91–110). https://doi.org/10.1016/j.colsurfa.2011.12.014

Jiang, D., Xing, L., Liu, L., Yan, X., Guo, J., Zhang, X., Zhang, Q., Wu, Z., Zhao, F., Huang, Y., Wei, S., Guo, Z. (2014). Interfacially reinforced unsaturated polyester composites by chemically grafting different functional POSS onto carbon fibers. *Journal of Materials Chemistry A*, *2*(43), 18293–18303. https://doi.org/10.1039/c4ta04055d

Jiang, L., Gao, L., & Sun, J. (2003). Production of aqueous colloidal dispersions of carbon nanotubes. *Journal of Colloid And Interface Science*, *260*, 89–94. https://doi.org/10.1016/S0021-9797(02)00176-5

Jimeno, A., Goyanes, S., Eceiza, A., Kortaberria, G., Mondragon, I., & Corcuera, M. A. (2009). Effects of Amine Molecular Structure on Carbon Nanotubes Functionalization. *Journal of Nanoscience and Nanotechnology*, *9*(10), 6222–6227. https://doi.org/10.1166/jnn.2009.1562

Käppler, I., Hund, R. D., & Cherif, C. (2014). Surface modification of carbon fibres using plasma technique. *Autex Research Journal*, *14*(1), 34–38. https://doi.org/10.2478/v10304-012-0048-y

Kaseem, M., Hamad, K., & Gun, Y. (2016). Fabrication and materials properties of polystyrene/carbon nanotube (PS/CNT) composites: A review. *European Polymer Journal*, *79*, 36–62. https://doi.org/10.1016/j.eurpolymj.2016.04.011

Kathi, J., & Rhee, K. Y. (2008). Surface modification of multi-walled carbon nanotubes using 3-aminopropyltriethoxysilane. *Journal of Materials Science*, *43*, 33–37. https://doi.org/10.1007/s10853-007-2209-2

Khan, M. U., Gomes, V. G., & Altarawneh, I. S. (2010). Synthesizing polystyrene / carbon nanotube composites by emulsion polymerization with non-covalent and covalent functionalization. *Carbon*, *48*(10), 2925–2933. https://doi.org/10.1016/j.carbon.2010.04.029

Kim, J. W., & Lee, J. S. (2016). Influence of interleaved films on the mechanical properties of carbon fiber fabric/polypropylene thermoplastic composites. *Materials*, *9(5): 344*, 1–12.

Kim, S. W., Kim, T., Kim, Y. S., Choi, H. S., Lim, H. J., Yang, S. J., & Park, C. R. (2011). Surface modifications for the effective dispersion of carbon nanotubes in solvents and polymers. *Carbon*, *50*, 3–33. https://doi.org/10.1016/j.carbon.2011.08.011

Kim, Y. J., Shin, T. S., Choi, H. Do, Kwon, J. H., Chung, Y. C., & Yoon, H. G. (2005). Electrical conductivity of chemically modified multiwalled carbon nanotube/epoxy composites. *Carbon*, *43*(1), 23–30. https://doi.org/10.1016/j.carbon.2004.08.015

Konyushenko, E. N., Stejskal, J., Trchová, M., Hradil, J., Kovářová, J., Prokeš, J., Cieslar, M., Hwang, J., Chen, K., Sapurina, I. (2006). Multi-wall carbon nanotubes coated with polyaniline. *Polymer*, *47*(16), 5715–5723. https://doi.org/10.1016/j.polymer.2006.05.059

Koumoulos, E. P., Trompeta, A., Santos, R., Martins, M., Iglesias, V., Böhm, R., & Gong, G. (2019). Research and Development in Carbon Fibers and Advanced High-Performance Composites Supply Chain in Europe : A Roadmap for Challenges and the Industrial Uptake. *Journal of Composite Science*, *3*(86), 1–28. https://doi.org/10.3390/jcs3030086

Koziol, K. K. K., Boncel, S., Shaffer, M. S. P., & Windle, A. H. (2011). Aligned carbon nanotube-polystyrene composites prepared by in situ polymerisation of stacked layers. *Composites Science and Technology*, *71*(13), 1606–1611. https://doi.org/10.1016/j.compscitech.2011.07.007

Lahelin, M., Annala, M., Nykänen, A., Ruokolainen, J., & Seppälä, J. (2011). In situ polymerized nanocomposites: Polystyrene/CNT and Poly(methyl methacrylate)/CNT composites. *Composites Science and Technology*, *71*(6), 900–907. https://doi.org/10.1016/j.compscitech.2011.02.005

Latif, M., Prabhakar, M. N., & Song, J. (2019). Fabrication of hybrid matrix / silane modi fi ed carbon fabric composites and study of their mechanical properties. *Journal of Applied Polymer Science*, *47695*, 1–9. https://doi.org/10.1002/app.47695

Le, T. H., Kim, Y., & Yoon, H. (2017). Electrical and electrochemical properties of conducting polymers. *Polymers*, *9*(150), 1–32. https://doi.org/10.3390/polym9040150

Lee, H., & Her, H. (2011). Study of electroactive shape memory polyurethane–carbon nanotube hybrids. *Soft Matter*, *7*, 3801–3807. https://doi.org/10.1039/c0sm01101k

Lee, H. S., Kim, S. Y., Noh, Y. J., & Kim, S. Y. (2014). Design of microwave plasma and enhanced mechanical properties of thermoplastic composites reinforced with microwave plasma-treated carbon fiber fabric. *Composites Part B: Engineering*, *60*, 621–626. https://doi.org/10.1016/j.compositesb.2013.12.064

Lei, M., Chen, Z., Lu, H., & Yu, K. (2019). Recent progress in shape memory polymer composites: methods, properties, applications and prospects. *Nanotechnology Reviews*, *8*, 327–351.

Lendlein, A., Jiang, H., Junger, O., Langer, R., Jünger, O., & Langer, R. (2005). Light-induced shape-memory polymers. *Nature*, *434*, 879–882. https://doi.org/10.1038/nature03496

Leng, J., Lv, H., Liu, Y., & Du, S. (2007). Electroactivate shape-memory polymer filled with nanocarbon particles and short carbon fibers. *Applied Physics Letters*, *91*(14), 222–224. https://doi.org/10.1063/1.2790497

Li, F., Liu, Y., & Leng, J. (2019). Progress of shape memory polymers and their composites in aerospace applications. *Smart Materials and Structures*, *28*, 1–23.

Liao, M., Yang, Y., & Hamada, H. (2016). Mechanical performance of glass woven fabric composite: Effect of different surface treatment agents. *Composites Part B: Engineering*, *86*, 17–26. https://doi.org/10.1016/j.compositesb.2015.08.084

Lin, T., Bajpai, V., Ji, T., & Dai, L. (2003). Chemistry of Carbon Nanotubes. *Aust. J. Chem.*, *56*, 635–651.

Ling, X., Wei, Y., Zou, L., & Xu, S. (2013). The effect of different order of purification treatments on the purity of multiwalled carbon nanotubes. *Applied Surface Science*, *276*, 159–166.

Liu, A., Honma, I., Ichihara, M., & Zhou, H. (2006). Poly(acrylic acid)-wrapped multi-walled carbon nanotubes composite solubilization in water: Definitive spectroscopic properties. *Nanotechnology*, *17*(12), 2845–2849. https://doi.org/10.1088/0957-4484/17/12/003

Liu, B., Xu, A., & Bao, L. (2017). Preparation of carbon thermoplastics with high fiber volume fraction and high properties. *Journal of Thermoplastic Composite Materials*, *30*, 724–737.

Liu, P., Huang, T., Lu, R., & Li, T. (2012). Tribological properties of modified carbon fabric/polytetrafluoroethylene composites. *Wear*, *289*, 17–25. https://doi.org/10.1016/j.wear.2012.04.021

Liu, Yang, Zhang, F., Leng, J., Fu, K., Lu, X. L., & Wang, L. (2019). Remotely and Sequentially Controlled Actuation of Electroactivated Carbon Nanotube/Shape Memory Polymer Composites. *Adv. Mater. Technol.*, *1900600*, 1–8. https://doi.org/10.1002/admt.201900600

Liu, Yanju, Du, H., Liu, L., & Leng, J. (2014). Shape memory polymers and their composites in aerospace applications: a review. *Smart Materials and Structures*, *23*, 1–22. https://doi.org/10.1088/0964-1726/23/2/023001

Liu, Yanju, Lv, H., Lan, X., Leng, J., & Du, S. (2009). Review of electro-active shape-memory polymer composite. *Composites Science and Technology*, *69*(13), 2064–2068.

Lu, H., Liu, Y., Gou, J., & Leng, J. (2010). Electrical properties and shape-memory behavior of self-assembled carbon nanofiber nanopaper incorporated with shape-memory polymer. *Smart Materials and Structures*, *19*, 1–7. https://doi.org/10.1088/0964-1726/19/7/075021

Lu, H., Wang, X., Yao, Y., Gou, J., Hui, D., Xu, B., & Fu, Y. Q. (2015). Synergistic effect of siloxane modified aluminum nanopowders and carbon fiber on electrothermal efficiency of polymeric shape memory nanocomposite. *Composites Part B: Engineering*, *80*, 1–6. https://doi.org/10.1016/j.compositesb.2015.05.035

Ma, Y., Ueda, M., Yokozeki, T., Sugahara, T., Yang, Y., & Hamada, H. (2017). A comparative study of the mechanical properties and failure behavior of carbon fiber/epoxy and carbon fiber/polyamide 6 unidirectional composites. *Composite Structures*, *160*, 89–99.

Ma, Y., Yokozeki, T., Ueda, M., Sugahara, T., Yang, Y., & Hamada, H. (2017). Effect of polyurethane dispersion as surface treatment for carbon fabrics on mechanical properties of carbon/Nylon composites. *Composites Science and Technology*, *151*, 268–281. https://doi.org/10.1016/j.compscitech.2017.08.031

Mahrholz, T., Mosch, J., Röstermundt, D., Riedel, U., & Herbeck, L. (2003). New High-peformance Fibre Reinforced Materials with Nanocomposites. *20th AAAF Colloquium – Materials for Aerospace Applications*, 1–7. Paris.

Mark, J. E. (1999). *Polymer Data Handbook*. Oxford University Press, Inc.

McClory, C., Po, P., & Mcnally, T. (2011). Influence of Screw Speed on Electrical and Rheological Percolation of Melt-Mixed High- Impact Polystyrene/MWCNT Nanocomposites. *Macromolecular Materials and Engineering*, *296*, 59–69. https://doi.org/10.1002/mame.201000220

Mekhilef, N., & Verhoogt, H. (1996). Phase inversion and dual-phase continuity in polymer blends: Theoretical predictions and experimental results. *Polymer*, *37*(18), 4069–4077. https://doi.org/10.1016/0032-3861(96)00254-6

Misumi, J., & Oyama, T. (2018). Low viscosity and high toughness epoxy resin modified by in situ radical polymerization method for improving mechanical properties of carbon fiber reinforced plastics. *Polymer*, *156*, 1–9. https://doi.org/10.1016/j.polymer.2018.09.050

Mittal, V. (2011). Carbon Nanotubes Surface Modifications : An Overview. In *Surface Modification of Nanotube Fillers* (pp. 1–23). Wiley-VCH Verlag GmbH & Co. KGaA.

Moreno Marcelino, J. E., Vigueras Santiago, E., López Téllez, G., & Hernández López, S. (2014). Chemical functionalization of carbon nanotubes and its effects on electrical conductivity. *Journal of Nano Research*, *28*, 51–61. https://doi.org/10.4028/www.scientific.net/JNanoR.28.51

Morris, B. A. (2016). The Science and Technology of Flexible Packaging: Multilayer Films from Resin and Process to End Use. In *The Science and Technology of Flexible Packaging: Multilayer Films from Resin and Process to End Use*.

Mu, T., Liu, L., Lan, X., Liu, Y., & Leng, J. (2018). Shape memory polymers for composites. *Composites Science and Technology*, *160*, 169–198.

Müller, M. T., Krause, B., Kretzschmar, B., & Pötschke, P. (2011). Influence of feeding conditions in twin-screw extrusion of PP/MWCNT composites on electrical and mechanical properties. *Composites Science and Technology*, *71*, 1535–1542. https://doi.org/10.1016/j.compscitech.2011.06.003

Njuguna, J., Pielichowski, K., & Fan, J. (2012). Polymer nanocomposites for aerospace applications. In *Advances in Polymer Nanocomposites: Types and Applications*. https://doi.org/10.1533/9780857096241.3.472

Noels, L. (2018). Fracture Mechanics. Retrieved from http://www.ltas-cm3.ulg.ac.be/FractureMechanics/

Oliver, J. (1999). Infrared Spectral Interpretation: A Systematich Approach. In *Journal of Chemical Information and Modeling* (Vol. 53). CRC Press.

Olmos, D., Martín, E. V., & González-Benito, J. (2014). New molecular-scale information on polystyrene dynamics in PS and PS-BaTiO3 composites from FTIR spectroscopy. *Physical Chemistry Chemical Physics*, *16*(44), 24339–24349. https://doi.org/10.1039/c4cp03516j

Ozdemir, N. G., Zhang, T., Hadavinia, H., Aspin, I., & Scarpa, F. (2016). Influence of nanorubber toughening on the tensile deformation and tensile fatigue behaviour of a carbon fibre-reinforced epoxy composite. *Journal of Composite Materials*, *50*(19), 2633–2645. https://doi.org/10.1177/0021998315609976

Palazzetti, R., & Zucchelli, A. (2017). Electrospun nanofibers as reinforcement for composite laminates materials – A review. *Composite Structures*, *182*(June), 711–727. https://doi.org/10.1016/j.compstruct.2017.09.021

Patole, A. S., Patole, S. P., Yoo, J., An, J., & Kim, T. (2013). Fabrication of Polystyrene/ Multiwalled Carbon Nanotube Composite Films Synthesized by In Situ Microemulsion Polymerization. *Polymer Engineering and Science*, *53*, 1327–1336. https://doi.org/10.1002/pen

Pedrazzoli, D., & Pegoretti, A. (2013). Silica nanoparticles as coupling agents for polypropylene/glass composites. *Composites Science and Technology*, *76*, 77–83. https://doi.org/10.1016/j.compscitech.2012.12.016

Pedrazzoli, D., & Pegoretti, A. (2014). Expanded graphite nanoplatelets as coupling agents in glass fiber reinforced polypropylene composites. *Composites Part A: Applied Science and Manufacturing*, *66*, 25–34. https://doi.org/10.1016/j.compositesa.2014.06.016

Pelin, C.-E., Pelin, G., Stefan, A., Andronescu, E., Dinca, I., Ficai, A., & Trusca, R. (2016). Mechanical properties of polyamide/carbon-fiber-fabric composites. *Materials and Technology*, *50*(5), 723–728.

Peng, F., Zhang, L., Wang, H., Lv, P., & Yu, H. (2005). Sulfonated carbon nanotubes as a strong protonic acid catalyst. *Carbon*, *43*(11), 2405–2408. https://doi.org/10.1016/j.carbon.2005.04.004

Ponnamma, D., El-Gawady, Y. M., Rajan, M., Goutham, S., Venkateswara, R. K., & Al-Maadeed, M. A. (2017). Shape Memory Behavior of Conducting Polymer Nanocomposites. In *Smart Polymer Nanocomposites* (pp. 321–343). https://doi.org/10.1007/978-3-319-50424-7

Porubská, M., Szöllös, O., Kóňová, A., Janigová, I., Jašková, M., Jomová, K., & Chodák, I. (2012). FTIR spectroscopy study of polyamide-6 irradiated by electron and proton beams. *Polymer Degradation and Stability*, *97*(4), 523–531. https://doi.org/10.1016/j.polymdegradstab.2012.01.017

Properties of (3-Aminopropyl)triethoxysilane. (2017). Retrieved from https://www.sigmaaldrich.com/catalog/product/aldrich/440140?lang=en&region=TR

Properties of (3-Trimethoxysilylpropyl)methacrylate. (2018). Retrieved from https://www.sigmaaldrich.com/catalog/product/aldrich/440159?lang=en&region=TR

Properties of AIBN. (2017). Retrieved from ttps://www.sigmaaldrich.com/catalog/product/aldrich/441090?lang=en&region=TR

Properties of Polyamide 6. (2018). Retrieved from http://www.eurotec-ep.com/s/1404/i/TDS_Tecomid_NB40_NL_E.pdf

Properties of Styrene Monomer. (2017). Retrieved from https://www.sigmaaldrich.com/catalog/product/sial/85959?lang=en&region=TR

Qi, X., Dong, P., Liu, Z., Liu, T., & Fu, Q. (2016). Selective localization of multi-walled carbon nanotubes in bi-component biodegradable polyester blend for rapid electroactive shape memory performance. *Composites Science and Technology*, *125*, 38–46.

Rajak, D. K., Pagar, D. D., Menezes, P. L., & Linul, E. (2019). Fiber-Reinforced Polymer Composites : Manufacturing, Properties, and Applications. *Polymers*, *11*, 1–37.

Ramanathan, T., Fisher, F. T., Ruoff, R. S., & Brinson, L. C. (2005). Amino-fimctionalized carbon nanotubes for binding to polymers and biological systems. *Chemistry of Materials*, *17*(6), 1290–1295. https://doi.org/10.1021/cm048357f

Rastogi, R., Kaushal, R., Tripathi, S. K., Sharma, A. L., Kaur, I., & Bharadwaj, L. M. (2008). Comparative study of carbon nanotube dispersion using surfactants. *Journal of Colloid and Interface Science*, *328*, 421–428. https://doi.org/10.1016/j.jcis.2008.09.015

Rosen, S. L. (1993). *Fundamental Principles of Polymeric Materials*. John Wiley & Sons.

Sahoo, N. G., Jung, Y. C., & Cho, J. W. (2007). Electroactive shape memory effect of polyurethane composites filled with carbon nanotubes and conducting polymer. *Materials and Manufacturing Processes*, *22*(4), 419–423. https://doi.org/10.1080/10426910701232857

Sang, L., Wang, Y. K., Chen, G., Liang, J., & Wei, Z. (2016). A comparative study of the crystalline structure and mechanical properties of carbon fiber/polyamide 6 composites enhanced with/without silane treatment. *RSC Advances*, *6*(109), 107739–107747.

Sarvi, A., & Sundararaj, U. (2014). Rheological percolation in polystyrene composites filled with polyaniline-coated multiwall carbon nanotubes. *Synthetic Metals*, *194*, 109–117.

https://doi.org/10.1016/j.synthmet.2014.04.031

Semitekolos, D., Kainourgios, P., Jones, C., Rana, A., Koumoulos, E. P., & Charitidis, C. A. (2018). Advanced carbon fi bre composites via poly methacrylic acid surface treatment ; surface analysis and mechanical properties investigation. *Composites Part B*, *155*, 237–243.

https://doi.org/10.1016/j.compositesb.2018.08.027

Şengör, İ. (2013). *Shape Memory Polymer Composites Containing Carbon Based Fillers*. METU, MSc. Thesis.

Sharma, M., & Bijwe, J. (2011). Influence of fiber – matrix adhesion and operating parameters on sliding wear performance of carbon fabric polyethersulphone composites. *Wear*, *271*(11–12), 2919–2927. https://doi.org/10.1016/j.wear.2011.06.012

Sharma, M., Bijwe, J., & Mitschang, P. (2011). Wear performance of PEEK – carbon fabric composites with strengthened fiber – matrix interface. *Wear*, *271*(9–10), 2261–2268. https://doi.org/10.1016/j.wear.2010.11.055

Shonaike, G. O. (2000). A preliminary investigation of tensile properties of glass-mat wovenfabric-reinforced thermoplastic elastomer composites. *Journal of Thermoplastic Composite Materials*, *13*, 102–118.

Su, F. H., Zhang, Z. Z., Wang, K., Jiang, W., & Liu, W. M. (2005). Tribological and mechanical properties of the composites made of carbon fabrics modified with various methods. *Composites Part A: Applied Science and Manufacturing*, *36*(12), 1601–1607. https://doi.org/10.1016/j.compositesa.2005.04.012

Su, F., & Zhang, Z. (2009). Friction and Wear Behavior of Glass Fabric / Phenolic Resin Composites with Surface-Modified Glass Fabric. *Journal of Applied Polymer Science*, *112*, 594–601. https://doi.org/10.1002/app

Su, S., Chiang, W., Lin, C., & Yokoyama, M. (2008). Multi-wall carbon nanotubes: Purification , morphology and field emission performance. *Physica E*, *40*, 2322–2326. https://doi.org/10.1016/j.physe.2007.09.087

Sun, T., Li, M., Zhou, S., Liang, M., Chen, Y., & Zou, H. (2020). Multi-scale structure construction of carbon fiber surface by electrophoretic deposition and electropolymerization to enhance the interfacial strength of epoxy resin composites. *Applied Surface Science*, *499*, 1–12. https://doi.org/10.1016/j.apsusc.2019.143929

Tan, S. H., Goak, J. C., Lee, N., & Kim, J. (2007). Functionalization of Multi-Walled Carbon Nanotubes with Poly(2-ethyl-2-oxazoline). *Macromol. Symp.*, 270–275. https://doi.org/10.1002/masy.200750344

Tang, Z., Kang, H., Wei, Q., Guo, B., & Zhang, L. (2013). Incorporation of graphene into polyester/carbon nanofibers composites for better multi-stimuli responsive shape memory performances. *Carbon*, *64*, 487–498. https://doi.org/10.1016/j.carbon.2013.07.103

Tang, Z., Sun, D., Yang, D., Guo, B., Zhang, L., & Jia, D. (2013). Vapor grown carbon nanofiber reinforced bio-based polyester for electroactive shape memory performance. *Composites Science and Technology*, *75*, 15–21. https://doi.org/10.1016/j.compscitech.2012.11.019

Technical Data Sheet of GLYMO. (2018). Retrieved from https://products-re.evonik.com/www2/uploads/productfinder/Dynasylan-GLYMO-EN.pdf

Technical Data Sheet of Kraton FG 1924 G. (2017). Retrieved from http://docs.kraton.com/pdfDocuments/20091005132104359652O2.PDF

Technical Data Sheet of MSPM. (2019). Retrieved from https://products-re.evonik.com/www2/uploads/productfinder/Dynasylan-MEMO-EN.pdf

Technical Data Sheet of NC7000. (2017). Retrieved from http://www.nanocyl.com/wp-content/uploads/2016/07/DM-TI-02-TDS-NC7000-V08.pdf

Technical Data Sheet of PS Crystal 1540. (2017). Retrieved from http://polymersproducts.total.com/site_collection_documents/Technical Datasheets/1540-EU-EN.pdf

Technical Data Sheet of PSMA. (2019). Retrieved from ttps://www.sigmaaldrich.com/catalog/product/aldrich/442380?lang=en&region=TR

Technical Data Sheet of SDBS. (2019). Retrieved from https://www.sigmaaldrich.com/catalog/substance/sodiumdodecylbenzenesulfonate348482515530011?lang=en&region=TR

Technical Data Sheet of SDS. (2019). Retrieved from https://www.sigmaaldrich.com/catalog/product/sial/436143?lang=en&region=TR

Technical Data Sheet of Triton X-100. (2019). Retrieved from https://www.sigmaaldrich.com/catalog/product/sial/x100?lang=en&region=TR

Thaher, I., Al-amer, A., P, S. T., Al-harthi, M., Adamu, S., Sougrat, R., & Ali, M. (2011). Effect of acid treated carbon nanotubes on mechanical , rheological and thermal properties of polystyrene nanocomposites. *Composites Part B*, *42*(6), 1554–1561. https://doi.org/10.1016/j.compositesb.2011.04.013

Tiwari, S, & Bijwe, J. (2014). Surface Treatment of Carbon Fibers - A Review. *Procedia Technology*, *14*, 505–512.

Tiwari, Sudhir, Bijwe, J., & Panier, S. (2011). Influence of Plasma Treatment on Carbon Fabric for Enhancing Abrasive Wear Properties of Polyetherimide Composites. *Tribology Letters*, *41*, 153–162. https://doi.org/10.1007/s11249-010-9694-1

Valesco-Santos, C., Martinez-Hernandez, A. L., & Castano, V. M. (2011). Silanization of Carbon Nanotubes: Surface Modification and Polymer Nanocomposites. In *Carbon Nanotubes - Polymer Nanocomposites* (pp. 251–280). https://doi.org/10.1016/j.colsurfa.2011.12.014

Wang, B., Fu, Q., Li, H., Qi, L., & Lu, Y. (2020). Synergistic effect of surface modification of carbon fabrics and multiwall carbon nanotube incorporation for improving tribological properties of carbon fabrics/resin composites. *Polymer Composites*, *41*(1), 102–111. https://doi.org/10.1002/pc.25349

Wang, B., Fu, Q., Yin, T., Li, H., Qi, L., & Fu, Y. (2018). Grafting CNTs on carbon fabrics with enhanced mechanical and thermal properties for tribological applications of carbon fabrics/phenolic composites. *Carbon*, *139*, 45–51. https://doi.org/10.1016/j.carbon.2018.06.032

Wang, J., Fang, Z., Gu, A., Xu, L., & Liu, F. (2006). Effect of amino-functionalization of multi-walled carbon nanotubes on the dispersion with epoxy resin matrix. *Journal of Applied Polymer Science*, *100*(1), 97–104. https://doi.org/10.1002/app.22647

Wei, F., Pan, B., & Lopez, J. (2018). The tribological properties study of carbon fabric/ epoxy composites reinforced by nano-TiO2 and MWNTs. *Open Physics*, *16*(1), 1127–1138. https://doi.org/10.1515/phys-2018-0133

Wei, H. F., Hsiue, G. H., & Liu, C. Y. (2007). Surface modification of multi-walled carbon nanotubes by a sol-gel reaction to increase their compatibility with PMMA resin. *Composites Science and Technology*, *67*(6), 1018–1026. https://doi.org/10.1016/j.compscitech.2006.06.005

Wei, K., Zhu, G., Tang, Y., & Li, X. (2012). The effects of carbon nanotubes on electroactive shape-memory behaviors of hydro-epoxy/carbon black composite. *Smart Materials and Structures*, *21*, 1–6. https://doi.org/10.1088/0964-1726/21/8/085016

Xie, X. L., Mai, Y. W., & Zhou, X. P. (2005). Dispersion and alignment of carbon nanotubes in polymer matrix: A review. *Materials Science and Engineering R: Reports*, *49*(4), 89–112. https://doi.org/10.1016/j.mser.2005.04.002

Xu, B., Fu, Y. Q., Ahmad, M., Luo, J. K., Huang, W. M., Kraft, A., Reuben, R., Pei, Y. T., Chen, Z. G., De Hosson, J. T. M. (2010). Thermo-mechanical properties of polystyrene-based shape memory nanocomposites. *Journal of Materials Chemistry*, *20*(17), 3442–3448.

Xu, F., Du, X. S., Liu, H. Y., Guo, W. G., & Mai, Y. W. (2016). Temperature effect on nano-rubber toughening in epoxy and epoxy/carbon fiber laminated composites. *Composites Part B: Engineering*, *95*, 423–432. https://doi.org/10.1016/j.compositesb.2016.04.019

Xu, H., Tong, X., Zhang, Y., Li, Q., & Lu, W. (2016). Mechanical and electrical properties of laminated composites containing continuous carbon nanotube film interleaves. *Composites Science and Technology*, *127*, 113–118. https://doi.org/10.1016/j.compscitech.2016.02.032

Yang, J., Xiao, J., Zeng, J., Bian, L., Peng, C., & Yang, F. (2013). Matrix modification with silane coupling agent for carbon fiber reinforced epoxy composites. *Fibers and Polymers*, *14*(5), 759–766.

Yang, T., Hu, Y., Deng, S., Du, L., Zhou, J., Hu, J., & Jian, X. (2019). Synthesis and thermal stability of a novel acetylene end-capped silicon-containing polyimide coupling agent with a silane pendant group. *High Performance Polymers*, *31*, 1259–1271.

Yang, Y., Zhang, Z., Ma, Y., Ueda, M., Yokozeki, T., Sugahara, T., & Hamada, H. (2018). Effect of polyurethane dispersion treatment on the performance improvement of carbon woven fabric-reinforced composites. *Journal of Thermoplastic Composite Materials*, *31*(3), 408–425.

https://doi.org/10.1177/0892705717704487

Yao, S., Jin, F., Yop, K., Hui, D., & Park, S. (2018). Recent advances in carbon-fiber-reinforced thermoplastic composites : A review. *Composites Part B*, *142*(July 2017), 241–250. https://doi.org/10.1016/j.compositesb.2017.12.007

Yapıcı, U., Pan, L., Xu, F., & Cao, J. (2014). Effect of functional groups on interfacial adhesion properties of PEEK/carbon fiber composites. *Applied Mechanics and Materials*, *598*, 66–72.

https://doi.org/10.4028/www.scientific.net/AMM.598.66

Yasar, M. (2014). *Performance of Modified Thermoplastic Poly(ether)ester elastomer in Multilayer Composites*. METU, MSc. Thesis.

Ye, Y., Chen, H., Wu, J., & Chan, C. M. (2011). Interlaminar properties of carbon fiber composites with halloysite nanotube-toughened epoxy matrix. *Composites Science and Technology*, *71*(5), 717–723.

https://doi.org/10.1016/j.compscitech.2011.01.018

Yeniova, C. E., & Yilmazer, U. (2010). Characteristics of Impact Modified Polystyrene / Organoclay Nanocomposites. *Polymer Composites*, 1853–1861. https://doi.org/10.1002/pc.20978

Yesil, S. (2010). *Processing and Characterization of Carbon Nanotube Based Conductive Polymer Composites*. METU, PhD Thesis.

Yesil, S., & Bayram, G. (2010). Effect of Carbon Nanotube Purification on the Electrical and Mechanical Properties of Poly (ethylene terephthalate) Composites with Carbon Nanotubes in Low Concentration. *Journal of Applied Polymer Science*, *119*, 3360–3371. https://doi.org/10.1002/app

Yesil, S., & Bayram, G. (2011). Poly(ethylene terephthalate)/Carbon Nanotube Composites Prepared With Chemically Treated Carbon Nanotubes. *Polymer Engineering and Science*, *51*, 1286–1300. https://doi.org/10.1002/pen

Yoo, H. J., Jung, Y. C., Sahoo, N. G., & Cho, J. W. (2006). Polyurethane-carbon nanotube nanocomposites prepared by in-situ polymerization with electroactive shape memory. *Journal of Macromolecular Science, Part B: Physics*, *45 B*(4), 441–451. https://doi.org/10.1080/00222340600767471

Youssry, M., Al-Ruwaidhi, M., Zakeri, M., & Zakeri, M. (2020). Physical functionalization of multi-walled carbon nanotubes for enhanced dispersibility in aqueous medium. *Emergent Materials*, *3*(1), 25–32. https://doi.org/10.1007/s42247-020-00076-3

Yuan, J., Fan, Z., Chen, X., Chen, X., Wu, Z., & He, L. (2009). Preparation of polystyrene-multiwalled carbon nanotube composites with individual-dispersed nanotubes and strong interfacial adhesion. *Polymer*, *50*, 3285–3291. https://doi.org/10.1016/j.polymer.2009.04.065

Zaragoza-Contreras, E. A., Lozano-Rodrıguez, E. D., Roman-Aguirre, M., Antunez-Flores, W., Hernandez-Escobar, C. A., Flores-Gallardo, S. G., & Aguilar-Elguezabal, A. (2009). Evidence of multi-walled carbon nanotube fragmentation induced by sonication during nanotube encapsulation via bulk-suspension polymerization. *Micron*, *40*, 621–627. https://doi.org/10.1016/j.micron.2009.02.007

Zhan, Z., He, H., Zhu, Z., Xue, B., Wang, G., Chen, M., & Xiong, C. (2019). Blends of rABS and SEBS: Influence of in-situ compatibilization on the mechanical properties. *Materials*, *12*(15). https://doi.org/10.3390/ma12152352

Zhang, B., Fu, R. W., Zhang, M. Q., Dong, X. M., Lan, P. L., & Qiu, J. S. (2005). Preparation and characterization of gas-sensitive composites from multi-walled carbon nanotubes/polystyrene. *Sensors and Actuators, B: Chemical*, *109*(2), 323–328. https://doi.org/10.1016/j.snb.2004.12.066

Zhang, Chao, Liu, T., & Lu, X. (2010). Facile fabrication of polystyrene / carbon nanotube composite nanospheres with core-shell structure via self-assembly. *Polymer*, *51*(16), 3715–3721. https://doi.org/10.1016/j.polymer.2010.06.021

Zhang, Cheng, Zhu, J., Ma, C., & Sumita, M. (2009). Conductive Network Formation and Electrical Properties of Poly(vinylidene fluoride)/Multiwalled Carbon Nanotube Composites: Percolation and Dynamic Percolation. *Journal of Applied Polymer Science*, *114*(5), 1405–1411. https://doi.org/10.1002/app

Zhang, J. (2013). Work of Adhesion and Work of Cohesion. In *Encyclopedia of Tribology*. https://doi.org/10.1007/978-0-387-92897-5

Zhang, X., Pei, X., Jia, Q., & Wang, Q. (2009). Effects of carbon fiber surface treatment on the tribological properties of 2D woven carbon fabric/polyimide composites. *Applied Physics A: Materials Science and Processing*, *95*(3), 793–799. https://doi.org/10.1007/s00339-009-5073-x

Zhang, X., Pei, X., & Wang, Q. (2008). Friction and wear properties of combined surface modified carbon fabric reinforced phenolic composites. *European Polymer Journal*, *44*, 2551–2557. https://doi.org/10.1016/j.eurpolymj.2008.06.013

Zhang, Z., Zhang, J., Chen, P., & Zhang, B. (2006). Enhanced interactions between multi-walled carbon nanotubes and polystyrene induced by melt mixing. *Carbon*, *44*, 692–698. https://doi.org/10.1016/j.carbon.2005.09.027

Zhao, D., Hamada, H., & Yang, Y. (2019). Influence of polyurethane dispersion as surface treatment on mechanical, thermal and dynamic mechanical properties of laminated woven carbon-fiber-reinforced polyamide 6 composites. *Composites Part B: Engineering*, *160*(December 2018), 535–545. https://doi.org/10.1016/j.compositesb.2018.12.105

Zhao, L., Liu, W., Liu, P., Tian, J., Xu, M., Sun, S., & Wang, Y. (2020). Study on atmospheric air glow discharge plasma generation and surface modification of carbon fiber fabric. *Plasma Processes and Polymers*, (July 2019), 1–11. https://doi.org/10.1002/ppap.201900148

APPENDICES

A. TGA Curve of As-Received Carbon Fabric Sample

In order to determine the working temperature of ash content analysis, TGA was performed to as-received CF sample. The TGA curve is given in Figure A.1.

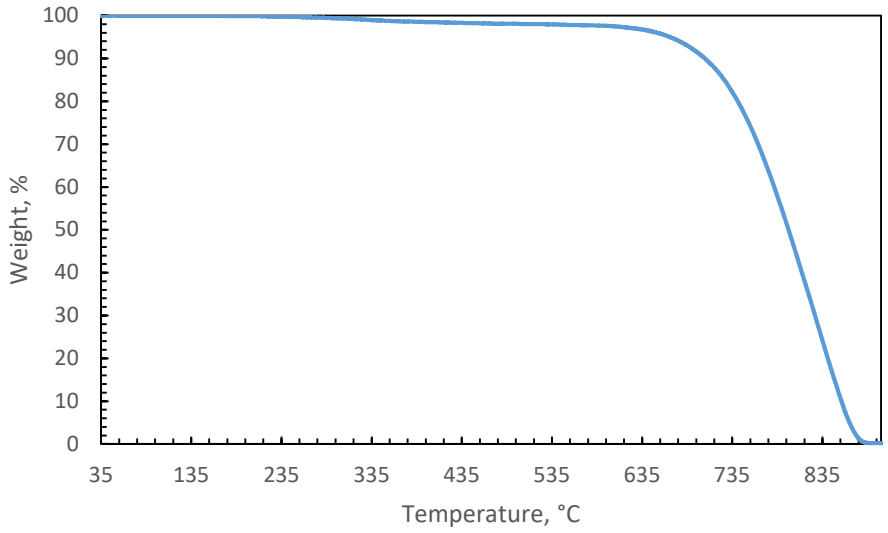

Figure A.1. TGA curve of as-received CF sample in air atmosphere.

B. Electrical Measurements

The results of electrical resistivities of the binary, ternary, and multilayer composites were measured with two-point probe method were given in Figures 4.4, 4.10, 4.25, and 4.4, respectively. The calculated volume resistivity values represented in these figures are given between Table B.1- B.5.

Table B.1 Electrical resistivity values of binary composites (PS-CNTs) prepared in first set for surface modifier selection.

Sample	Volume Resistivity, Ω.cm			
	PS-CNT	**PS-SDBS-A-CNT**	**PS-TX100-A-CNT**	**PS-MSPM-A-CNT**
1	3.33×10^{4}	7.83×10^{7}	1.05×10^{5}	8.24×10^{7}
2	2.81×10^{5}	4.75×10^{7}	1.01×10^{5}	5.71×10^{7}
3	2.73×10^{5}	5.95×10^{7}	1.03×10^{5}	1.91×10^{9}
4	6.13×10^{5}	2.27×10^{8}	1.02×10^{5}	8.38×10^{7}
5	3.90×10^{6}	2.98×10^{8}	1.01×10^{5}	8.52×10^{7}
6	1.60×10^{4}	9.08×10^{7}	2.49×10^{8}	2.23×10^{8}
7	2.00×10^{4}	6.88×10^{8}	1.26×10^{8}	7.50×10^{7}
8	1.05×10^{5}	1.03×10^{8}	1.08×10^{8}	1.82×10^{8}
9	5.08×10^{4}	1.15×10^{8}	6.05×10^{7}	3.26×10^{8}
10	8.84×10^{3}	1.98×10^{8}	8.35×10^{7}	2.40×10^{8}
11	2.47×10^{2}	3.66×10^{8}	3.73×10^{6}	1.98×10^{8}
12	2.16×10^{2}	3.60×10^{8}	2.16×10^{5}	2.45×10^{8}
13	2.15×10^{2}	3.10×10^{8}	1.21×10^{5}	1.30×10^{8}
14	2.15×10^{3}	3.28×10^{8}	1.53×10^{5}	2.16×10^{8}
15	2.15×10^{4}	2.20×10^{8}	1.15×10^{5}	1.17×10^{8}
Avg.	3.53×10^{5}	2.33×10^{8}	4.21×10^{7}	2.78×10^{8}
log(Avg.)	5.55	8.37	7.63	8.44

Table B.2 Electrical resistivity values of binary composites (PS-CNTs) prepared in second set for surface modifier selection.

Sample	Volume Resistivity, Ω.cm			
	PS-CNT	**PS-SDBS-A-CNT**	**PS-TX100-A-CNT**	**PS-MSPM-A-CNT**
1	4.76×10^{3}	2.33×10^{8}	4.75×10^{7}	1.24×10^{8}
2	2.95×10^{3}	6.68×10^{7}	7.51×10^{7}	5.30×10^{7}
3	2.68×10^{3}	8.55×10^{8}	4.63×10^{7}	8.92×10^{7}
4	2.81×10^{3}	5.98×10^{7}	4.94×10^{7}	1.07×10^{8}
5	2.65×10^{3}	5.87×10^{7}	1.92×10^{8}	3.85×10^{8}
6	4.20×10^{4}	6.88×10^{7}	1.79×10^{8}	5.06×10^{7}
7	2.59×10^{4}	7.73×10^{8}	6.75×10^{7}	7.96×10^{7}
8	2.72×10^{4}	5.96×10^{7}	6.75×10^{7}	5.10×10^{7}
9	2.70×10^{4}	7.09×10^{7}	7.43×10^{7}	7.10×10^{7}
10	2.89×10^{3}	5.72×10^{7}	4.42×10^{7}	6.00×10^{7}
11	3.40×10^{3}	7.81×10^{7}	8.69×10^{7}	3.26×10^{8}
12	3.60×10^{3}	5.69×10^{7}	4.81×10^{7}	5.48×10^{7}
13	3.30×10^{3}	5.34×10^{7}	4.79×10^{7}	9.27×10^{7}
14	3.54×10^{3}	2.62×10^{8}	5.08×10^{7}	2.41×10^{8}
15	3.37×10^{3}	5.24×10^{7}	1.09×10^{8}	5.00×10^{7}
Avg.	1.23×10^{4}	1.87×10^{8}	7.91×10^{7}	1.22×10^{8}
log(Avg.)	4.09	8.27	7.90	8.09

Table B.3 Electrical resistivities of ternary composites (PS-E-CNTs).

Sample	Volume Resistivity, Ω.cm				
	PS-E-CNT	**PS-E-A-CNT**	**PS-E-SDBS-A-CNT**	**PS-E-TX100-A-CNT**	**PS-E-MSPM-A-CNT**
1	1.10×10^{9}	4.76×10^{7}	1.40×10^{8}	2.41×10^{8}	1.03×10^{8}
2	4.50×10^{9}	1.52×10^{8}	1.26×10^{8}	7.36×10^{8}	8.81×10^{7}
3	2.88×10^{9}	6.88×10^{7}	3.52×10^{8}	8.55×10^{9}	2.07×10^{8}
4	7.59×10^{8}	6.01×10^{7}	1.23×10^{8}	8.55×10^{9}	1.02×10^{8}
5	3.79×10^{8}	1.20×10^{8}	2.30×10^{8}	2.30×10^{9}	1.10×10^{8}
6	3.48×10^{8}	1.76×10^{8}	1.54×10^{8}	1.01×10^{8}	7.67×10^{7}
7	6.73×10^{7}	5.96×10^{8}	6.93×10^{7}	3.87×10^{8}	4.81×10^{8}
8	5.32×10^{7}	5.75×10^{7}	2.87×10^{8}	2.95×10^{8}	1.34×10^{8}
9	5.72×10^{7}	4.85×10^{7}	2.91×10^{8}	9.85×10^{7}	2.02×10^{8}
10	6.27×10^{7}	7.93×10^{7}	2.44×10^{8}	2.09×10^{8}	9.33×10^{7}
11	2.78×10^{7}	2.36×10^{8}	5.21×10^{8}	8.47×10^{7}	8.93×10^{7}
12	1.41×10^{8}	3.43×10^{8}	2.20×10^{8}	1.82×10^{8}	1.02×10^{8}
13	3.17×10^{8}	2.39×10^{8}	4.85×10^{9}	2.96×10^{8}	5.77×10^{7}
14	2.92×10^{8}	1.68×10^{8}	1.61×10^{8}	2.96×10^{8}	1.20×10^{8}
15	6.23×10^{7}	1.20×10^{8}	1.70×10^{8}	5.43×10^{8}	1.77×10^{8}
Avg.	7.63×10^{8}	1.67×10^{8}	5.29×10^{8}	1.52×10^{9}	1.47×10^{8}
log(Avg.)	8.87	8.22	8.72	9.18	8.17

Table B.4 Electrical resistivities of the multilayer composites (PS-E-CNTs as polymer layers and one layer of CF).

Sample	Volume Resistivity, Ω.cm					
	PS-E-CF		PS-E-CNT-CF		PS-E-MSPM-A-CNT-CF	
	Method 1	Method 2	Method 1	Method 2	Method 1	Method 2
1	0.069	0.083	0.040	0.068	0.058	0.112
2	0.069	0.075	0.038	0.062	0.059	0.103
3	0.069	0.072	0.038	0.060	0.057	0.101
4	0.068	0.073	0.038	0.059	0.056	0.098
5	0.079	0.072	0.114	0.103	0.131	0.074
6	0.080	0.070	0.134	0.094	0.127	0.071
7	0.082	0.069	0.127	0.090	0.125	0.071
8	0.081	0.070	0.132	0.088	0.118	0.070
9	0.076	0.091	0.044	0.084	0.100	0.089
10	0.073	0.085	0.048	0.084	0.094	0.080
11	0.072	0.080	0.046	0.083	0.089	0.076
12	0.072	0.079	0.044	0.084	0.090	0.074
13	0.079	0.148	0.065	0.083	0.078	0.083
14	0.092	0.145	0.054	0.076	0.076	0.079
15	0.089	0.150	0.052	0.073	0.074	0.078
16	0.084	0.143	0.050	0.072	0.073	0.076
17	0.057	0.123	0.050	0.068	0.049	0.062
18	0.056	0.095	0.049	0.062	0.048	0.055
19	0.057	0.092	0.049	0.060	0.047	0.053
20	0.058	0.086	0.048	0.059	0.045	0.052
Avg.	0.073	0.095	0.063	0.076	0.080	0.078
log(Avg.)	-1.14	-1.02	-1.20	-1.12	-1.10	-1.11

Table B.5 Electrical resistivities of the multilayer composites (PS-E-CNTs as polymer layers and one, three and five layers of CFs).

Sample	Volume Resistivity, Ω.cm			
	PS-1-CF	**PS-3-CFs**	**PS-5-CFs**	**PS-5-MSPM-CFs**
1	0.170	0.086	0.081	0.061
2	0.147	0.079	0.071	0.059
3	0.169	0.074	0.064	0.059
4	0.175	0.073	0.056	0.058
5	0.153	0.085	0.046	0.085
6	0.143	0.080	0.044	0.083
7	0.137	0.078	0.042	0.083
8	0.132	0.076	0.041	0.080
9	0.118	0.064	0.039	0.066
10	0.113	0.058	0.038	0.061
11	0.112	0.056	0.036	0.059
12	0.111	0.054	0.036	0.058
13	0.164	0.067	0.034	0.064
14	0.160	0.063	0.032	0.062
15	0.158	0.062	0.039	0.062
16	0.156	0.061	0.037	0.061
Avg.	0.145	0.070	0.046	0.066
log(Avg.)	-0.84	-1.16	-1.34	-1.18

C. **Mechanical Properties**

The results of mechanical properties of the composites are measured with tensile test and impact test were given for binary composites in Figures 4.5-4.8 and for ternary composites in Figures 4.11-4.14. The tensile test results of multilayer composites are given in Figures 4.26-4.28 and for multilayer composites prepared with one, three and five layers of CFs tensile test results were given in Figures 4.44-4.46. The calculated values of the mechanical properties of the composites are given in Figures C.1-C.14.

Table C.1 Tensile strength values of the binary composites (PS-CNTs).

Sample	Tensile Strength, MPa									
	PS		PS-CNT		PS-SDBS-A-CNT		PS-TX100-A-CNT		PS-MSPM-A-CNT	
	First Set	Second Set	First Set	Second Set	First Set	Second Set	First Set	Second Set	First Set	Second Set
1	33.07	50.20	18.41	34.99	33.25	42.20	28.58	40.92	29.04	41.34
2	32.57	44.25	24.39	32.11	33.05	46.18	24.79	40.07	35.02	42.66
3	35.09	45.57	24.81	35.98	34.20	45.02	20.65	44.31	29.09	45.01
4	33.59	39.71	21.46	36.37	35.29	45.85	23.43	45.04	34.72	41.10
5	35.31	39.90	18.98	34.25	26.60	42.22	29.73	45.97	32.40	43.78
Avg.	33.93	43.92	21.61	34.74	32.48	44.29	25.44	43.26	32.05	42.78
Std. Dev.	1.22	4.36	2.97	1.69	3.40	1.95	3.73	2.61	2.91	1.65

Table C.2 Tensile moduli of the binary composites (PS-CNTs).

Sample	Tensile Modulus, MPa									
	PS		PS-CNT		PS-SDBS-A-CNT		PS-TX100-A-CNT		PS-MSPM-A-CNT	
	First Set	Second Set	First Set	Second Set	First Set	Second Set	First Set	Second Set	First Set	Second Set
1	2576.3	2874.6	2828.6	3436.5	2985.1	2708.8	2945.2	3567.4	2799.5	3296.8
2	2991.9	2701.6	2902.9	3206.8	2596.9	2656.9	3225.6	2611.8	2815.5	2995.1
3	2790.1	2504.8	2869.5	2790.0	34571.7	2913.8	2757.8	3123.3	2775.8	3743.1
4	2899.4	2887.1	2982.6	3641.2	2717.5	2896.3	3035.5	2868.8	2778.1	2881.3
5	2855.3	2689.2	2899.7	2632.7	2852.9	2975.6	2631.4	2940.4	2839.2	3053.9
Avg.	2822.6	2731.5	2896.7	3141.4	2922.0	2830.3	2919.1	3022.3	2801.6	3194.0
Std. Dev.	156.0	157.1	56.6	425.3	332.9	139.0	232.9	355.7	26.6	342.4

Table C.3 Elongation at break values of the binary composites (PS-CNTs).

Sample	Elongation at Break, %									
	PS		PS-CNT		PS-SDBS-A-CNT		PS-TX100-A-CNT		PS-MSPM-A-CNT	
	First Set	Second Set	First Set	Second Set	First Set	Second Set	First Set	Second Set	First Set	Second Set
1	2.10	2.55	0.81	1.41	1.66	1.99	1.29	1.69	1.35	1.93
2	1.67	2.20	1.03	1.44	1.97	2.51	1.01	1.88	1.91	2.02
3	2.04	2.24	1.10	1.57	1.57	2.41	0.98	2.02	1.36	2.08
4	1.61	1.90	0.86	1.42	1.93	2.30	0.98	2.26	1.93	1.86
5	2.20	1.92	0.78	1.54	1.21	1.99	1.52	2.38	1.59	2.08
Avg.	1.93	2.16	0.91	1.48	1.67	2.24	1.16	2.05	1.63	1.99
Std. Dev.	0.27	0.27	0.14	0.07	0.31	0.24	0.24	0.28	0.28	0.09

Table C.4 Impact strength values of the binary composites (PS-CNTs) for surface modifier selection.

Sample	Impact Strength, kJ/m^2									
	PS		PS-CNT		PS-SDBS-A-CNT		PS-TX100-A-CNT		PS-MSPM-A-CNT	
	First Set	Second Set	First Set	Second Set	First Set	Second Set	First Set	Second Set	First Set	Second Set
1	9.68	12.20	8.73	9.75	9.58	9.55	9.65	8.35	8.45	9.13
2	9.93	10.93	8.38	9.68	9.78	9.55	9.45	9.90	8.50	9.35
3	8.93	12.65	8.13	9.55	9.45	9.93	9.65	9.13	8.63	9.05
4	9.13	11.83	8.38	9.38	9.78	9.38	9.65	8.38	8.70	8.93
5	9.08	12.03	8.93	9.75	9.70	9.38	9.15	8.83	8.70	9.48
Avg.	9.35	11.93	8.60	9.62	9.66	9.56	9.51	8.92	8.60	9.19
Std. Dev.	0.43	0.64	3.85	0.16	0.14	0.26	0.22	0.64	0.12	0.29

Table C.5 Tensile strengths of the ternary composites (PS-E-CNTs).

Sample	Tensile Strength, MPa					
	PS-E	**PS-E-CNT**	**PS-E-A-CNT**	**PS-E-SDBS-A-CNT**	**PS-E-TX100-A-CNT**	**PS-E-MSPM-A-CNT**
1	5.13	4.63	5.87	5.57	5.24	4.12
2	4.13	5.98	5.62	6.65	5.44	4.43
3	4.80	5.44	6.36	6.43	5.06	4.26
4	4.79	4.65	5.62	5.92	5.33	4.35
5	5.63	5.43	4.18	5.00	5.31	5.51
Avg.	4.90	5.23	5.53	5.92	5.28	4.53
Std. Dev.	0.42	0.58	0.81	0.66	0.16	0.13

Table C.6 Tensile moduli of the ternary composites (PS-E-CNTs).

Sample	Tensile Modulus, MPa					
	PS-E	**PS-E-CNT**	**PS-E-A-CNT**	**PS-E-SDBS-A-CNT**	**PS-E-TX100-A-CNT**	**PS-E-MSPM-A-CNT**
1	653.0	645.4	682.7	638.5	585.6	634.4
2	716.1	636.6	661.5	708.9	606.1	575.6
3	694.1	606.1	699.2	682.7	602.2	628.0
4	738.7	622.2	655.2	664.1	710.3	676.9
5	709.0	673.7	629.1	666.5	668.4	654.1
Avg.	702.1	636.8	665.6	672.1	634.5	633.8
Std. Dev.	36.5	25.5	26.8	26.0	56.9	41.6

Table C.7 Elongation at breaks of the ternary composites (PS-E-CNTs).

Sample	Elongation at Break, %					
	PS-E	**PS-E-CNT**	**PS-E-A-CNT**	**PS-E-SDBS-A-CNT**	**PS-E-TX100-A-CNT**	**PS-E-MSPM-A-CNT**
1	11.84	15.48	14.34	16.99	15.86	6.74
2	10.30	13.35	17.14	14.24	7.02	7.48
3	5.82	7.02	15.90	15.23	16.33	9.15
4	7.76	7.66	14.79	16.23	11.81	13.44
5	6.20	11.81	17.52	11.81	18.32	14.70
Avg.	8.38	11.07	15.94	14.90	13.87	10.30
Std. Dev.	2.67	3.65	1.40	2.01	4.33	3.00

Table C.8 Impact strengths of ternary composites (PS-E-CNTs).

Sample	Impact Strength, kJ/m^2					
	PS-E	**PS-E-CNT**	**PS-E-A-CNT**	**PS-E-SDBS-A-CNT**	**PS-E-TX100-A-CNT**	**PS-E-MSPM-A-CNT**
1	35.93	44.18	41.55	49.80	41.40	60.35
2	39.25	49.80	46.18	51.68	58.15	66.73
3	42.55	37.40	45.80	48.40	46.18	61.18
4	36.45	36.38	38.28	51.58	50.55	61.05
5	31.40	40.05	44.90	44.08	42.80	59.00
Avg.	37.12	41.56	43.34	49.11	47.82	61.66
Std. Dev.	3.31	1.90	2.57	1.86	8.63	3.92

Table C.9 Tensile strengths of the multilayer composites (PS-E-CNTs as polymer layers and one layer of CF).

Sample	Tensile Strength, MPa					
	PS-E-CF		PS-E-CNT-CF		PS-E-MSPM-A-CNT CF	
	Method 1	Method 2	Method 1	Method 2	Method 1	Method 2
1	76.45	59.81	96.31	61.36	119.10	80.21
2	53.26	58.65	68.51	62.26	102.37	74.96
3	56.34	66.07	80.13	72.14	91.52	72.77
4	72.54	64.66	85.10	64.64	94.07	83.95
5	75.45	55.68	85.91	64.79	93.73	65.60
Avg.	66.81	60.97	83.19	65.04	100.16	75.50
Std. Dev.	11.11	4.31	10.10	4.24	11.37	7.06

Table C.10 Tensile moduli of the multilayer composites (PS-E-CNTs as polymer layers and one layer of CF).

Sample	Tensile Modulus, MPa					
	PS-E-CF		PS-E-CNT-CF		PS-E-MSPM-A-CNT CF	
	Method 1	Method 2	Method 1	Method 2	Method 1	Method 2
1	7465.0	3644.9	4906.2	4695.1	7168.1	5354.4
2	5529.3	3533.0	4985.6	3654.8	7672.4	4087.3
3	6739.7	4102.7	3584.0	3181.8	6012.9	5533.3
4	4973.9	3921.8	4165.2	2899.8	6399.4	4372.4
5	6898.6	3405.5	4024.0	4394.4	5835.0	5356.2
Avg.	6321.3	3721.6	4333.0	3765.2	6617.6	4940.7
Std. Dev.	1031.9	285.8	599.8	768.5	781.2	660.7

Table C.11 Elongation at breaks of the multilayer composites (PS-E-CNTs as polymer layers and one layer of CF).

Sample	Elongation at break, %					
	PS-E-CF		PS-E-CNT-CF		PS-E-MSPM-A-CNT-CF	
	Method 1	Method 2	Method 1	Method 2	Method 1	Method 2
1	1.87	2.09	2.66	1.94	2.76	2.59
2	1.94	2.21	2.36	2.13	2.84	2.49
3	1.75	1.98	2.76	2.68	2.44	1.87
4	2.38	2.19	2.85	2.57	2.20	2.38
5	1.95	2.50	3.08	2.26	2.51	2.21
Avg.	1.98	2.19	2.74	2.32	2.55	2.31
Std. Dev.	0.24	0.20	0.26	0.31	0.26	0.28

Table C.12 Tensile strengths of the multilayer composites (PS-E-CNTs as polymer layers and one, three and five layers of CFs).

Sample	Tensile Strength, MPa			
	PS-1-CF	PS-3-CFs	PS-5-CFs	PS-5-MSPM-CFs
1	15.79	62.37	145.94	123.52
2	26.27	72.01	119.11	146.78
3	21.55	54.27	103.59	164.86
4	14.66	53.63	93.93	148.51
5	15.47	54.67	125.34	155.98
Avg.	18.75	59.39	117.58	147.93
Std. Dev.	5.02	7.90	20.14	15.40

Table C.13 Tensile moduli of the multilayer composites (PS-E-CNTs as polymer layers and one, three and five layers of CFs).

Sample	Tensile Modulus, MPa			
	PS-1-CF	**PS-3-CFs**	**PS-5-CFs**	**PS-5-MSPM-CFs**
1	1813.4	4236.5	5271.7	4230.3
2	2266.5	3308.2	4558.0	3632.4
3	2126.7	3053.3	4773.5	3688.8
4	1919.2	3392.8	4521.0	3653.1
5	2330.8	4109.9	4433.3	4008.4
Avg.	2091.3	3620.1	4711.5	3842.6
Std. Dev.	221.4	522.0	337.2	265.3

Table C.14 Elongation at breaks of the multilayer composites (PS-E-CNTs as polymer layers and one, three and five layers of CFs).

Sample	Elongation at Break, %			
	PS-1-CF	**PS-3-CFs**	**PS-5-CFs**	**PS-5-MSPM-CFs**
1	1.51	1.76	3.69	3.51
2	1.76	2.22	3.12	4.53
3	1.34	2.50	2.80	4.91
4	1.18	1.86	2.78	4.44
5	1.05	1.72	3.24	5.06
Avg.	1.37	2.01	3.12	4.49
Std. Dev.	0.28	0.34	0.37	0.60

D. **Shape Recovery**

Shape recovery times and shape recovery ratios of multilayer composites are given in Table D.1-D.4.

Table D.1 Shape recovery times of the bending test results of the multilayer composite samples (PS-E-CNTs as polymer layers and one layer of CF) triggered with heat.

Sample	**Shape Recovery Time, sec**					
	PS-E-CF		**PS-E-umCNT-CF**		**PS-E-MSPM-A-CNT-CF**	
	Method 1	**Method 2**	**Method 1**	**Method 2**	**Method 1**	**Method 2**
1	136	36	127	21	75	20
2	37	27	282	17	31	32
3	149	11	172	12	26	28
4	96	13	174	18	28	23
5	112	38	116	24	35	23
Avg.	106	25	174	18	39	25
Std. Dev.	44	13	66	5	20	5

Table D.2 Shape recovery ratios of the bending test results of the multilayer composite samples (PS-E-CNTs as polymer layers and one layer of CF) triggered with heat.

Sample	**Shape Recovery Ratio, %**					
	PS-E-CF		**PS-E-umCNT-CF**		**PS-E-MSPM-A-CNT-CF**	
	Method 1	**Method 2**	**Method 1**	**Method 2**	**Method 1**	**Method 2**
1	96.1	100.0	92.9	100.0	100.0	100.0
2	97.5	100.0	81.7	100.0	100.0	100.0
3	100.0	100.0	94.2	100.0	100.0	100.0
4	97.6	100.0	85.1	100.0	100.0	100.0
5	95.3	100.0	100.0	100.0	100.0	100.0
Avg.	97.3	100.0	90.8	100.0	100.0	100.0
Std. Dev.	2	0	7	0	0	0

Table D.3 Shape recovery times of the bending test results of the multilayer composite samples (PS-E-CNTs as polymer layers and one layer of CF) triggered with electricity.

Sample	Shape Recovery Time, sec					
	PS-E-CF		PS-E-umCNT-CF		PS-E-MSPM-A-CNT-CF	
	Method 1	Method 2	Method 1	Method 2	Method 1	Method 2
1	22	30	13	16	20	24
2	22	19	15	21	17	12
3	30	25	25	23	21	25
4	38	27	10	16	38	24
5	30	16	9	14	41	15
Avg.	28	23	14	18	27	20
Std. Dev.	7	6	6	4	11	6

Table D.4 Shape recovery times of the bending test results of the multilayer composite samples (PS-E-CNTs as polymer layers and one, three and five layers of CFs) triggered with electricity

Sample	Shape Recovery Time, sec			
	PS-1-CF	PS-3-CFs	PS-5-CFs	PS-5-MSPM-CFs
1	64.0	66.0	43.0	49.0
2	54.0	54.0	51.0	59.0
3	58.0	51.0	57.0	48.0
4	60.0	52.0	46.0	53.0
5	56.0	56.0	50.0	48.0
Avg.	58.4	55.8	49.4	51.4
Std. Dev.	3.8	6.0	5.3	4.7

E. **Viscosity Average Molecular Weight (M_v) Measurement**

In order to calculate the viscosity average molecular weight, intrinsic viscosity value is needed to be determined. Intrinsic viscosity is defined as the fractional change in the viscosity of a solution per unit concentration of a polymer at infinite dilution.

Dilute PS solutions were prepared from 0.28 g/dL to 1.2 g/dL. Flow times of the solvent and the solutions were measured at 30°C by using an Ubbelohde viscometer and are given in Table E.1.

Table E.1 Measured flow times of the solvent and the solutions of PS Crystal 1540.

Mesurements Concentration, g/dL	**Flow Times, s**					**Avg.**	**Std.Dev.**
	1	**2**	**3**	**4**	**5**		
Toluene	223	222	222	221	222	222.0	0.7
0.27 g/dL	272	271	269	274	273	271.8	1.9
0.34 g/dL	287	285	287	282	284	285.0	2.1
0.90 g/dL	404	400	400	404	403	402.2	2.0
1.20 g/dL	479	483	480	479	477	479.6	2.2

Sample calculation for the 0.34 g/dL concentration is given in Table E.2.

Table E.2 Solution viscosity calculations at 0.34 g/dL concentration of PS Crystal 1540 (Rosen, 1993).

Quantitiy	Abbreviations	Formula
$\boldsymbol{\eta}$	η: Solution Viscosity η_s: Pure solvent Viscosity T: Temperature c: Concentration M: Molecular Weight	$\eta = \eta(\eta_s, T, \text{polymer}, \text{solvent}, c, \text{entanglements}, M)$
$\boldsymbol{\eta_r}$	η_r: Relative Viscosity	$\eta_r = \frac{\eta}{\eta_s} = \frac{285}{222} = 1.284$
$\boldsymbol{\eta_{sp}}$	η_{sp}: Specific Viscosity	$\eta_{sp} = \eta_r - 1 = 1.284 - 1 = 0.284$
$\boldsymbol{\eta_{red}}$	η_{red}: Reduced Viscosity	$\eta_{red} = \frac{\eta_{sp}}{c} = \frac{(\eta/\eta_s) - 1}{c} = 0.827\ \text{dL/g}$
$\boldsymbol{\eta_{inh}}$	η_{inh}: Inherent Viscosity	$\eta_{inh} = \frac{\ln(\eta_r)}{c} = 0.728\ \text{dL/g}$

Solution viscosity values calculated for different concentrations are given in Table E.3.

Table E.3 Solution viscosity calculations.

Concentration, g/dL	$\boldsymbol{\eta_r}$	$\boldsymbol{\eta_{sp}}$	$\boldsymbol{\eta_{red}}$ (dL/g)	$\boldsymbol{\eta_{inh}}$ (dL/g)
0.27	1.224	0.224	0.820	0.740
0.34	1.284	0.284	0.827	0.728
0.90	1.812	0.812	0.904	0.661
1.20	2.160	1.160	0.971	0.645

Reduced and inherent viscosities are plotted with respect to concentration to determine intrinsic viscosity. The average of the intercept values of the both plots gives the intrinsic viscosity (Figure E.1).

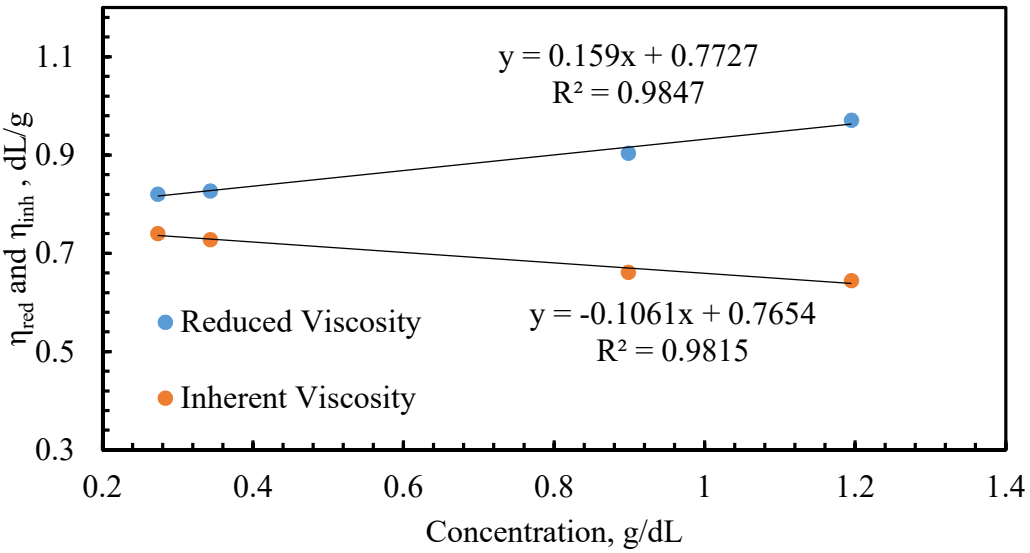

Figure E.1. PS-E-CF samples prepared with different amount of elastomer (SEBS-gMA) addition.

M_v was calculated from Mark-Houwink-Sakurada equation, which was given in Equation 2.6, by taking [η] as the average of the intercepts.

$$M_v = \left(\frac{[\eta]}{K}\right)^{\frac{1}{a}} = \left(\frac{0.77}{1.2 \times 10^{-4}}\right)^{\frac{1}{0.71}} = 229960 \text{ g/mol}$$

F. **Calculations of Surface Free Energy and Work of Adhesion**

The Owens-Wendt-Kaelble equation (Equation F.1) was used for the calculation of dispersion and polar component of surface free energy. In this equation dispersion (London-van der Waals), orientation (Keesom-van der Waals), induction (Debye-van der Waals and Lifshitz-van der Waals forces) and non-dispersion contributions (deriving from electrostatic, metallic, hydrogen bonding and dipole-dipole interactions) of surface free energy is defined (Baldan, 2012).

$$\frac{\gamma_l(1+\cos\theta)}{2} = \left[\left(\gamma_l^d\gamma_s^p\right)^{1/2} + \left(\gamma_l^p\gamma_s^d\right)^{1/2}\right] \qquad \text{F.1}$$

where:

θ: the average contact angle for the test liquid on the test specimen.

γ_l: the surface tension of the test liquid in mJ/m^2.

γ_l^d and γ_s^d: the dispersion component of surface tension of the test liquid and solid, respectively.

γ_l^p and γ_s^p: the polar component of surface tension of the test liquid and solid, respectively.

Sample calculation for the surface energy components is given below. By using the surface free energy components of probe liquids Equation F.1 was simplified and Equations F.4 and F.5 were reached.

$$\frac{72.8(1+\cos\theta_W)}{2} = \left[\left(51.0\,\gamma_s^p\right)^{1/2} + \left(21.8\,\gamma_s^d\right)^{1/2}\right] \qquad \text{F.2}$$

$$\frac{50.8(1+\cos\theta_{DIM})}{2} = \left[\left(1.3\,\gamma_s^p\right)^{1/2} + \left(49.5\,\gamma_s^d\right)^{1/2}\right] \qquad \text{F.3}$$

$$(36.4)(1+\cos\theta_W) = \left[(7.14)(\gamma_s^p)^{1/2} + (4.67)(\gamma_s^d)^{1/2}\right] \qquad \text{F.4}$$

$$(25.4)(1+\cos\theta_{DIM}) = \left[(1.14)(\gamma_s^p)^{1/2} + (7.03)(\gamma_s^d)^{1/2}\right] \qquad \text{F.5}$$

To change these two equations with two unknowns to a single equation with one unknown; both sides of Equation F.4 was multiplied by (-7.03/4.67) in order to eliminate γ_s^d, this new equation was added with Equation F.5 to obtain Equation F.6:

$$(54.8)(1+\cos\theta_W)-(25.4)(1+\cos\theta_{DIM})=\left[(9.61)(\gamma_s^p)^{1/2}\right] \qquad \text{F.6}$$

For example; on the sample PS-E-MSPM-A-CNT the water contact angle was 99.68°, so $\cos\theta_W$ = -0.17, and the diiodomethane contact angle was 47.99°, $\cos\theta_{DIM}$ = 0.67. Therefore, the expression resulting from the subtraction becomes;

$$(54.8)(1-0.17)-(25.4)(1+0.67)=\left[(9.61)(\gamma_s^p)^{1/2}\right] \qquad \text{F.7}$$

$$\gamma_s^p = 0.11\ \text{mJ/m}^2$$

Dispersive component was calculated from the equation for water;

$$(36.4)(1-0.17)=\left[(7.14)(0.11)^{1/2}+(4.67)(\gamma_s^d)^{1/2}\right] \qquad \text{F.8}$$

$$\gamma_s^d = 35.73\ \text{mJ/m}^2$$

The sum of these two values gives the total solid surface tension (γ_s^{total}), which in this case is 35.84 mJ/m^2. Average angles and calculated values of surface free energy components and total surface free energy values were given in Table 4.7.

Work of adhesion (W_a) between two substrates were calculated by using the Young-Dupre equation (Equation F.9) (Baldan, 2012).

$$W_a = 2\left[(\gamma_l^d\gamma_s^d)^{1/2}+(\gamma_l^p\gamma_s^p)^{1/2}\right] \qquad \text{F.9}$$

The calculated W_a values were given in Figure 4.31. For example; W_a between PS-E-MSPM-CNT polymer surface and as-received CF surfaces were calculated as follows;

$$W_a = 2\left[(37.81 \times 35.73)^{1/2} + (1.16 \times 0.11)^{1/2}\right] \quad \text{F. 10}$$

$$W_a = 74.21\ \mathrm{mJ/m^2}$$

G. **Peel Strength**

T-peel test results were given in Figure 4.41. The calculated values of peel strength of the composites are given in Table G.1. The experiments were performed seven times for CF sample and five times for other samples. The absent measurements were represented with '-' sign.

Table G.1 Peel strength dependence on different surface modifications applied to CF.

Sample	Peel Strength, N/m									
	CF	**Desized-CF**	**MSPM-CF**	**Desized-MSPM-CF**	**PSMA-CF**	**sPS-CF**	**sPS-E-CF**	**sPS-E-MSPM-CF**	**PA6-CF**	**PA6-APTES-CF**
1	1696.2	1628.5	1871.9	1640.6	475.7	237.4	722.2	1570.5	202.5	1802.2
2	1508.9	1376.5	1928.5	1536.6	1213.9	409.8	760.6	1415.0	168.4	1627.6
3	1518.3	1668.3	2057.6	1640.9	789.5	371.0	741.3	1408.5	187.3	1639.5
4	1677.8	1224.1	2032.8	1778.2	1405.9	266.4	740.6	1018.3	181.2	1662.9
5	1567.6	1455.5	1920.0	1530.9	679.6	275.1	750.3	1566.6	196.1	1462.3
6	1558.4	-	-	-	-	-	-	-	-	-
7	1858.5	-	-	-	-	-	-	-	-	-
Avg.	1626.5	1470.6	1962.1	1625.5	912.9	311.9	743.0	1353.1	187.1	1638.9
Std. Dev.	125.8	183.0	79.3	100.8	385.5	74.2	14.2	235.4	13.3	121.0

CURRICULUM VITAE

PERSONAL INFORMATION

Surname, Name: Erkmen, Berrak
Nationality: Turkish (TC)
Date and Place of Birth: 1 August 1990, Zonguldak
Marital Status: Single
Phone: +90 538 529 30303
Fax: -
email: e206007@metu.edu.tr

EDUCATION

Degree	Institution	Year of Graduation
MS	Ankara University Chemical Engineering	2014
BS	Ankara University Chemical Engineering	2011
High School	Kdz. Ereğli Anatolian High School, Zonguldak	2007

WORK EXPERIENCE

Year	Place	Enrollment
2019-Present	SOCAR Turkey	Product Development Chief Engineer
2013-2019	METU Dept. of Chemical Eng.	Research Assistant
2010 August	Henkel AG & Company, KGaA, Ankara	Intern Eng. Student
2009 August	Lafarge Ereğli Çimento A.Ş., Zonguldak	Intern Eng. Student

FOREIGN LANGUAGES

Advanced English, Pre-Intermediate German

PUBLICATIONS

1. Erkmen, B., Bayram, G., Investigation of Multifunctional Behavior of the Polystyrene-based Carbon Fiber Reinforced Polymer Composites Containing Carbon Nanotubes. Article. Submitted to: Journal of Applied Polymer Science, 2020.
2. Erkmen, B., Bayram, G., Improvement of Adhesion between the Layers of Polystyrene-Based Carbon Fabric-Reinforced Composites. Oral Presentation. 35th International Conference of the Polymer Processing Society (PPS-35), 26-30 May 2019, İzmir.
3. Erkmen, B., Bayram, G., Polystyrene-Based Carbon Fabric Reinforced Multilayer Composites: Preparation and Characterization. Poster Presentation. Eastern Mediterranean Chemical Engineering Conference (EMCC-9), 31 August-2 September 2018, METU, Ankara.
4. Erkmen, B., Bayram, G., Impact Modified Polystyrene-Based Nanocomposites: Mechanical and Shape Memory Properties. Oral Presentation. 13th Nanoscience and Nanotechnology Conference (NANOTR-13), 22-25 October 2017, Antalya.
5. Erkmen, B., Bayram, G., Preparation and Improvement of Polystyrene Based Multilayer Composites. Poster Presentation. Ulusal Polimer Bilim ve Teknoloji Kongresi-6, 04-07 Semptember 2016, Hacettepe University, Ankara.
6. Aksoy, C. B., Erkmen, B., Bayram, G., Improvement of Adhesion in Multilayer Polymer Composites, Poster Presentation. Ankara Kimya Mühendisliği Bölümleri Birlikteliği (AKMBB), May 2015, Gazi University, Ankara.
7. Erkmen, B., Soysal, F., Çiçek, B. 2014. Carbon Nanotube Production with Cold-Walled Chemical Vapor Deposition. Oral presentation, UKMK-11, 02-05 September 2014, Eskişehir Osmangazi University, Eskişehir.
8. Soysal, F., Erkmen, B., Çiçek, B. 2014. Effect of Magnetron Sputtering Parameters on the Coating Thickness of Iron and Aluminum. Oral presentation, ISTS-2014, 25-27 June 2014, Istanbul Technical University, Istanbul.
9. Yağlıkçı, S., Soysal, F., Erkmen, B., Çiçek, B. 2013. Comparison of carbon nanotubes produced by hot wall and cold wall chemical vapor deposition. Oral presentation, NanoTR-9, 24-28 June 2013, Atatürk University, Erzurum.